JOURNAL OF PETROLOGY | VOLUME 46 | NUMBER 12 | PAGES 2427–2464 | 2005 | doi:10.1093/petrology/egi060

Hafnium Isotope and Trace Element Constraints on the Nature of Mantle Heterogeneity beneath the Central Southwest Indian Ridge (13°E to 47°E)

P. E. JANNEY[1]*, A. P. LE ROEX[2] AND R. W. CARLSON[1]

[1]DEPARTMENT OF TERRESTRIAL MAGNETISM, CARNEGIE INSTITUTION OF WASHINGTON, 5241 BROAD BRANCH ROAD, NW, WASHINGTON, DC 20015, USA

[2]DEPARTMENT OF GEOLOGICAL SCIENCES, UNIVERSITY OF CAPE TOWN, PRIVATE BAG, RONDEBOSCH 7701, SOUTH AFRICA

RECEIVED JULY 6, 2004; ACCEPTED JUNE 10, 2005
ADVANCE ACCESS PUBLICATION JULY 20, 2005

Hafnium isotope and incompatible trace element data are presented for a suite of mid-ocean ridge basalts (MORB) from 13 to 47°E on the Southwest Indian Ridge (SWIR), one of the slowest spreading and most isotopically heterogeneous mid-ocean ridges. Variations in Nd–Hf isotope compositions and Lu/Hf ratios clearly distinguish an Atlantic–Pacific-type MORB source, present west of 26°E, characterized by relatively low ε_{Hf} values for a given ε_{Nd} relative to the regression line through all Nd–Hf isotope data for oceanic basalts (termed the 'Nd–Hf mantle array line'; the deviation from this line is termed $\Delta\varepsilon_{Hf}$) and low Lu/Hf ratios, from an Indian Ocean-type MORB signature, present east of 32°E, characterized by relatively high $\Delta\varepsilon_{Hf}$ values and Lu/Hf ratios. Additionally, two localized, isotopically anomalous areas, at 13–15°E and 39–41°E, are characterized by distinctly low negative and high positive $\Delta\varepsilon_{Hf}$ values, respectively. The low $\Delta\varepsilon_{Hf}$ MORB from 13 to 15°E appear to reflect contamination by HIMU-type mantle from the nearby Bouvet mantle plume, whereas the trace element and isotopic compositions of MORB from 39 to 41°E are most consistent with contamination by metasomatized Archean continental lithospheric mantle. Relatively small source-melt fractionation of Lu/Hf relative to Sm/Nd, compared with MORB from faster-spreading ridges, argues against a significant role for garnet pyroxenite in the generation of most central SWIR MORB. Correlations between $\Delta\varepsilon_{Hf}$ and Sr and Pb isotopic and trace element ratios clearly delineate a high-$\Delta\varepsilon_{Hf}$ 'Indian Ocean mantle component' that can explain the isotope composition of most Indian Ocean MORB as mixtures between this component and a heterogeneous Atlantic–Pacific-type MORB source. The Hf, Nd and Sr isotope compositions of Indian Ocean MORB appear to be most consistent with the hypothesis that this component represents fragments of subduction-modified lithospheric mantle beneath Proterozoic orogenic belts that foundered into the nascent Indian Ocean upper mantle during the Mesozoic breakup of Gondwana.

KEY WORDS: *mid-ocean ridge basalt; isotopes; incompatible elements; Indian Ocean*

INTRODUCTION

The Southwest Indian Ridge (SWIR) is among the slowest-spreading of all mid-ocean ridges (spreading rate $\leq$18 mm/year; Dick *et al.*, 2003) and is arguably the most geochemically heterogeneous ridge system on Earth (e.g. Hamelin & Allègre, 1985; Mahoney *et al.*, 1992). The high degree of tectonic segmentation and low magma supply at this spreading center (Fisher & Goodwillie, 1997; Cannat *et al.*, 1999) appear to have hindered the dispersal of geochemical anomalies arising from nearby mantle plumes (e.g. le Roex *et al.*, 1983, 1992) and/or passive heterogeneities possibly derived from deeply or shallowly recycled continental material (e.g. Mahoney *et al.*, 1992).

The greatest geochemical variations observed in mid-ocean ridge basalt (MORB) along the SWIR occur in the central portion of the ridge, between the Shaka fracture

*Corresponding author. Present address: Department of Geology, The Field Museum of Natural History, 1400 S. Lake Shore Drive, Chicago, IL 60605, USA. Telephone: (312) 665-7099. Fax: (312) 665-7641. E-mail: pjanney@fieldmuseum.org

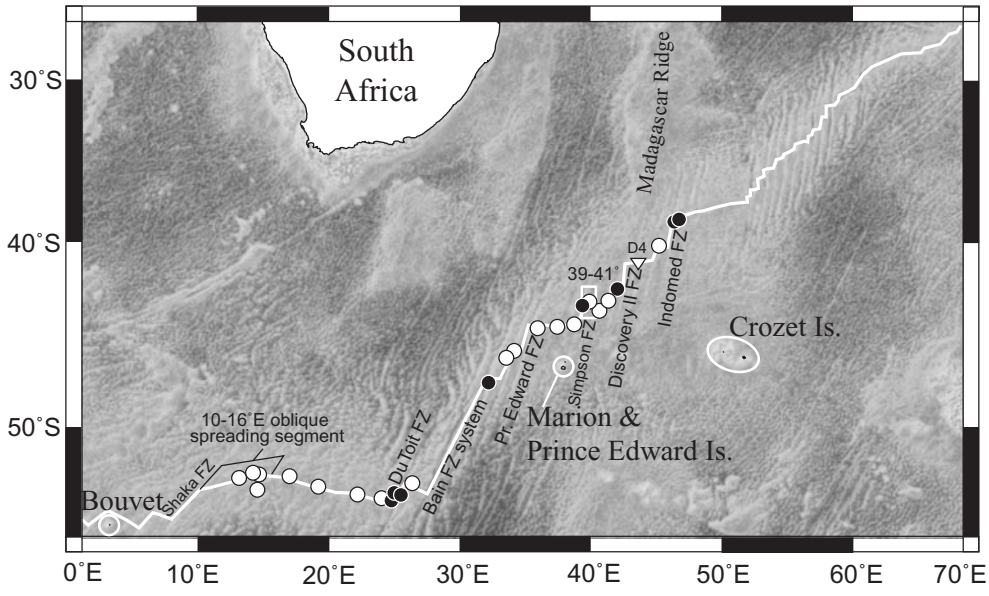

Fig. 1. Map of the Southwest Indian Ridge showing the locations of samples examined in this study. Filled symbols indicate a fracture zone dredge location; open symbols indicate an on-ridge dredge location. The triangle indicates the position of dredge MD34-D4, for which Hf isotope data have been published elsewhere (Hamelin & Allègre, 1985; Chauvel & Blichert-Toft, 2001). White box surrounds the 39–41°E segment.

zone at roughly 10°E and the Indomed Fracture Zone at roughly 47°E (Fig. 1). These variations include localized isotopic anomalies at 13–15°E, which have yielded the most radiogenic $^{206}Pb/^{204}Pb$ values yet measured for Indian Ocean MORB (le Roex *et al.*, 1992), and the so-called 'DUPAL' segment at 39–41°E, which encompasses the lowest $^{206}Pb/^{204}Pb$ values and among the lowest $^{143}Nd/^{144}Nd$ values of any MORB yet reported (Hamelin & Allègre, 1985; Mahoney *et al.*, 1992). Superimposed on these short-wavelength features is a broad isotopic transition across the region from Atlantic–Pacific-type normal MORB (N-MORB) compositions in the west, with relatively radiogenic $^{206}Pb/^{204}Pb$, moderate $^{143}Nd/^{144}Nd$ and unradiogenic $^{87}Sr/^{86}Sr$, to Indian Ocean-type depleted MORB compositions in the east, with unradiogenic $^{206}Pb/^{204}Pb$ (but relatively high $^{207}Pb/^{204}Pb$ and $^{208}Pb/^{204}Pb$), and variable $^{143}Nd/^{144}Nd$ and $^{87}Sr/^{86}Sr$ (Mahoney *et al.*, 1992).

Basalts generated at Indian Ocean spreading centers have long been known to have isotope compositions that are largely distinct from MORB produced in the Atlantic and Pacific oceans (e.g. Subbarao & Hedge, 1973; Dupré & Allègre, 1983). The Indian Ocean mantle signature is characterized by $^{87}Sr/^{86}Sr$ values that are more radiogenic and $^{206}Pb/^{204}Pb$ values that are less radiogenic, particularly for a given $^{143}Nd/^{144}Nd$, $^{207}Pb/^{204}Pb$ or $^{208}Pb/^{204}Pb$ value, than are encountered in Atlantic or Pacific MORB (e.g. Dosso *et al.*, 1986; Price *et al.*, 1986; Mahoney *et al.*, 1989, 1992, 2002). The origin of this signature has long been the source of controversy, having been attributed to addition of plume material, deeply recycled pelagic sediments, subduction-modified mantle wedge material and continental lithosphere to the Indian Ocean upper mantle (e.g. Storey *et al.*, 1989; Mahoney *et al.*, 1992; Weis & Frey, 1996; Rehkamper & Hofmann, 1997; Kempton *et al.*, 2002; Escrig *et al.*, 2004; Hanan *et al.*, 2004; Zhang *et al.*, 2005).

The Lu–Hf isotope system provides a unique perspective on the origin of mantle heterogeneity (e.g. Patchett & Tatsumoto, 1980*a*; Salters & Hart, 1991). Lu is slightly more compatible in mantle phases than Hf and in most circumstances the Lu–Hf system closely mirrors the Sm–Nd isotope system, leading to a high degree of correlation between Hf and Nd isotope ratios in oceanic basalts (Patchett & Tatsumoto, 1980*a*). However, Lu/Hf ratios are more readily fractionated than Sm/Nd by several processes, including melting in the presence of garnet (in which Lu is highly compatible; Irving & Frey, 1978) and metasomatism by carbonated or hydrous fluids (in which Hf is relatively insoluble, e.g. Nelson *et al.*, 1988; Ayers *et al.*, 1997). Also, because of the slower diffusion of Hf relative to Nd in some mantle minerals, particularly garnet, metasomatized mantle peridotites can have radiogenic Hf—a signature of ancient melt depletion—combined with unradiogenic Nd contributed by the metasomatic agent (Bedini *et al.*, 2004; Carlson *et al.*, 2004). Additionally, pelagic sediments display significant decoupling between Hf and Nd isotopes and Lu/Hf and Sm/Nd ratios (e.g. Patchett *et al.*, 1984; Vervoort *et al.*, 1999).

Here, we present Hf isotope and incompatible trace element data for a suite of MORB samples from the central SWIR (Fig. 1) as well as for basalts from the neighboring Bouvet, Marion and Prince Edward islands, and alkalic basalts from the Madagascar large igneous province, which appear to have resulted from the Late Cretaceous activity of the Marion hotspot. This study has three main objectives. The first is to better characterize the geochemistry of MORB from the central SWIR using our extensive trace element and Hf isotope datasets. The second is to use these data in an attempt to constrain the mineralogy and composition of the mantle sources of these basalts and identify the materials and processes responsible for the extreme isotopic compositions present along this ridge, particularly the anomalous DUPAL segment at 39–41°E. The third is to use the geochemical contrast between the unusually clear Atlantic–Pacific and Indian Ocean-type mantle signatures juxtaposed along the central SWIR, as revealed by Hf isotopes, to evaluate the various models that have been proposed for the origin of the Indian Ocean MORB signature.

SAMPLES AND ANALYTICAL METHODS

Samples analyzed in this study are from the PROTEA 05 expedition of the R.V. *Melville* (indicated by prefix 'P' in the sample name), cruises 22 and 53 of the S.A. *Agulhas* (indicated by prefixes 'AG22' or 'AG53'), cruise 34 of the R.V. *Marion Dufresne* (indicated by prefix 'MD34') and cruise ANT IV/4 of the F.S. *Polarstern* (indicated by prefix 'PS4'). For the most part, these samples have been described previously for major and some trace element abundances and Sr, Nd and Pb isotope ratios (Hamelin & Allègre, 1985; le Roex *et al.*, 1989, 1992; Mahoney *et al.*, 1992). Because not all of the MORB samples for which we present data have had major element data reported in the published literature, we provide a full set of major element data for these samples in an electronic appendix, which can be accessed at http://petrology.oupjournals.org/ or obtained from the first author upon request.

The vast majority of sample materials analyzed were whole-rock powders made from fresh pillow interiors; a minority were fresh glasses from chilled pillow rinds (indicated with a 'G' suffix). All whole-rock samples selected for analysis have loss on ignition (LOI) values of $<2{\cdot}5$ wt %, with most samples having LOI <1 wt %. The paucity of available glass is largely due to three factors. First, fresh glass appears to be less abundant at ultra-slow-spreading ridges than at other types of spreading centers because of the longer time intervals between eruptions. Second, the dredging strategy used, particularly on the PROTEA 5 cruise, focused on fracture zones and inside-corner highs to recover peridotites and lower crustal material, rather than focusing on recovery of glassy lavas on-axis. Third, much of the glass that was recovered has been consumed by previous geochemical investigations. However, we have analyzed trace element abundances in two glass–whole-rock pairs (P25-211–P25-211G and P37-2–P37-2G) and found excellent agreement (Table 1).

Trace element analyses were performed on dissolved sample solutions by inductively coupled plasma mass spectrometry (ICPMS) using a Perkin Elmer/SCIEX Elan 6000 quadrupole instrument at the Department of Geological Sciences, University of Cape Town. Sample solutions were run in peak-hopping mode, using In, Re and Bi as internal standards. Calibration was performed using multi-element standard solutions. Accuracy and precision were checked by repeated analysis of USGS basalt standard BHVO-1 and in-house MORB glass standard V40-56 (see Table 1 for measured and reference values for these standards).

Hafnium separation and isotope ratio measurements were performed at the Department of Terrestrial Magnetism of the Carnegie Institution of Washington (DTM). Hf separations were conducted using a three-column, cation–anion–cation separation procedure in a HCl–HF medium adapted from Patchett & Tatsumoto (1980*b*) and Blichert-Toft *et al.* (1997). Hf recoveries were $>75\%$ with Yb/Hf and Lu/Hf ratios of $<0{\cdot}0005$ and $<0{\cdot}0002$, respectively. Hf blanks are <25 pg and thus are negligible; no blank corrections were applied. Analysis of Hf isotope ratios was performed by ICPMS on a VG Plasma 54 multicollector system (equipped with nine Faraday collectors) in static mode, with ^{173}Yb and ^{175}Lu monitored to allow correction of ^{176}Hf for isobaric interferences by ^{176}Yb and ^{176}Lu. All Faraday cup efficiencies were set to unity and Hf isotope ratios were fractionation-corrected to a ^{179}Hf/^{177}Hf value of 0·7325. The Hf isotope data presented here were collected during two analysis periods within a 1 year interval (April 2000 to April 2001). Fifty-three analyses of the JMC 475 Hf standard, run as every third sample, yielded a mean ^{176}Hf/^{177}Hf ratio of 0·282152 with a 2σ uncertainty of $\pm 0{\cdot}000012$. To facilitate comparison, all sample data have been normalized to a JMC 475 ^{176}Hf/^{177}Hf ratio of 0·28216. Two SWIR samples that we analyzed for Hf isotope composition (MD34-D5 and MD34-D6) were also analyzed by Chauvel & Blichert-Toft (2001). For both samples, our values agree within 2σ analytical uncertainties.

Supplementary Sr, Nd and Pb isotope ratios were determined on a subset of samples. Nd and Pb isotope ratio measurements were performed on the VG Plasma 54 at DTM. Sr was separated using standard cation exchange techniques and Sr isotope ratios were measured in multi-dynamic mode by thermal ionization mass spectrometry on the VG 354 instrument at DTM. Sr isotope ratios were fractionation-corrected to

Table 1: Trace element concentrations of SWIR lavas

Section:	13–15°E				17–26°E										
Sample:	PS4-6-2	PS4-4-101	PS4-3-14	PS4-2-1	AG22-1-1	AG22-3-4	AG22-9-2	AG22-12-26	AG22-8-1	P14-81	P14-89	P14-90	P11-17	P12-12	P9-1G
Latitude (°S):	52·35	52·1	53·12	52·22	52·3	52·76	53·11	53·39	53·41	53·12	53·12	53·12	53·16	53·18	52·58
Longitude (°E):	13·13	14·12	14·50	14·63	16·98	19·10	22·20	23·19	24·76	25·32	25·32	25·32	25·49	25·51	26·34
Setting:	R	R	R	R	R	R	R	R	R	FZ	FZ*	FZ*	FZ	FZ	R
Rb (ppm)	7·97	22·7	69·2	11·2	1·58	3·68	0·35	1·20	1·74	3·00	6·83	4·43	0·57	1·09	1·52
Sr	202	424	407	351	129[a]	164[a]	123[a]	152[a]	160[a]	137·3[b]	160·7[b]	154·1[b]	126·4[b]	158·4[b]	194
Zr	162	310	174	107	98[a]	130[a]	81[a]	108[a]	139[a]	117[c]	39[c]	29[c]	157[c]	171[c]	177
Y	36·2	43·6	29·2	20·4	29·3	33·0	23·9	28·5	34·5	31·8	18·5	13·5	34·5	41·5	39·5
Nb	14·5	47·0	52·1	23·9	3·28	4·85	1·58	2·29	3·25	2·23	1·10	0·57	3·69	5·23	4·21
Cs	0·12	0·29	2·29	0·20	0·02	0·11	0·01	0·03	0·06	0·14	0·26	0·20	0·05	0·07	0·01
Ba	82·4	266	411	190	14·5	21·5	4·79	7·24	8·37	8·05	66·9	54·4	5·66	9·66	13·0
La	11·0	30·9	30·2	14·6	3·69	5·54	2·61	3·63	4·83	3·78	2·70	1·69	5·37	5·95	6·32
Ce	26·0	65·3	55·4	28·4	11·3	16·0	8·37	11·8	15·3	11·9	7·84	5·09	17·0	18·5	20·0
Pr	3·65	8·91	6·68	3·40	1·90	2·58	1·53	2·01	2·56	2·10	1·19	0·79	2·81	3·03	3·22
Nd	16·7	38·2	26·1	13·9	10·1	13·4	8·19	10·7	13·6	11·2	6·16	4·17	14·3	15·4	16·0
Sm	4·52	9·11	5·58	3·38	3·42	4·23	2·80	3·47	4·29	3·76	2·05	1·43	4·46	4·76	4·87
Eu	1·52	2·92	1·78	1·19	1·26	1·50	1·06	1·26	1·53	1·35	0·81	0·60	1·54	1·63	1·66
Gd	5·25	9·07	5·43	3·63	4·37	5·14	3·69	4·28	5·31	4·88	2·76	1·96	5·55	5·98	6·14
Tb	0·91	1·39	0·86	0·60	0·75	0·90	0·65	0·75	0·92	0·86	0·49	0·35	0·97	1·03	1·06
Dy	5·70	7·85	4·92	3·48	5·01	5·78	4·21	4·90	5·98	5·58	3·25	2·38	6·24	6·61	6·90
Ho	1·23	1·54	1·00	0·70	1·04	1·21	0·88	1·02	1·26	1·16	0·70	0·51	1·27	1·35	1·44
Er	3·59	4·09	2·77	1·93	2·94	3·49	2·50	2·98	3·64	3·32	2·04	1·48	3·51	3·73	4·13
Tm	0·52	0·55	0·39	0·27	0·44	0·50	0·38	0·43	0·52	0·50	0·31	0·23	0·51	0·56	0·63
Yb	3·31	3·35	2·43	1·66	2·71	3·21	2·33	2·76	3·36	3·10	1·96	1·46	3·03	3·46	3·91
Lu	0·51	0·48	0·36	0·24	0·41	0·48	0·34	0·42	0·50	0·47	0·31	0·23	0·44	0·49	0·60
Hf	3·43	6·82	3·62	2·35	2·54	3·17	2·02	2·61	3·30	2·84	1·18	0·82	2·35	2·82	4·04
Pb	1·08	2·19	2·03	1·36	0·40	0·70	0·33	0·57	0·72	0·65	1·67	1·47	0·54	0·48	0·78
Th	1·23	3·32	4·54	2·12	0·24	0·36	0·090	0·15	0·20	0·14	0·47	0·28	0·12	0·18	0·25
U	0·33	0·94	1·20	0·58	0·10	0·16	0·048	0·070	0·12	0·074	0·15	0·089	0·041	0·11	0·095

Section:		32–34°E					36–39°E						39–41°E		
Sample:	P9-4	P15-54	AG53-1-34	AG53-1-35	P17-22	AG53-3-3	P25-211	P25-211G	P25-217	MD34-D7	P26-1	MD34-D6	P27-2	P28-8G	P28-9
Latitude (°S):	52·58	47·7	47·17	47·17	46·39	46·03	44·82	44·82	44·82	44·81	44·74	44·18	43·62	43·37	43·37
Longitude (°E):	26·34	32·16	32·66	32·66	33·52	34·07	35·85	35·85	35·85	36·30	37·08	38·80	39·31	39·86	39·86
Setting:	R*	FZ	FZ	FZ	FZ	FZ	R	R	R	R	R	R	FZ	FZ	FZ
Rb (ppm)	11·9	6·21	1·93	5·88	0·53	3·39	9·00	8·46	9·19	10·2	10·4	3·08	4·48	7·14	6·16
Sr	152	132·8[b]	120	150[a]	119·4[b]	160[a]	193·2[b]	196	93·4[b]	202[c]	134[b]	146[c]	183[c]	162	202[c]
Zr	77	109[c]	84[a]	83[a]	72[c]	120[c]	122[c]	122	76[c]	115[c]	128[c]	117[c]	73[c]	122	111[c]
Y	35·2	34·3	26·8	24·1	24·1	32·8	33·2	35·0	31·9	30·8	38·0	34·2	21·4	39·0	27·3
Nb	1·13	2·53	1·50	1·48	1·46	5·54	14·5	14·8	4·4	12·6	10·5	7·32	7·48	8·09	5·70
Cs	0·56	0·44	0·05	0·33	0·03	0·04	0·13	0·09	0·11	0·25	0·25	0·04	0·07	0·07	0·14
Ba	137	19·2	4·18	4·64	7·30	32·3	84·9	91·9	22·0	80·8	66·8	52·9	89·4	159	103
La	4·30	3·64	2·47	2·48	2·25	5·24	10·3	10·8	3·31	9·94	8·11	7·03	7·02	8·31	6·03
Ce	12·9	11·6	8·29	8·44	7·38	14·7	23·3	24·0	9·36	22·5	19·4	17·9	15·4	20·0	14·7
Pr	2·00	1·98	1·49	1·46	1·30	2·32	3·13	3·24	1·55	3·09	2·84	2·64	2·07	2·94	2·14
Nd	10·3	10·5	8·12	7·87	7·11	11·8	14·3	14·7	8·34	14·2	13·9	13·0	9·42	14·3	10·3
Sm	3·52	3·63	2·87	2·67	2·58	3·83	4·07	4·29	3·08	4·06	4·33	4·01	2·70	4·45	3·12
Eu	1·31	1·34	1·10	1·06	1·04	1·34	1·39	1·43	1·16	1·46	1·51	1·37	1·01	1·52	1·15
Gd	4·85	5·06	3·79	3·54	3·61	4·87	4·90	5·13	4·58	5·04	5·71	5·24	3·35	5·50	4·17
Tb	0·87	0·90	0·70	0·65	0·64	0·88	0·87	0·91	0·83	0·86	1·02	0·91	0·59	1·00	0·72
Dy	5·69	5·96	4·78	4·30	4·25	5·83	5·70	5·75	5·58	5·56	6·69	6·04	3·84	6·41	4·79
Ho	1·29	1·26	1·02	0·92	0·89	1·23	1·19	1·26	1·20	1·14	1·40	1·26	0·79	1·40	1·02
Er	3·80	3·65	2·90	2·60	2·55	3·50	3·38	3·60	3·49	3·19	4·01	3·64	2·22	4·07	2·94
Tm	0·55	0·56	0·45	0·40	0·39	0·53	0·51	0·53	0·53	0·48	0·61	0·55	0·33	0·60	0·44
Yb	3·65	3·49	2·78	2·49	2·36	3·31	3·17	3·32	3·32	2·97	3·79	3·41	2·07	3·76	2·78
Lu	0·56	0·53	0·43	0·38	0·36	0·50	0·48	0·50	0·51	0·45	0·57	0·52	0·31	0·57	0·43
Hf	2·23	2·67	2·08	1·97	1·46	2·87	2·96	3·02	2·12	2·85	3·23	2·88	1·50	3·12	2·25
Pb	4·17	0·56	0·31	0·32	0·24	0·51	0·93	0·93	0·35	1·03	0·91	0·70	0·55	1·06	0·85
Th	0·84	0·18	0·10	0·10	0·071	0·39	1·15	1·18	0·28	1·00	0·86	0·67	0·52	0·63	0·46
U	0·23	0·061	0·068	0·093	0·021	0·13	0·32	0·30	0·090	0·30	0·25	0·17	0·11	0·14	0·14

Table 1: continued

Section:	42–47°E										Standards					
Sample:	P28-26	P28-120	MD34-5	P29-34	P30-75	P37-1	P37-2	P37-2G	P41-49	P42-11	BHVO-1	% RSD	BHVO-1	V40-56	%RSD	V40-56
Latitude (°S):	43·37	43·37	43·89	42·69	42·69	40·13	40·13	40·13	38·66	38·42	($n = 39$)		Eggins	($n = 15$)		Le Roex
Longitude (°E):	39·86	39·86	40·65	41·90	41·99	45·76	45·76	45·76	46·63	46·72			*et al.*			*et al.*
Setting:	FZ	FZ	R	FZ	FZ	R	R	R	FZ	RTI			(1997)			(2002*a*)
Rb (ppm)	9·18	5·57	2·51	5·27	6·96	14·0	7·66	6·63	4·42	4·14	9·52	1·7	9·5	2·98	0·6	2·87
Sr	188·0[b]	163[c]	240	132·9[b]	125[c]	307[c]	190[c]	154	119[c]	100[c]	398	1·2	390	203	0·7	203
Zr	109[c]	87[c]	39	153[c]	154[c]	82[c]	134[c]	111	68[c]	70[c]	177	2·0	180	175	0·7	174
Y	32·9	26·7	14·5	36·3	46·6	15·8	30·0	30·6	27·9	27·7	27·3	1·4	28	37·9	0·5	37·8
Nb	7·44	5·50	2·61	3·47	4·14	19·1	10·6	9·70	5·45	3·27	19·5	2·8	19·5	8·46	3·3	8·39
Cs	0·20	0·16	0·03	0·21	0·27	0·14	0·09	0·07	0·05	0·11	0·10	2·8	0·1	0·03	3·6	
Ba	138	105	64·0	17·3	26·1	178	82·1	80·8	48·6	27·5	131	2·9	133	29·9	0·9	30
La	7·65	5·83	3·31	4·16	5·32	13·4	7·91	7·45	4·32	3·07	15·5	3·3	15·5	8·02	0·7	8·12
Ce	18·5	14·2	7·83	13·2	16·8	25·8	18·7	17·4	10·5	8·41	38·6	3·5	38	22·5	0·8	22·8
Pr	2·70	2·08	1·17	2·26	2·91	3·01	2·65	2·53	1·58	1·38	5·35	3·3	5·45	3·42	0·8	
Nd	13·0	9·99	5·81	12·2	15·5	11·9	12·5	12·0	7·93	7·41	24·5	4·6	24·7	16·7	0·6	17
Sm	3·94	3·05	1·92	4·11	5·25	2·67	3·78	3·70	2·64	2·67	6·09	4·5	6·17	4·98	0·8	5·03
Eu	1·40	1·13	0·87	1·42	1·81	0·96	1·33	1·27	0·99	1·02	2·04	2·4	2·06	1·75	1·4	1·74
Gd	5·01	4·01	2·41	5·56	7·07	2·83	4·69	4·58	3·77	3·94	6·04	1·9	6·22	6·14	1·3	6·1
Tb	0·88	0·70	0·41	0·98	1·24	0·47	0·82	0·81	0·67	0·71	0·91	2·3	0·95	1·06	1·3	
Dy	5·85	4·72	2·51	6·42	8·18	2·89	5·36	5·09	4·47	4·78	5·15	2·3	5·25	6·81	1·4	6·64
Ho	1·22	1·00	0·53	1·35	1·72	0·58	1·12	1·11	0·95	1·02	0·96	1·8	1·00	1·41	1·8	
Er	3·47	2·86	1·44	3·90	4·93	1·60	3·18	3·16	2·75	2·95	2·50	1·6	2·56	3·99	1·7	4·06
Tm	0·53	0·44	0·20	0·58	0·75	0·24	0·47	0·45	0·42	0·45	0·32	1·8		0·60	1·6	
Yb	3·29	2·73	1·25	3·65	4·69	1·43	2·92	2·87	2·62	2·82	1·93	1·7	1·98	3·71	1·7	3·68
Lu	0·50	0·42	0·18	0·56	0·71	0·22	0·44	0·42	0·40	0·43	0·27	1·6	0·278	0·56	1·1	
Hf	2·84	2·18	1·04	3·09	3·95	1·82	2·89	2·69	1·83	1·85	4·31	2·6	4·3	4·08	1·8	
Pb	0·91	0·77	0·60	0·54	0·69	1·17	0·85	0·79	0·43	0·33	2·00	1·7	2·1	0·92	4·4	
Th	0·61	0·44	0·20	0·24	0·30	1·93	0·86	0·79	0·48	0·31	1·32	2·6	1·26	0·47	2·3	0·53
U	0·16	0·14	0·051	0·12	0·17	0·43	0·22	0·19	0·14	0·10	0·45	2·0	0·42	0·19	1·6	0·19

Data shown represent averages of three or more individual analyses. Analytical methods are described in text. Mean measured and literature trace element values for BHVO-1 and in-house MORB standard V40-56 (Eggins *et al.*, 1997; Le Roux *et al.*, 2002*a*) are provided for comparison. R, FZ and RTI stand for ridge, fracture zone and ridge–transform intersection, respectively. Because of problems with Sr and Zr concentrations in calibration standards in one analytical session, some Sr and Zr concentrations were not determined. Data shown with superscripts are XRF and isotope dilution values from [a]A. P. le Roex (unpublished data, 1988), [b]Mahoney *et al.* (1992) and [c]le Roex *et al.* (1989). %RSD indicates the relative standard deviation between replicate analyses in percent.
*Samples suspected to be ice-rafted volcanic material from the South Sandwich Islands (see text).

$^{86}Sr/^{88}Sr = 0{\cdot}1194$. Repeat analyses of NBS 987 gave a mean $^{87}Sr/^{86}Sr$ value of $0{\cdot}710275 \pm 18$ (2σ, $n = 6$), but all data reported are normalized to a $^{87}Sr/^{86}Sr$ value of 0·710250. Nd was separated from the other rare earth elements (REE) using EiChrom 'Lanthanide' resin and measured in static mode. ^{140}Ce and ^{147}Sm were monitored to correct for isobaric interferences of Ce and Sm on ^{142}Nd and ^{144}Nd, respectively. Nd isotope ratios were fractionation-corrected to a $^{146}Nd/^{144}Nd$ value of 0·7219. Repeat analysis of the La Jolla Nd standard yielded a mean $^{143}Nd/^{144}Nd$ value of $0{\cdot}511835 \pm 12$ (2σ, $n = 10$), but sample values were normalized to La Jolla $^{143}Nd/^{144}Nd = 0{\cdot}51185$. Pb was separated by anion exchange chromatography in an HBr medium and Pb isotope ratio measurements were performed in static mode using the thallium normalization technique (Rehkämper & Halliday, 1998) for mass bias correction. All Tl normalized samples and standards were prepared with $^{208}Pb/^{205}Tl$ ratios of $0{\cdot}2 \pm 0{\cdot}04$. Pb isotope measurements were conducted by bracketing the analysis of each sample with analyses of the NBS 981 Pb standard. Measured Pb isotope ratios for NBS 981 using Tl normalization yielded $^{206}Pb/^{204}Pb$ and $^{207}Pb/^{204}Pb$ values within 0·015 and $^{208}Pb/^{204}Pb$ values within 0·030 of the reference values of Todt *et al.* (1996), to which the Pb isotope ratio values of all samples were normalized. Procedural blanks for Sr, Nd and Pb are less than 150 pg, 20 pg and 100 pg, respectively, and are negligible.

RESULTS

Incompatible trace elements

MORB from the central SWIR display wide ranges of incompatible trace element concentrations (Table 1) and ratios that suggest derivation by variable degrees and depths of partial melting of a number of variably depleted and enriched mantle sources. Seawater alteration appears to have had little effect on the trace element compositions of the samples. Only the highly mobile elements Rb and Cs and, to a lesser extent, U show evidence for alteration-related disturbance relative to less mobile elements such as Th, Nb and the light rare earth elements (LREE) in the whole-rock samples (Fig. 2).

One characteristic shared by nearly all of the SWIR samples is a slight depletion in the heavy REE (HREE) relative to the middle REE (MREE), resulting in $(Tb/Yb)_N$ ratios (the subscript N indicates normalization to chondritic values; Evensen *et al.*, 1978) that are slightly higher [mean $= 1{\cdot}22 \pm 0{\cdot}08$ (1σ) excluding samples with $(La/Sm)_N > 1$] than those of average N-MORB from slow- to fast-spreading centers [>2 mm/year full rate; mean $= 1{\cdot}08 \pm 0{\cdot}11(1\sigma)$ excluding samples with $(La/Sm)_N > 1$; PETDB MORB database, 2004, available at http://www.petrology.oupjournals.org]. This mild HREE depletion appears to be common to MORB from ultra-slow-spreading centers, as it is also found in MORB from the Mid-Cayman Rise, American–Antarctic Ridge and Gakkel Ridge (le Roex *et al.*, 1985; Mühe *et al.*, 1993, 1997; Elthon *et al.*, 1995).

Along axis, one of the most notable regional (as opposed to local) variations in incompatible element composition occurs between 26°E and 32°E, where there is a marked eastward increase in Lu/Hf ratio both overall (Fig. 3a) and for a given Sm/Nd ratio (Fig. 3b). This shift in Lu/Hf values also marks a major division in the Hf–Nd–Sr isotopic composition of central SWIR MORB, as will be shown in the next section. The regional Lu/Hf variations therefore appear to represent long-lived features of the mantle source, and are not simply caused by regional variations in depth of melting or source mineralogy. The incompatible element compositions of central SWIR MORB, divided into six sections, are described below.

13–15°E: enriched MORB

Dredging of the 13–15°E portion of the extremely slow oblique-spreading ridge segment at 10–16°E (8 mm/year effective spreading rate; Dick *et al.*, 2003) recovered lava types ranging from olivine tholeiites to moderately nepheline-normative alkali basalts. The four samples from this segment selected for trace element analysis encompass nearly the full range of incompatible element enrichment and silica saturation or undersaturation of the suite reported by le Roex *et al.* (1992). The samples are characterized by the highest $(La/Sm)_N$ and Nb/Zr ratios yet found for SWIR MORB (1·5–3·4 and 0·09–0·31, respectively; and primitive mantle-normalized incompatible element patterns with strong positive Nb anomalies (Fig. 2a). The two most incompatible-element enriched alkali basalts (PS4-3-14 and PS4-4-101) are nearly indistinguishable from Bouvet Island basalts in terms of their incompatible element compositions.

17–26°E: normal (N-type) MORB

Samples in this section come from the long orthogonal spreading segment at 16–25°E, as well as the DuToit Fracture Zone (hereafter termed 'DuToit FZ') and the western portion of the short 26–28°E spreading segment between the DuToit and Bain fracture zones (Fig. 1). Most of the lavas from this area are normal (N-type) MORB with $(La/Sm)_N$ (0·63–0·82), Ba/Nb (1·5–4·4) and Nb/Zr (0·02–0·04) ratios that vary from slightly below to slightly above average N-MORB values (see Hofmann, 1988; Sun & McDonough, 1989). The trace element patterns for the five on-axis samples from the 16–25°E segment and sample P9-1G from the 26–28°E segment are very similar, particularly for the mildly incompatible elements (i.e. Sm to Lu; Fig. 2b). As a result, these lavas display restricted ranges of $(Sm/Yb)_N$ and $(Lu/Hf)_N$

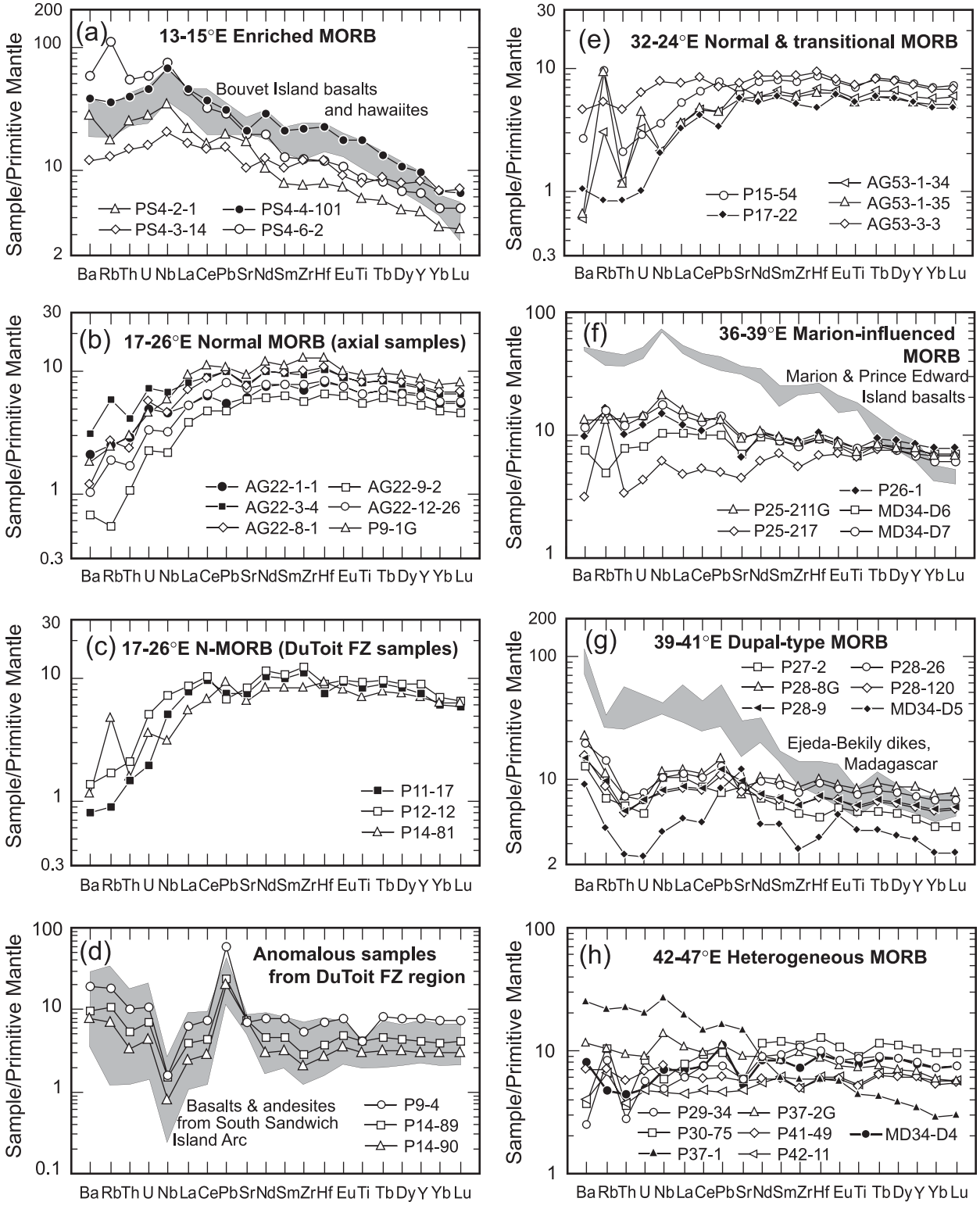

Fig. 2. Primitive mantle-normalized incompatible element diagrams for central SWIR MORB. Primitive mantle values are from Sun & McDonough (1989). Shown on these diagrams are fields for Bouvet Island lavas (le Roex & Erlank, 1982; Weaver *et al.*, 1986), basalts and andesites from the South Sandwich Arc (Pearce *et al.*, 1995), Marion and Prince Edward Island basalts (Table 2) and Ejeda–Bekily dike samples MAD 8, MAD 10 and MAD 52 (Dostal *et al.*, 1992) analyzed for Hf isotopes. Pattern for sample MD34-D4 is from Chauvel & Blichert-Toft (2001).

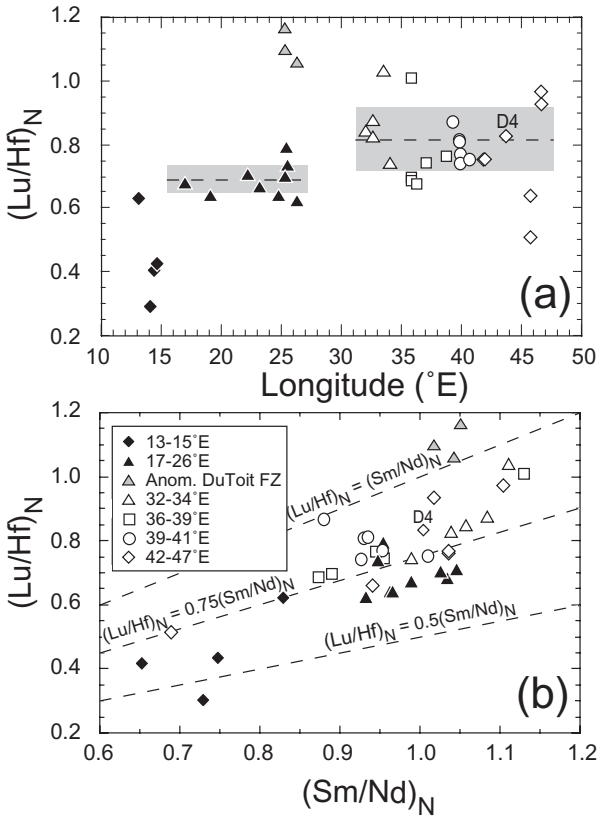

Fig. 3. (a) Longitude vs $(Lu/Hf)_N$, and (b) $(Sm/Nd)_N$ vs $(Lu/Hf)_N$. Dashed lines and gray bars in (a) indicate the mean and 1σ variation of $(Lu/Hf)_N$ in the 17–26°E and 32–47°E regions, respectively. D4 indicates composition of sample MD34-D4 from Chauvel & Blichert-Toft (2001).

ratios (1·29–1·41 and 0·63–0·71, respectively). In contrast, the three MORB samples from the DuToit FZ show greater variability in their trace element patterns for this range of elements, and two of the three samples (P11-17 and P12-12) have mild negative Hf anomalies and slightly higher ratios of MREE to HREE, giving them relatively high $(Sm/Yb)_N$ and $(Lu/Hf)_N$ ratios (1·48–1·58 and 0·75–0·79, respectively; Fig. 2c). The cause of the negative Hf anomalies in these fracture zone samples is unknown, as their Zr and Ti contents are not similarly depleted.

In addition to the N-MORB lavas described above, a small number of vesicular basalts and andesites lacking glassy rinds were recovered in PROTEA Expedition dredges 14 and 9 (Fisher *et al.*, 1985), located in the DuToit FZ and on the 26–28°E spreading segment, respectively. These samples include P14-89, P14-90, and P9-4 described by le Roex *et al.* (1989), Mahoney *et al.* (1992) and this study, and P9-7 described only by Mahoney *et al.* (1992). They are remarkable in that they have extreme depletions in Nb and very strong relative enrichments in Ba and Pb (e.g. Ba/Nb = 60–120, Ce/Pb = 3·1–4·7, le Roex *et al.*, 1989; Mahoney *et al.*, 1992; Fig. 2d). These traits are more extreme than those for any other MORB sample yet published (see Kamenetsky *et al.*, 2001; Le Roux *et al.*, 2002*a*; Fig. 2d). The combination of their unusual appearance and major element similarity to arc tholeiites (le Roex *et al.*, 1989), led Mahoney *et al.* (1992) to speculate that these rocks are exotic lava fragments originating at the South Sandwich island arc and carried eastward as ice-rafted debris. Figure 2d clearly shows that the incompatible element patterns for these anomalous lavas display an extraordinary similarity to those for the dominantly tholeiitic, basaltic to andesitic lavas forming the South Sandwich Islands (Pearce *et al.*, 1995). This strong trace element similarity, along with isotopic similarities between these dredge samples and South Sandwich Island lavas (Cohen & O'Nions, 1982; Mahoney *et al.*, 1992; Pearce *et al.*, 1995), appears to confirm the hypothesis of Mahoney *et al.* (1992) for the exotic origin of these lavas.

32–34°E: normal and transitional MORB

Five MORB samples were analyzed from this area of the ridge, obtained from one dredge in the northeastern part of the Bain Fracture Zone and three dredges on the short 32·5°–34°E spreading segment between the Bain and Prince Edward fracture zones. Although roughly half as many MORB samples were analyzed from this section as compared with 17–26°E, these samples display greater variation in their ratios of highly and moderately incompatible elements [e.g. $(La/Sm)_N = 0·62$ to 0·86, Nb/Zr = 0·02 to 0·05; Ba/Nb = 3·1 to 7·6; Table 1]. As noted above, these samples also tend to display higher $(Lu/Hf)_N$ ratios than those from the 17–26°E section (0·74 to 1·0 vs 0·63 to 0·79, respectively; Fig. 3a).

36–39°E: Marion-influenced MORB

The segment at 36–39°E, located between the Prince Edward and Simpson fracture zones, is the portion of the SWIR that lies closest to Marion and Prince Edward Islands, and presumably to the present-day location of the Marion hotspot. Most lavas dredged from this segment are mildly enriched in incompatible elements, but one sample (P25-217) is moderately depleted (e.g. La/Sm_N = 0·7–1·5, Nb/Zr = 0·05–0·12, Ba/Nb = 5·0–7·2). All samples have primitive mantle-normalized incompatible element patterns with positive Nb anomalies. In this, they resemble lavas from Marion and Prince Edward Islands (Table 2, Fig. 2f), although they do not attain the same degree of incompatible element enrichment as these ocean island lavas (e.g. La/Sm_N = 2·1–2·8, Nb/Zr = 0·14–0·17, Ba/Nb = 7–8).

Table 2: Major and trace element data for Marion and Prince Edward Island lavas

Sample:	MAR-11	MAR-12	PREI 13
Location:	Marion Is.	Marion Is.	Pr. Edward Is.
XRF			
SiO_2 (wt %)	46·45	47·31	47·07
TiO_2	3·62	3·48	3·95
Al_2O_3	15·48	16·04	15·62
$Fe_2O_3^t$	13·75	13·24	13·62
MnO	0·18	0·17	0·18
MgO	5·86	5·53	5·04
CaO	9·37	8·97	8·75
Na_2O	3·29	3·95	3·83
K_2O	1·31	1·39	1·45
P_2O_5	0·70	0·53	0·70
H_2O^-	0·54	0·37	0·84
LOI	−0·67	−0·93	−0·96
Total	99·89	100·06	100·08
Ni (ppm)	51	45	28
Cr	96	47	5·9
V	294	261	280
ICPMS			
Rb (ppm)	30·0	27·5	23·4
Sr	657	695	759
Zr	293	295	355
Y	29	28	41
Nb	50	49	48
Cs	0·24	0·19	0·13
Ba	341	335	334
La	34	31	37
Ce	75	69	80
Pr	9·32	8·57	10·9
Nd	38·2	34·9	47·4
Sm	8·21	7·50	11·1
Eu	2·72	2·61	3·57
Gd	7·43	6·83	10·38
Tb	1·09	1·01	1·51
Dy	6·06	5·56	8·02
Ho	1·09	1·00	1·48
Er	2·79	2·53	3·68
Tm	0·38	0·35	0·48
Yb	2·23	2·03	2·77
Lu	0·32	0·29	0·39
Hf	6·75	6·79	8·09
Ta	2·74	2·76	2·88
Pb	2·40	2·21	3·02
Th	3·77	3·68	3·09
U	1·08	1·01	0·864

XRF data were obtained at the University of Cape Town (UCT) using the method of le Roex (1985). H_2O^- and LOI indicate the weight change during heating at 110°C for 8 h and at 1000°C for 4 h, respectively. ICPMS data were acquired at UCT during the same period and with the same conditions as in Table 1.

39–41°E: 'Dupal-type' MORB

Basalts from the 39–41°E segment are among the most isotopically unusual basalts recovered from the global mid-ocean ridge system (e.g. Hamelin & Allègre, 1985; Hart *et al.*, 1986; Mahoney *et al.*, 1992), and are particularly notable for their extremely unradiogenic $^{143}Nd/^{144}Nd$ and $^{206}Pb/^{204}Pb$ ratios, combined with relatively high $^{207}Pb/^{204}Pb$ and $^{208}Pb/^{204}Pb$ for a given $^{206}Pb/^{204}Pb$ value (i.e. high Δ7/4 and Δ8/4; Hart, 1984). These samples are characterized by mild enrichments in the LREE [$(La/Sm)_N = 1·1–1·6$], and, relative to the LREE, strong enrichments in Ba (Ba/La = 13–19, Na/Nb = 12/24, Ba/Th = 172–312), variable enrichments in Pb (Ce/Pb = 13–28) and strong depletions in Th and U (Fig. 2g). Unlike the anomalous lavas from the DuToit Fracture Zone region, these samples are non-vesicular, have glassy chilled margins and are, from appearance, indistinguishable from other SWIR MORB. It should also be noted that these characteristics are displayed by both whole-rock lavas and fresh basaltic glass (e.g. sample P28-8G) and thus appear to be primary features and not the result of seawater alteration.

The strong enrichments in Ba and Pb and, in the case of the most isotopically extreme sample (MD34-D5), relative depletions in Zr and Hf, are suggestive of the addition of a subduction or continental component to the sources of these lavas. Ba and Pb enrichments and high field strength element depletions are characteristic of many arc lavas, as well as mean continental crust, pelagic clays and some types of metasomatized peridotite xenoliths from the continental lithospheric mantle (e.g. Rudnick & Fountain, 1995; Plank & Langmuir, 1998; Grégoire *et al.*, 2003).

42–47°E: heterogeneous MORB

This portion of the ridge, extending from the Discovery II to the Indomed fracture zones, was only sparsely sampled by the PROTEA 5 and *Marion Dufresne* 34 cruises, but the recovered samples span a wide geochemical range. They include incompatible element-depleted normal MORB, relatively undepleted transitional MORB and incompatible element-enriched (E-type) MORB [e.g. Nb/La = 0·8–1·4; Nb/Zr = 0·02 to 0·23; $(La/Sm)_N = 0·63–3·14$; Fig. 2h]. The E-MORB samples come from a single on-axis dredge (PROTEA 5 dredge 37) near 46°E, just west of the Indomed fracture zone and far from any known intraplate volcanic features. These samples display incompatible element patterns with negative slopes from Ba to Lu and mild positive Nb anomalies. The most enriched of these, P37-1, a mildly fractionated, nepheline-normative basalt, has an incompatible element pattern similar to that of average ocean island basalt (OIB) (Sun & McDonough, 1989). Also from this region is the sample MD34-D4, which has, along with positive Ba and Pb

anomalies (Fig. 2h), a remarkably radiogenic Hf isotope composition (Chauvel & Blichert-Toft, 2001).

Hafnium isotope characteristics of central SWIR MORB

Hafnium isotope data for 30 central SWIR MORB samples investigated in this study are presented in Table 3 together with their Sr, Nd and Pb isotopic compositions. The data span a wide range of $^{176}Hf/^{177}Hf$ values (0·28279–0·28327; $\varepsilon_{Hf} = +0·6$ to $+17·7$) encompassing the values of most OIB and MORB (e.g. Salters, 1996; Chauvel & Blichert-Toft, 2001). Plotted vs longitude (Fig. 4), ε_{Hf} values display a roughly linear gradient from about +10 in the west to about +17 in the east of the study area, punctuated by localized regions of low ε_{Hf} at 13–15°E, 39–41°E, and 46°E. This pattern is similar to that observed for Nd isotopes, which show a gradual eastward increase in ε_{Nd} (from approximately +7·5 to +10; Mahoney *et al.*, 1992), although the gradient in Hf isotopes is significantly greater relative to the total range of variation. The trend of ε_{Hf} vs longitude is essentially the inverse of that for $^{206}Pb/^{204}Pb$ with the major exception of the 39–41°E segment, which produced MORB having both unradiogenic $^{206}Pb/^{204}Pb$ and $^{176}Hf/^{177}Hf$ ratios. No systematic gradient is present in $^{87}Sr/^{86}Sr$ values, but the three regions characterized by anomalously unradiogenic Hf are also characterized by radiogenic $^{87}Sr/^{86}Sr$.

As with Nd isotope compositions (Fig. 5), Hf isotope compositions of central SWIR MORB correlate negatively with both $^{87}Sr/^{86}Sr$ and $^{206}Pb/^{204}Pb$ (Fig. 6). However, the ε_{Hf} values correlate markedly worse with $^{87}Sr/^{86}Sr$ ($r^2 = 0·55$ vs 0·78) and better with $^{206}Pb/^{204}Pb$ ($r^2 = 0·79$ vs 0·39, if the 39–41°E samples are excluded) than do ε_{Nd} values for the same samples. The relatively poor correlation of ε_{Hf} with $^{87}Sr/^{86}Sr$ is due to the fact that the data form two elongated, roughly parallel groupings in $^{87}Sr/^{86}Sr$–ε_{Hf} space (Fig. 6a), composed of samples from 13 to 26°E and 32 to 47°E, that are vertically offset from each other by ~5 ε_{Hf} units. No such clear separation is apparent in the plot of $^{87}Sr/^{86}Sr$ vs ε_{Nd} (Fig. 5a). The good correlation of ε_{Hf} with $^{206}Pb/^{204}Pb$ (apart from the 39–41°E samples) is due to the strong, nearly linear east–west gradients in both of these isotopic tracers (Fig. 6b). In contrast, the milder and less well-defined east–west gradient in Nd isotope composition yields a flatter overall slope and a large spread in $^{206}Pb/^{204}Pb$ ratios (17·8–19·0) at intermediate ε_{Nd} values of +7 to +9 (Fig. 5b), resulting in a relatively poor correlation.

Like nearly all data for oceanic basalts, the central SWIR MORB samples investigated fall within 5 ε_{Hf} units of the 'Nd–Hf mantle array' line on a plot of ε_{Nd} vs ε_{Hf} (Fig. 7). This line is the linear regression through the oceanic basalt Nd–Hf isotope dataset, defined by the equation $\varepsilon_{Hf} = 1·33 \times \varepsilon_{Nd} + 3·19$ (Vervoort *et al.*, 1999). Small, regionally coherent deviations from this line do occur. As in the plot of $^{87}Sr/^{86}Sr$ vs ε_{Hf} (Fig. 6a), samples from the western (13–26°E) and eastern (32–47°E) regions have systematically lower and higher ε_{Hf} values, respectively, for a given ε_{Nd} value. Whereas samples from the western region fall below the Nd–Hf mantle array line by 1–4 ε_{Hf} units, those from the eastern region fall either near or above this line (i.e. between 1 ε_{Hf} unit below and 3 ε_{Hf} units above this line). Sample MD34-D4 from 43°E (Chauvel & Blichert-Toft; 2001) has the highest ε_{Hf} value (+21) reported for an Indian Ocean MORB outside the Australian–Antarctic Discordance (AAD; see Hanan *et al.*, 2004) and plots 6·7 ε_{Hf} units above the Nd–Hf mantle array (Fig. 7).

The Nd–Hf isotopic data arrays for the 13–26°E and 32–47°E regions have slopes of 1·30 ($r^2 = 0·85$) and 1·17 ($r^2 = 0·88$), respectively, that vary only slightly from each other and that of the Nd–Hf mantle array line (1·33; Vervoort *et al.*, 1999). Without the 39–41°E segment data (which exert a strong control on the slope), the remaining samples from 32 to 47°E form a shallower but less coherent array with a slope of 0·99 ($r^2 = 0·54$).

The large ranges in Hf isotope composition (6–10 ε_{Hf} units) of SWIR MORB at both relatively depleted and enriched Sr and Nd isotope compositions (i.e. at $^{87}Sr/^{86}Sr < 0·7027$ and $> 0·7035$, respectively, and $\varepsilon_{Nd} > +8$ and $< +5$, respectively) suggests the presence of multiple depleted, as well as enriched mantle source components beneath the central SWIR, each with a distinct time-integrated decoupling of Lu/Hf from Sm/Nd relative to compositions lying on the Nd–Hf isotopic mantle array line. A useful way to constrain the isotopic and trace element characteristics of these end-members is to determine whether the variability in Hf isotope ratios of SWIR MORB at a given Nd isotopic composition varies systematically with other isotopic and trace element ratios. This can be accomplished through the use of the parameter $\Delta\varepsilon_{Hf}$ (Johnson & Beard, 1993), which is defined as the vertical displacement of a given sample in ε_{Hf} units from the Nd–Hf isotopic mantle array line. Across the study area, $\Delta\varepsilon_{Hf}$ displays a roughly linear increase with longitude (Fig. 8). Figures 9 and 10 illustrate that the $\Delta\varepsilon_{Hf}$ values of most samples (apart from those from 13 to 15°E and 39 to 41°E) correlate weakly to very well with $^{87}Sr/^{86}Sr$, $^{206}Pb/^{204}Pb$, $\Delta 7/4$ and $\Delta 8/4$ and some trace element ratios, such as Ba/Nb and Ba/Th. Interestingly, most data from other Indian Ocean ridges lie on or near these same correlation trends (Salters, 1996; Chauvel & Blichert-Toft, 2001), indicating that the processes responsible for decoupling Lu/Hf from Sm/Nd affect other isotope and trace element ratios in a similar fashion throughout the Indian Ocean mantle domain. Significantly, samples from the 39–41°E 'Dupal'

Table 3: Hf, Sr, Nd and Pb isotope ratios of mid-ocean ridge basalts from the central SWIR

Sample	Long. (°E)	$^{176}Hf/^{177}Hf$	$2\sigma_m$	ε_{Hf}	$\Delta\varepsilon_{Hf}$	$^{87}Sr/^{86}Sr$	$^{143}Nd/^{144}Nd$	ε_{Nd}	$^{206}Pb/^{204}Pb$	$^{207}Pb/^{204}Pb$	$^{208}Pb/^{204}Pb$
PS4-6-2[a]	13·13	0·283100	9	11·6	−1·1	0·70290	0·513004	7·1	18·741	15·551	38·541
PS4-4-101[a]	14·12	0·282901	13	4·6	−4·2	0·70368	0·512852	4·2	19·564	15·649	39·157
PS4-3-14[a]	14·50	0·282963	7	6·8	−1·6	0·70352	0·512837	3·9	19·254	15·642	39·305
PS4-2-1[a]	14·63	0·283002	8	8·1	−1·2	0·70338	0·512876	4·6	19·243	15·632	39·315
AG22-1-1[b]	16·98	0·283078	9	10·8	−3·2	0·70248	0·513056	8·2	19·045	15·557	38·554
AG22-3-4	19·10	0·283069	6	10·5	−3·3	0·70267	0·513048	8·0	18·968	15·551	38·767
AG22-9-2[b]	22·20	0·283120	10	12·3	−2·9	0·70256	0·513101	9·0	18·418	15·492	37·965
AG22-8-1	24·76	0·283120	7	12·3	−2·4	0·70268	0·513082	8·7	18·417	15·500	38·012
P14-81[b]	25·32	0·283116	10	12·2	−2·9	0·70253	0·513096	8·9	18·246	15·481	37·841
P14-89[b]	25·32	0·283149	8	13·3	1·1	0·70374	0·512986	6·8	18·608	15·600	38·496
P14-90[b]	25·32	0·283138	9	12·9	0·5	0·70387	0·512995	7·0	18·616	15·605	38·503
P11-17[b]	25·49	0·283137	7	12·9	−1·2	0·70258	0·513058	8·2	18·458	15·485	38·049
P12-12[b]	25·51	0·283148	10	13·3	−1·1	0·70259	0·513070	8·4	18·568	15·561	38·265
P9-1G[b]	26·34	0·283102	8	11·7	−2·1	0·70255	0·513046	8·0	18·339	15·478	37·987
P15-54[b]	32·16	0·283184	10	14·6	0·9	0·70318	0·513040	7·8	18·138	15·473	37·950
P17-22[b]	33·52	0·283199	8	15·1	1·0	0·70303	0·513060	8·2	18·118	15·501	37·870
AG53-3-3[b]	34·07	0·283164	8	13·9	−1·0	0·70276	0·513089	8·8	18·223	15·469	37·781
P25-211[b]	35·85	0·283162	7	13·8	−0·4	0·70291	0·513062	8·3	18·271	15·484	37·977
P25-217[b]	35·85	0·283227	8	16·1	−0·4	0·70268	0·513151	10·0	18·052	15·473	37·694
MD34-D6[b]	38·80	0·283215	12	15·7	1·5	0·70288	0·513060	8·2	18·366	15·503	38·066
P27-2[b]	39·31	0·282949	9	6·3	1·5	0·70440	0·512697	1·2	17·449	15·505	37·706
P28-9[b]	39·86	0·283022	7	8·8	1·8	0·70399	0·512785	2·9	17·152	15·418	37·318
P28-26[b]	39·86	0·283050	7	9·8	2·2	0·70410	0·512808	3·3	17·083	15·414	37·296
MD34-D5[b]	40·65	0·282792	7	0·7	2·7	0·70488	0·512437	−3·9	16·867	15·470	37·249
MD34-D5dup	40·65	0·282786	10	0·5	2·5						
P29-34[b]	41·90	0·283260	9	17·3	−0·9	0·70258	0·513213	11·2	17·859	15·436	37·418
P30-75[b]	41·99	0·283273	8	17·7	0·3	0·70268	0·513188	10·7	17·829	15·448	37·486
P37-1[b]	45·76	0·283018	8	8·7	1·7	0·70383	0·512785	2·9	18·351	15·544	38·644
P37-2[b]	45·76	0·283158	6	13·7	1·3	0·70325	0·512992	6·9	18·040	15·469	38·160
P41-49	46·63	0·283203	8	15·2	2·8	0·70289	0·512995	7·0	18·058	15·502	38·107
P42-11	46·72	0·283211	8	15·5	2·3	0·70321	0·513025	7·5	18·179	15·495	37·972

Sr, Nd and Pb isotope data for samples shown with superscripts are from: [a]le Roex *et al.* (1992) and [b]Mahoney *et al.* (1992). Other Sr, Nd and Pb isotope data are from this study. Sample MD34-D5dup is a duplicate analysis of MD34-D5. In-run uncertainties in $^{176}Hf/^{177}Hf$ pertain to last significant figures. Epsilon values (ε_{Hf} and ε_{Nd}) were calculated using $^{176}Hf/^{177}Hf_{CHUR} = 0{\cdot}282772$ (Blichert-Toft & Albarède, 1997) and $^{143}Nd/^{144}Nd_{CHUR} = 0{\cdot}512638$. $\Delta\varepsilon_{Hf}$ values were calculated using the equation $\Delta\varepsilon_{Hf} = \varepsilon_{Hf} - (1{\cdot}33\varepsilon_{Nd} + 3{\cdot}19)$ (Vervoort *et al.*, 1999). (See text for analytical details.)

JOURNAL OF PETROLOGY VOLUME 46 NUMBER 12 DECEMBER 2005

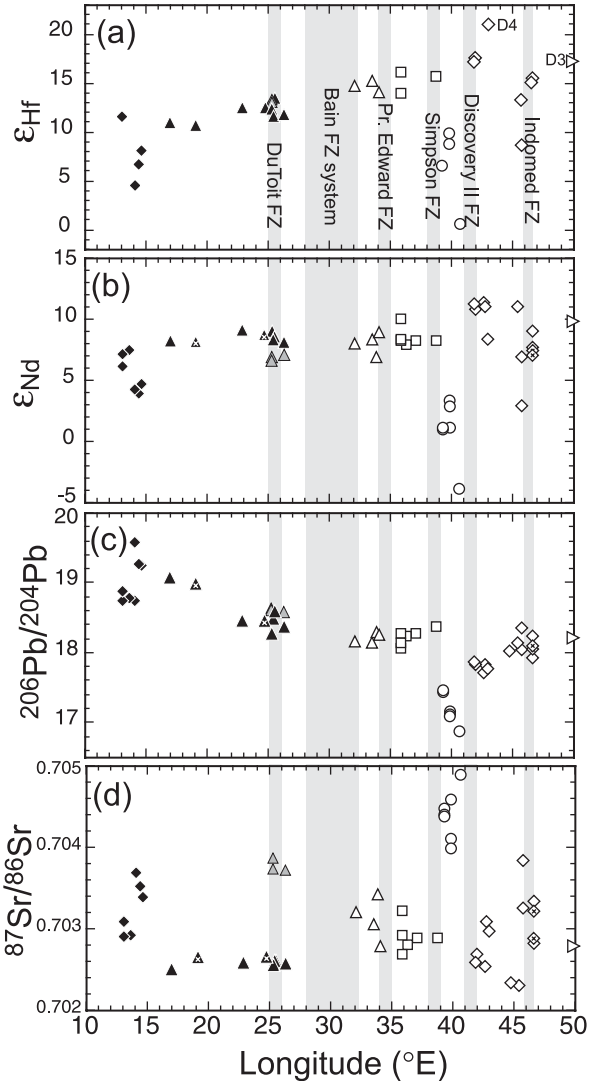

Fig. 4. Plots of longitude vs (a) ε_{Hf}, (b) ε_{Nd}, (c) $^{206}Pb/^{204}Pb$ and (d) $^{87}Sr/^{86}Sr$ isotope ratios for the central SWIR. Sample symbols are the same as in Fig. 3. D3 and D4 indicate Hf isotope compositions for samples MD34-D3 and MD34-D4, respectively, from Chauvel & Blichert-Toft (2001). ×, New Sr, Nd and Pb data from this study. Other Sr, Nd and Pb isotope data are from Hamelin & Allègre (1985), Mahoney *et al.* (1989, 1992) and le Roex *et al.* (1992).

segment constitute vectors in these figures that are strongly oblique to the main data arrays.

Hafnium isotope characteristics of intraplate samples

Hf, and supplementary Sr, Nd and Pb isotope ratios were determined for basalts and hawaiites from Bouvet, Marion and Prince Edward Islands, volcanic islands presumably marking the present location of the Bouvet and Marion hotspots, as well as for Cretaceous alkali basalt and basanite dikes from southern Madagascar (Table 4). The age and location of the latter suggests that they are the products of Cretaceous activity of the Marion hotspot. They also have strong Sr, Nd and Pb isotopic similarities to 39–41°E SWIR MORB (Mahoney *et al.*, 1991).

In Nd–Hf isotope space (Fig. 7), the Bouvet samples fall slightly below the mantle array and within the field for St. Helena OIB (Salters & White, 1998), consistent with its moderate HIMU Sr–Nd–Pb isotope signature (e.g. Sun, 1980). The Marion and Prince Edward Island lavas also fall below the mantle array, but at higher ε_{Nd} values intermediate between St. Helena OIB and Atlantic–Pacific MORB. Interestingly, three samples analyzed from the 10–16°E oblique-spreading segment of the SWIR have Nd–Hf (as well as Sr and Pb) isotopic compositions similar to lavas from Bouvet Island, even though these MORB samples were emplaced over 600 km to the east. In contrast, MORB from the 36–39°E segment of the SWIR, emplaced less than 250 km from Marion and Prince Edward Islands, show little to no Nd–Hf isotopic similarity to OIB from these islands and lie at significantly higher ε_{Nd} and ε_{Hf} values (Fig. 7).

The alkaline Ejeda–Bekily dike samples analyzed are part of the 88 Ma Madagascar large igneous province (LIP; Mahoney *et al.*, 1991; Dostal *et al.*, 1992). The Madagascar LIP encompasses tholeiitic and alkalic lava sequences and dikes emplaced mainly in the eastern and western coastal regions of Madagascar, and the adjacent submarine Madagascar Plateau, a large basaltic edifice extending south of the island (Storey *et al.*, 1998). This igneous province lies along the Late Cretaceous trace of the Marion hotspot (Hartnady & le Roex, 1985) and a significant portion of the lavas bear an isotopic resemblance to those of Marion Island (Mahoney *et al.*, 1991; Storey *et al.*, 1998). The Ejeda–Bekily dikes of southern Madagascar are composed of relatively primitive alkali basalts and basanites that are notable for having radiogenic Sr and unradiogenic Nd and Pb isotope ratios approaching or matching those of MORB from the 39–41°E 'Dupal' segment of the SWIR (e.g. $\varepsilon_{Nd} \geq -2{\cdot}5$, $^{206}Pb/^{204}Pb \geq 17{\cdot}4$; Mahoney *et al.*, 1991). Like these unusual MORB, the dike samples tend to have high ε_{Hf} for their relatively unradiogenic Nd isotope compositions ($\varepsilon_{Hf} = +0{\cdot}3$ to $+9{\cdot}9$, $\Delta\varepsilon_{Hf} = +0{\cdot}4$ to $+3{\cdot}5$; Fig. 7).

DISCUSSION AND CONCLUSIONS

The Hf isotope and trace element data presented above allow us to place new constraints on the mineralogy, composition and origin of mantle sources present beneath the central SWIR. We use these data in the discussion below to address four questions. First, do the Sm–Nd and Lu–Hf isotope systematics of central SWIR MORB indicate that garnet pyroxenite was a regionally important source component in their genesis, as has been recently inferred for MORB from the western SWIR

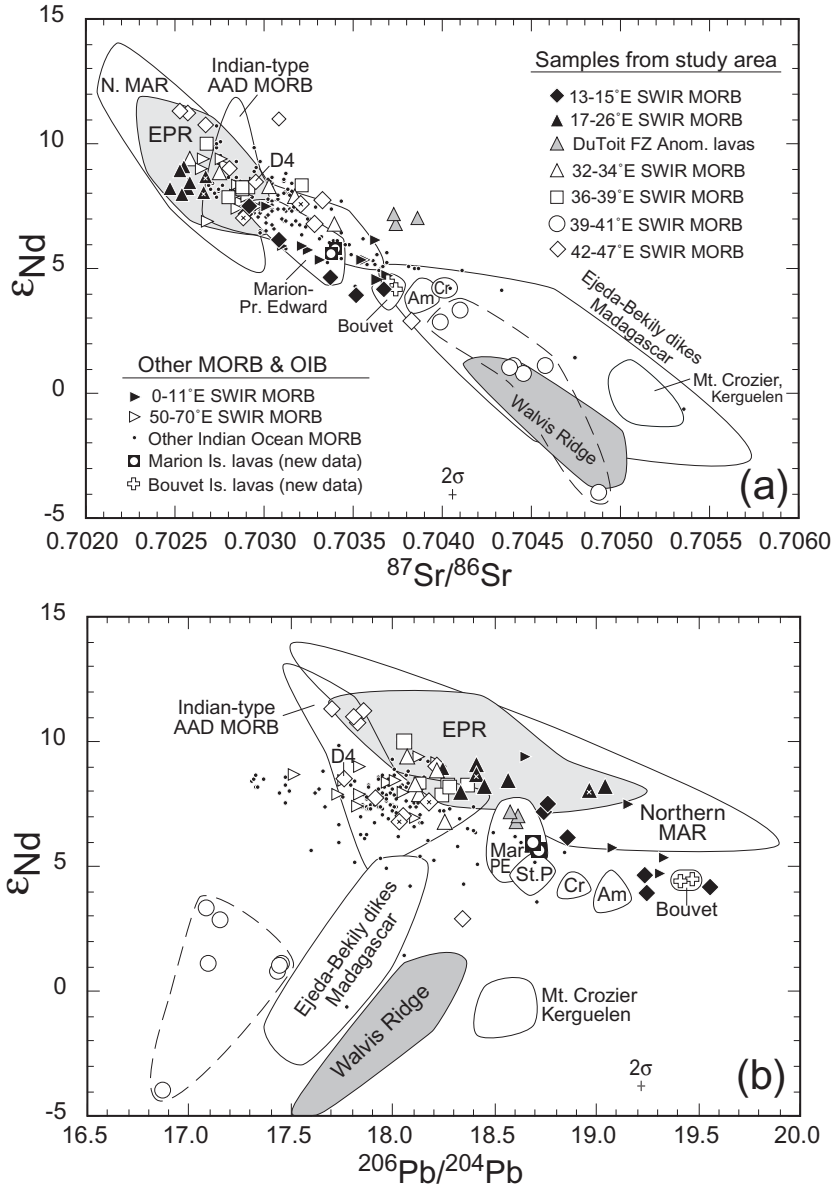

Fig. 5. Plots of ε_{Nd} vs (a) $^{87}Sr/^{86}Sr$ and (b) $^{206}Pb/^{204}Pb$ for SWIR MORB and other Indian Ocean MORB and OIB. Plotted Indian Ocean MORB data are from le Roex *et al.* (1983, 1992), Hamelin & Allègre (1985), Michard *et al.* (1986), Price *et al.* (1986), Dosso *et al.* (1988), Mahoney *et al.* (1989, 1992, 2002) and Rehkämper & Hofmann (1997). ×, New MORB isotope data from this study. Data sources for MORB and OIB fields are too numerous to list. Data field for Ejeda–Bekily dikes (Madagascar) are from Mahoney *et al.* (1991). Lavas from Mt. Crozier (Kerguelen Archipelago) are believed to most closely approximate the present composition of the Kerguelen plume source (Mattielli *et al.*, 2002). Am, Cr, Mar-PE and St.P stand for Amsterdam, Crozet, Marion–Prince Edward and St. Paul Islands, respectively. N.MAR, northern Mid-Atlantic Ridge; EPR, East Pacific Rise; AAD, Australian–Antarctic Discordance. Analytical uncertainties shown are for data collected in this study.

(Salters & Dick, 2002)? Second, what is the most likely origin of the extreme geochemical signature expressed by MORB from 39 to 41°E? Third, what are the regionally important mantle source components responsible for the main isotopic variations of central SWIR MORB? Fourth, what constraints do Hf isotope data place on the origin of the distinct isotopic characteristics of Indian Ocean MORB?

Constraints on the role of garnet pyroxenite as a melt source in central SWIR MORB

An apparent inconsistency exists between the relatively shallow depths of magma generation necessary to produce the observed thickness of oceanic crust (typically 5–7 km) as inferred from major element-based melting models (e.g. Klein & Langmuir, 1987; Niu & Batiza,

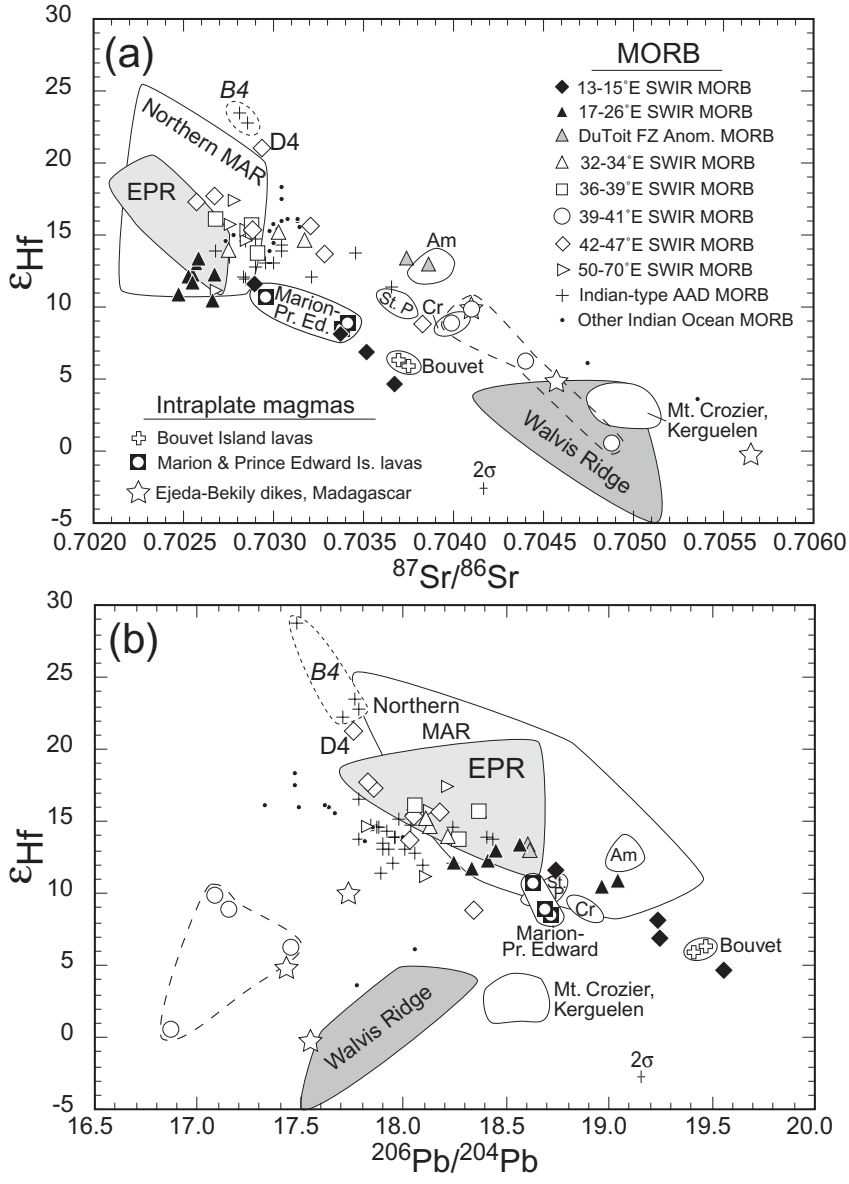

Fig. 6. Plots of ε_{Hf} vs (a) $^{87}Sr/^{86}Sr$ and (b) $^{206}Pb/^{204}Pb$ for SWIR MORB and other Indian Ocean MORB and OIB. MORB data sources are as in Fig. 5 and also from Salters (1996), Nowell *et al.* (1998), Chauvel & Blichert-Toft (2001), Kempton *et al.* (2002) (on-axis samples only) and Hanan *et al.* (2004). The four AAD MORB symbols outlined in the dashed field are isotopically extreme samples from zone B4 of the AAD (Hanan *et al.*, 2004). D4 indicates sample MD34-D4 from Chauvel & Blichert-Toft (2001). Data sources for ocean island and Madagascar samples are from Mahoney *et al.* (1991), Salters & Hart (1991), Salters & White (1998), Mattielli *et al.* (2002) and Doucet *et al.* (2004). Abbreviations are as in Fig. 5. Uncertainties shown are for data collected in this study.

1991) and the apparent requirement from trace element and isotope constraints (e.g. Salters & Hart, 1989; Bourdon *et al.*, 1996) that significant amounts of MORB melting has occurred in the presence of garnet. This has prompted the hypothesis that pods or veins of highly fertile garnet pyroxenite are widespread in the upper mantle (e.g. Hirschmann & Stolper, 1996). Garnet in such pyroxenite veins would probably be stable to depths significantly shallower than the top of the garnet stability field in peridotite (~70 km; O'Neill, 1981) and, because garnet pyroxenite has a lower solidus temperature than peridotite, these veins should contribute disproportionately to melts generated during MORB genesis (Perterman & Hirschmann, 2003). Although some recent studies of clinopyroxene partitioning (e.g. Blundy *et al.*, 1998) and trace element variations (Chauvel & Blichert-Toft, 2001) have suggested that garnet need not be involved in the genesis of most MORB, this contention

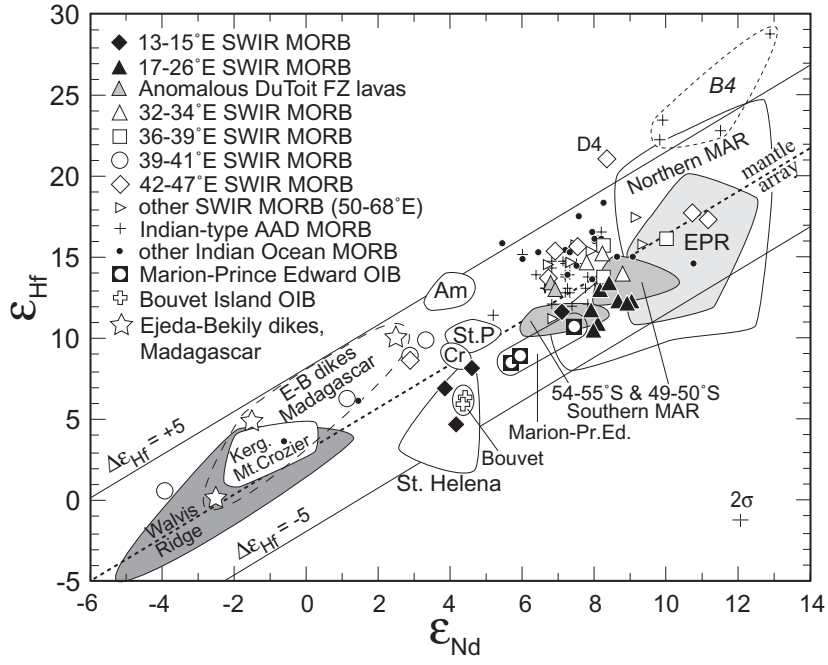

Fig. 7. Plot of ε_{Nd} vs ε_{Hf} showing data for SWIR MORB, other Indian Ocean MORB and OIB. Data sources and abbreviations are as in Figs 5 and 6, with the addition of Andres *et al.* (2002) for the southern MAR. The dashed line labeled 'mantle array' represents the regression line of Vervoort *et al.* (1999) through all Nd and Hf isotope data for oceanic basalts ($\varepsilon_{Hf} = 1{\cdot}33\varepsilon_{Nd} + 3{\cdot}19$). The lines labeled '$\Delta\varepsilon_{Hf} = +5$' and '$\Delta\varepsilon_{Hf} = -5$' are offset 5 ε_{Hf} units above and below the Nd–Hf mantle array line, respectively. Uncertainties shown are for data collected in this study.

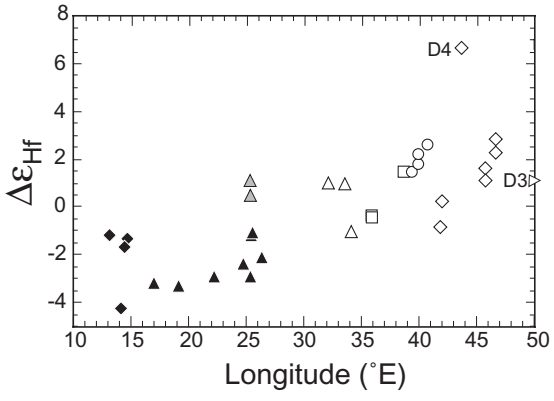

Fig. 8. Diagram of longitude vs $\Delta\varepsilon_{Hf}$. Symbols are as in Figs 3–7. The roughly linear increase in $\Delta\varepsilon_{Hf}$ from west to east should be noted. D3 and D4 indicate samples MD34-D3 and MD34-D4 from Chauvel & Blichert-Toft (2001).

remains hotly debated (e.g. Salters & Longhi, 1999; Salters *et al.*, 2002). Nevertheless, the notion of an upper mantle veined with garnet pyroxenite is an intriguing and frequently explored hypothesis for both the origin of the apparent garnet signature in MORB and as a source of compositional heterogeneity in the upper mantle (e.g. Lassiter *et al.*, 2000; Le Roux *et al.*, 2002*b*; Salters & Dick, 2002).

If garnet pyroxenite does indeed contribute a melt component during MORB genesis, then one might expect this component to be least diluted in lavas erupted at deep, ultra-slow-spreading centers such as the SWIR, the Mid-Cayman Rise, American–Antarctic Ridge and the Gakkel Ridge. Both the mean degree and rate of melting at such ridges are low, as indicated by lava chemistry and low crustal thickness (Bown & White, 1994; Robinson *et al.*, 1996). Because of the lower solidus temperatures of pyroxenite relative to peridotite (e.g. Hirschmann & Stolper, 1996) melting at an ultra-slow-spreading center should generate melts with a larger contribution from a garnet pyroxenite component (if present), than melting beneath a faster-spreading center.

Globally, N-MORB from ultra-slow-spreading centers tend to have slightly greater depletions in HREE relative to MREE than N-MORB from slow- to fast-spreading ridges [with $(Tb/Yb)_N$ means of $1{\cdot}22 \pm 0{\cdot}06$ and $1{\cdot}08 \pm 0{\cdot}11$ (1σ), respectively, excluding enriched samples with $(La/Sm)_N > 1$; le Roex *et al.*, 1985; Price *et al.*, 1986; Mühe *et al.*, 1993, 1997; Elthon *et al.*, 1995; Müller *et al.*, 1997; Lamont PETDB petrological database]. Although this difference is not statistically significant, it may indicate that MORB from ultra-slow-spreading centers received a greater contribution from melts of garnet-bearing mantle lithologies than MORB from faster-spreading ridges. Because melting is believed to commence at

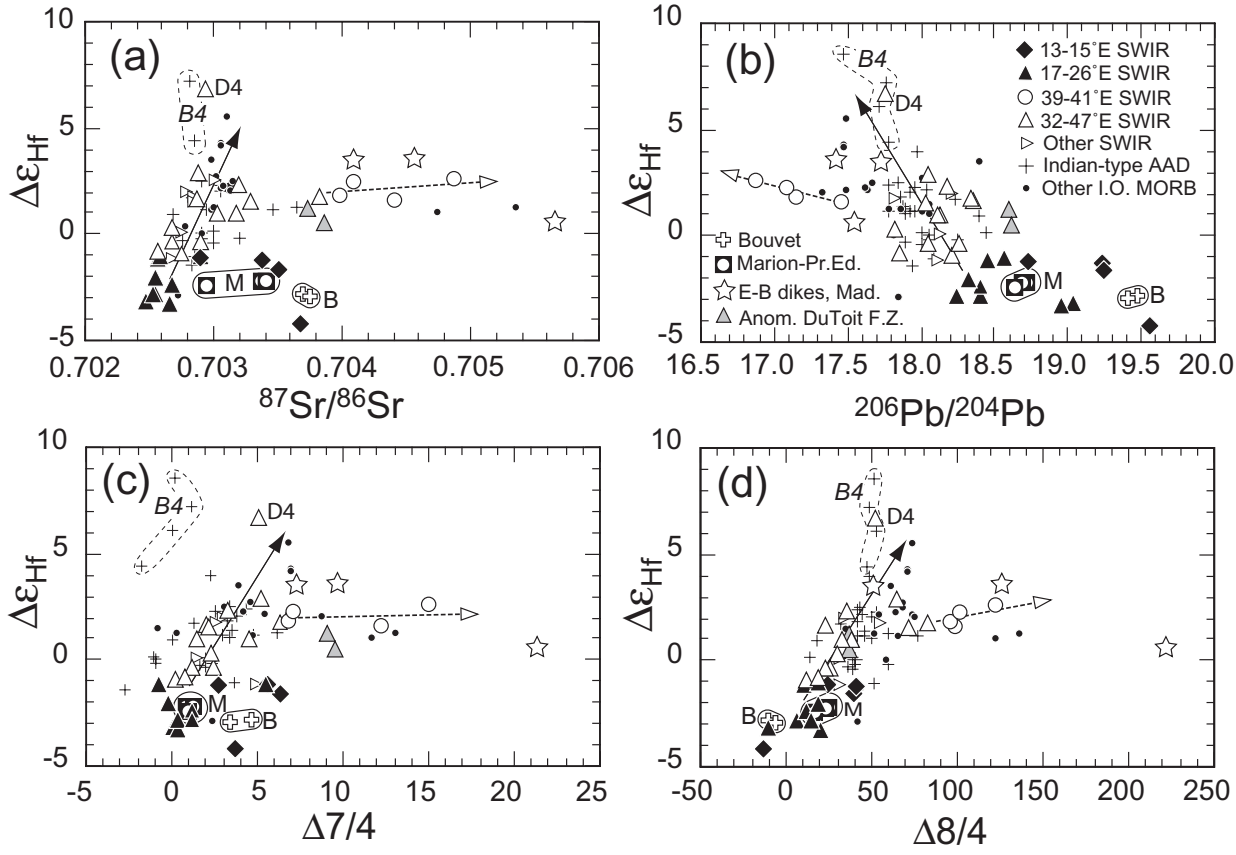

Fig. 9. Plots of (a) $^{87}Sr/^{86}Sr$, (b) $^{206}Pb/^{204}Pb$, (c) Δ7/4 and (d) Δ8/4, all vs $\Delta\varepsilon_{Hf}$. Data sources are as in Figs 5 and 6. M and B indicate Marion–Prince Edward and Bouvet Islands, respectively. Other abbreviations are as in Fig. 7. Continuous-line and dashed arrows indicate data arrays defined by 32–47°E and 39–41°E SWIR MORB, respectively. In particular, the good correlations between $\Delta\varepsilon_{Hf}$ and $^{87}Sr/^{86}Sr$, Δ7/4 and Δ8/4, and the similarities between 39–41°E MORB and the Ejeda–Bekily dike samples, should be noted.

relatively shallow depths beneath these deep spreading centers (Klein & Langmuir, 1987), the apparent garnet signature in the REE patterns of basalts from ultra-slow-spreading ridges would be consistent with the presence of shallow garnet pyroxenite veins in the underlying mantle.

The $^{176}Hf/^{177}Hf$ and $^{143}Nd/^{144}Nd$ ratios of MORB allow us to estimate the time-integrated Lu/Hf and Sm/Nd ratios of each sample's source. This information, combined with measured Lu/Hf and Sm/Nd ratios, makes it possible to calculate the extent of fractionation of Lu/Hf and Sm/Nd between source and melt. These fractionations are termed $\delta_{(Lu/Hf)}$ and $\delta_{(Sm/Nd)}$, and are defined as

$$\delta_{(Lu/Hf)} = (^{176}Lu/^{177}Hf_{source} - {}^{176}Lu/^{176}Hf_{sample})/(^{176}Lu/^{177}Hf_{source}) \quad (1)$$

with $\delta_{(Sm/Nd)}$ being similarly defined. The term $^{176}Lu/^{177}Lu_{source}$ is determined as the $^{176}Lu/^{177}Hf$ value on a mantle isochron (formed by fractionating a chondritic reservoir at 2 Ga) that corresponds to the sample's $^{176}Hf/^{177}Hf$ ratio (Salters & Hart, 1989). The choice of a 2 Ga age for the MORB source in this formulation is not critical: the use of an older or younger age would affect the absolute, but not the relative values of $\delta_{(Lu/Hf)}$ and $\delta_{(Sm/Nd)}$.

Garnet fractionates Lu from Hf to a much greater extent than Sm from Nd (e.g. Irving & Frey, 1978). Therefore, garnet pyroxenite, which typically has substantially higher garnet modes than suboceanic garnet lherzolite (e.g. Bodinier *et al.*, 1987), should yield melts having compositions falling near the low end of the range of Lu/Hf ratios measured in MORB. Garnet pyroxenite melts should also record significantly larger $\delta_{(Lu/Hf)}$ values relative to a given $\delta_{(Sm/Nd)}$ than other MORB (i.e. show a significantly greater decrease in Lu/Hf for a given decrease in Sm/Nd during melting; Hirschmann & Stolper, 1996).

Contrary to these expectations, the central SWIR lavas analyzed (excluding samples that are obviously the product of isotopically anomalous mantle sources, i.e. those

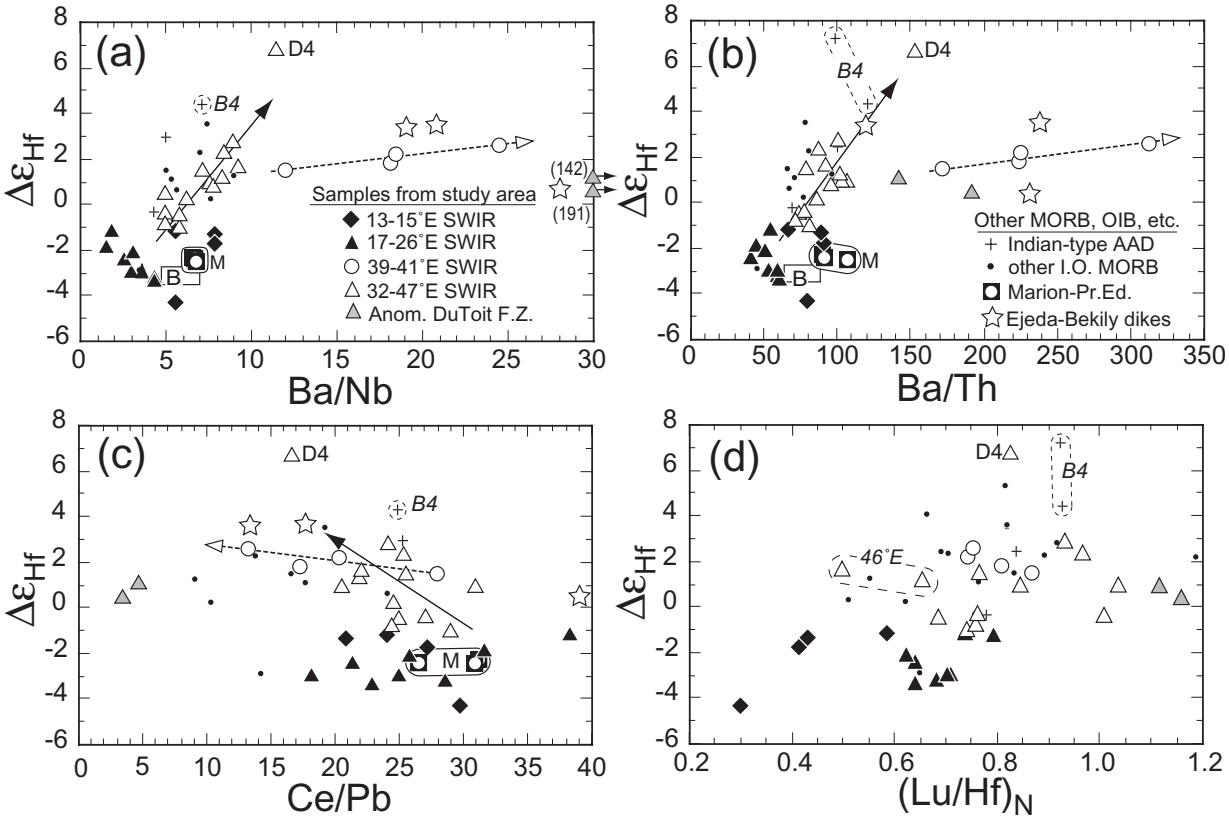

Fig. 10. Plots of (a) Ba/Nb, (b) Ba/Th, (c) Ce/Pb and (d) $(Lu/Hf)_N$, all vs $\Delta\varepsilon_{Hf}$. In particular, the excellent correlations between $\Delta\varepsilon_{Hf}$ and Ba/Nb and Ba/Th ratios should be noted. Data sources and abbreviations are as in Fig. 9, with the addition of Pyle *et al.* (1995).

from 13 to 15°E, 39 to 41°E, and 46°E) display a range of Lu/Hf values similar to that of MORB from the Atlantic and Pacific Oceans (Fig. 11). On the plot of $^{176}Lu/^{177}Hf$ vs $^{176}Hf/^{177}Hf$ (Fig. 11a) and $\delta_{(Lu/Hf)}$ vs $\delta_{(Sm/Nd)}$ (Fig. 11b) all but two of these 'normal' SWIR samples lie within the fields defined by data for MORB from the East Pacific Rise (EPR) and northern Mid-Atlantic Ridge (MAR; Salters, 1996; Nowell *et al.*, 1998). More significantly, none of these samples have $\delta_{(Lu/Hf)}$ or $\delta_{(Sm/Nd)}$ values that fall significantly above the 40% contour (of Salters & Hart, 1989) for the percentage of melting occurring in the garnet stability field. This suggests that they have had even less contribution of melt from garnet-bearing lithologies than many samples from the northern MAR.

The fact that the central SWIR lavas record relatively small Lu/Hf fractionations during melting, and have $\delta_{(Lu/Hf)}$ and $\delta_{(Sm/Nd)}$ values very similar to that of MORB from the EPR (which has substantially higher rates and mean degrees of melting), argues against an origin for the garnet signature in most SWIR lavas from shallow melting of garnet pyroxenite veins. Rather, it suggests that, like EPR MORB, these lavas were generated by melting that began within the field of garnet stability in peridotite. A pyroxenitic source component is more plausible for MORB from 13 to 15°E on the obliquely spreading section of the SWIR, which have both low Lu/Hf and particularly high $\delta_{(Lu/Hf)}$ for their $\delta_{(Sm/Nd)}$ values, most of which fall above the 40% contour for the percentage of melting in the presence of garnet (Fig. 11). Indeed, Salters & Dick (2002) found independent evidence for a garnet pyroxenite component in this region as a result of the lack of overlap in Nd isotopic composition and REE concentrations between peridotites (or calculated equilibrium melts of peridotites) and basalts from this segment. In contrast, the relatively high $^{176}Lu/^{177}Hf$ ratios (for their low $^{176}Hf/^{177}Hf$ ratios) and low $\delta_{(Lu/Hf)}$ and $\delta_{(Sm/Nd)}$ values for 39–41°E MORB appear to be inconsistent with a major source contribution from garnet pyroxenite.

A full discussion of how the low degrees of melting, thin crust (<4 km, Dick *et al.*, 2003) and relatively great depths of melt generation inferred for the SWIR can be reconciled is outside the scope of this paper. However, we note that N-MORB from the central SWIR are characterized by lower Si_8/Fe_8 ratios (Si_8 and Fe_8 are SiO_2 and FeO

Table 4: Hf, Sr, Nd, and Pb isotope data for western Indian Ocean island basalts and alkaline dikes from Madagascar

Sample	Age	$^{176}Hf/^{177}Hf$	$2\sigma_m$	$^{176}Hf/^{177}Hf_i$	$\varepsilon_{Hf}(t)$	$\Delta\varepsilon_{Hf}$	$^{87}Sr/^{86}Sr$	$^{143}Nd/^{144}Nd$	$\varepsilon_{Nd}(t)$	$^{206}Pb/^{204}Pb$	$^{207}Pb/^{204}Pb$	$^{208}Pb/^{204}Pb$
Marion Island												
MAR-11	0	0·283013	12		8·5	−2·2	0·70338	0·512928	5·7	18·715	15·529	38·509
MAR-12	0	0·283022	9		8·8	−2·3	0·70341	0·512944	6·0	18·688	15·529	38·471
Prince Edward Island												
PREI-13[a]	0	0·283073	12		10·6	−2·4	0·70295	0·513018	7·4	18·633	15·521	38·328
Bouvet Island												
WJM-2B	0	0·282948	12		6·2	−2·9	0·70370	0·512865	4·4	19·479	15·65	39·086
WJM-16B	0	0·282939	14		5·9	−3·1	0·70376	0·512861	4·4	19·418	15·631	39·050
Ejeda–Bekily dikes, Madagascar												
MAD-8[b]	90 Ma	0·283026	16	0·282994	9·9	3·4	0·70410		2·5	17·735	15·487	37·588
MAD-10[b]	90 Ma	0·282881	15	0·282847	4·7	3·5	0·70458		−1·5	17·429	15·478	37·963
MAD-52[b]	90 Ma	0·282761	18	0·282722	0·3	0·4	0·70566		−2·5	17·550	15·608	39·071

In-run uncertainties apply to last significant figures. Hf isotope ratios for the Ejeda–Bekily dikes were age-corrected using Lu and Hf concentrations of Dostal *et al*. (1992). ε_{Hf} values were calculated assuming $^{176}Lu/^{177}Hf$ and $^{176}Hf/^{177}Hf$ values of 0·0332 and 0·282772, respectively, for CHUR (Blichert-Toft & Albarède, 1997). Sr, Nd and Pb data for samples shown with superscripts are from [a]Mahoney *et al*. (1992) and [b]Mahoney *et al*. (1991). Major and trace element data for the Bouvet and Madagascar samples have been given by le Roex & Erlank (1982) and Dostal *et al*. (1992).

contents corrected for fractionation to 8 wt % MgO) than are typical for MORB from other ultra-slow-spreading centers (∼5 for the SWIR vs ∼6–7 for the American–Antarctic Ridge and Mid-Cayman Rise; le Roex *et al*., 1985, 1989; Elthon *et al*., 1995; Robinson *et al*., 1996), which are indicative of higher mean pressures of melting (Niu & Batiza, 1991). The extremely high degree of tectonic segmentation of most of the central SWIR may have resulted in unusually effective conductive cooling of the uppermost mantle, deepening the top of the mantle melting column beneath the SWIR (e.g. Bown & White, 1994). If mantle melting beneath ultra-slow-spreading ridges does typically commence within the garnet stability field (even slightly below the garnet–spinel transition), the suppression of melting in the upper part of the spinel stability field, normally the interval of highest melt productivity beneath spreading centers (Asimow *et al*., 1997), would result in a higher than normal proportion of melting occurring in the garnet stability field. MORB from this environment might have proportions of melts derived from garnet and spinel lherzolite similar to that of MORB produced at more vigorous, faster-spreading ridges, where the melting interval both starts at greater depth and ends at shallower depth than beneath the central SWIR. Comparisons of the $\delta_{(Lu/Hf)}$ and $\delta_{(Sm/Nd)}$ values of the central SWIR lavas with those of MORB from less segmented ultra-slow ridges, such as the Gakkel Ridge (which are not yet available), would be useful for testing this hypothesis.

The origin of 39–41°E MORB signature

The extremely unradiogenic Nd and Pb isotopic compositions of MORB from the 39–41°E segment require that their source contain a time-integrated LREE-enriched, low μ ($^{238}U/^{204}Pb$) component. On the basis of depleted mantle Nd model ages for these samples, which provide only minimum age constraints, this enriched component must have been isolated from the convecting mantle for at least 1·5 Gyr. Several different origins have been proposed to explain the extreme isotopic signature of the 39–41°E segment lavas. These include contamination of the upper mantle by (1) one or more mantle plumes in the region (e.g. Mahoney *et al*., 1989, 1992), (2) focused recycling into the upper mantle of ancient recycled pelagic sediments (Hamelin & Allègre, 1985; le Roex *et al*., 1989), (3) disrupted or delaminated ancient continental lithospheric mantle (Hamelin & Allègre, 1985; Mahoney *et al*., 1989, 1992) or (4) lower continental crust (Escrig *et al*., 2004). These hypotheses are not necessarily mutually exclusive, as mantle plumes are widely considered to be a likely agency of both disruption of continental lithosphere and transport of ancient, deeply recycled pelagic sediments into the upper mantle (e.g. Storey, 1995; Blichert-Toft *et al*., 1999).

The new trace element and Hf isotope data presented here offer the opportunity to place tighter constraints on the origin of the 39–41°E MORB source. More broadly, it is important to identify the exotic component responsible for the extreme isotopic composition of 39–41°E

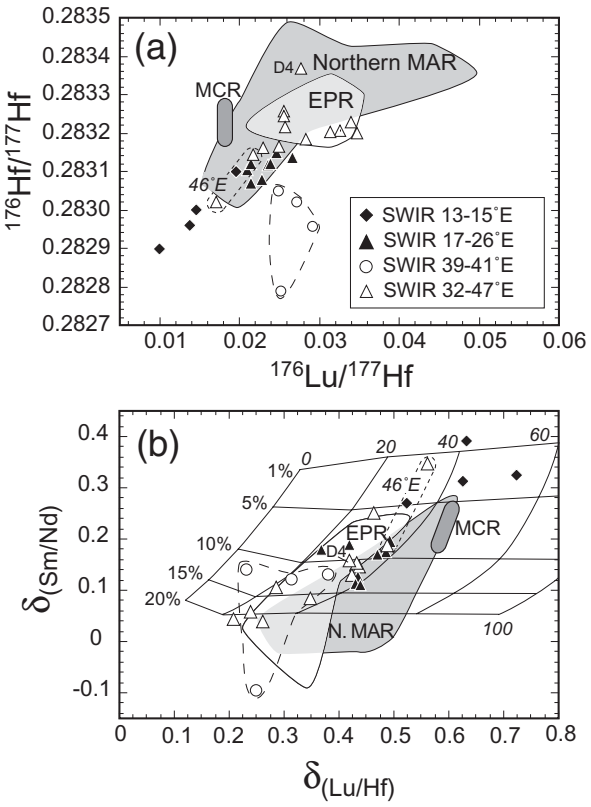

Fig. 11. (a) Plot of $^{176}Lu/^{177}Hf$ vs $^{176}Hf/^{177}Hf$ ratios and (b) $\delta_{(Lu/Hf)}$ vs $\delta_{(Sm/Nd)}$ values for SWIR MORB. Data sources are as in Figs 5–7. The melting grid in (b) is from Salters & Hart (1989) and shows the degree of melting on the subhorizontal grid lines and the percentage of melting in the garnet peridotite stability field on the subvertical grid lines, according to their melting model. It should be noted that all SWIR MORB, except those with long-term incompatible element enrichment (i.e. from 13–15°E, 39–41°E and 46°E) overlap or fall very near the fields for North Atlantic and Pacific MORB. MCR, Mid-Cayman Rise.

MORB because each of the candidate materials mentioned above has also been proposed to be responsible for the distinct isotopic signature of the Indian Ocean mantle domain as a whole (Storey *et al.*, 1989; Mahoney *et al.*, 1992; Weis & Frey, 1996; Rehkämper & Hofmann, 1997; Chauvel & Blichert-Toft, 2001; Escrig *et al.*, 2004; Hanan *et al.*, 2004). Establishing that one or more of these exotic materials was involved in producing the localized MORB signature at 39–41°E would make the involvement of that or similar materials in the entire Indian Ocean mantle domain more credible.

The isotopic signature of the 39–41°E MORB is unlikely to be wholly due to direct contamination by mantle plumes. The Nd and Pb isotopic compositions of basalts generated by all Indian Ocean plumes (e.g. Reunion, Marion, Crozet, Amsterdam–St. Paul and Kerguelen) are simply too radiogenic to account for the isotopic characteristics of these MORB (Mahoney *et al.*, 1992). The location of the 39–41°E segment adjacent to the trace of the Marion hotspot does suggest, however, that the Marion plume may have played an important indirect role in mixing the enriched 'DUPAL' component into the local asthenosphere.

Over 1–2 Gyr, subducted pelagic sediments should evolve highly radiogenic $^{87}Sr/^{86}Sr$ and strongly unradiogenic Nd and Pb isotope ratios (e.g. Ben Othman *et al.*, 1989; Rehkamper & Hofmann, 1997), making them plausible as the material responsible for the 'DUPAL' isotope signature of 39–41°E MORB. Because they are deficient in zircon (a major host of Hf in the continental crust), pelagic marine sediments also tend to have low Sm/Nd and relatively high Lu/Hf, which results in decoupled unradiogenic $^{143}Nd/^{144}Nd$ and relatively radiogenic $^{176}Hf/^{177}Hf$ ratios with time (e.g. Patchett *et al.*, 1984; Vervoort *et al.*, 1999). The addition of such material to the sources of oceanic basalts causes their compositions to plot off the mantle array toward low ε_{Nd} values, resulting in ε_{Nd}–ε_{Hf} arrays displaced above the mantle array (e.g. Blichert-Toft *et al.*, 1999), similar to that observed for the 39–41°E segment lavas.

Significant differences in the incompatible element compositions of pelagic sediment and 39–41° MORB, however, indicate a problem with ancient pelagic sediments as the 'DUPAL' component present at 39–41°E. Although the the 39–41°E MORB are characterized by relative enrichments in Ba and Pb, qualitatively similar to pelagic and global subducting sediment, these MORB are also characterized by pronounced depletions in U and Th relative to elements of similar incompatibility such as Nb and La. This results in 39–41°E MORB having Nb/U ratios similar to those of the depleted mantle (39–68). Pelagic sediments and altered oceanic crust, in contrast, are typically enriched in U and have low Nb/U ratios (typically 5–10; Staudigel *et al.*, 1996; Plank & Langmuir, 1998). It is clear from a plot of Nb/U vs La/Th (Fig. 12) that mixtures of subducting sediment and altered oceanic crust cannot explain the trace element ratios of 39–41°E MORB. Moreover, the maximum contribution that subducting sediments could have made to the mantle sources of these MORB is very small, <0·1%. Thus, pelagic sediments do not provide an adequate explanation for the geochemical features of 39–41°E MORB.

Ancient metasomatized continental lithospheric mantle and lower continental crust are both plausible source materials for isotopically anomalous oceanic basalts in the South Atlantic and Indian Oceans (Hamelin & Allègre, 1985; Mahoney *et al.*, 1989, 1992; Milner & le Roex, 1996; Douglass *et al.*, 1999; Kamenetsky *et al.*, 2001). Isotopic studies of peridotite xenoliths from Archean cratons and lower crustal granulite xenoliths from Archean and Proterozoic terranes in the Gondwanan continents have shown that both of these materials may have sufficiently unradiogenic $^{143}Nd/^{144}Nd$ and

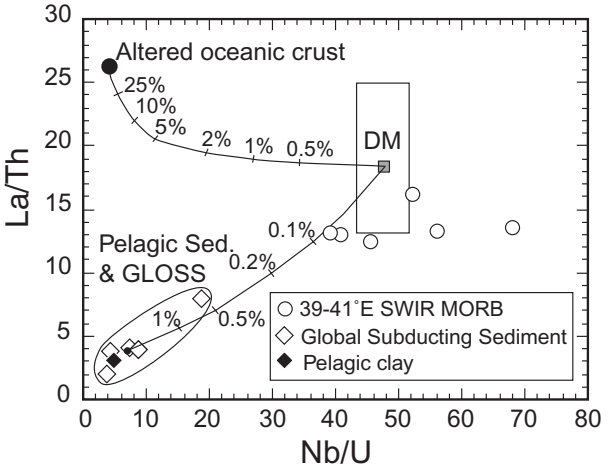

Fig. 12. Nb/U vs La/Th for 39–41°E SWIR MORB, showing mixing curves between depleted mantle [DM; showing the range of depleted mantle estimates from Jacobsen (1999), Salters & Stracke (2004) and Workman & Hart (2005)], pelagic sediments [subducting sediment compositions of Plank & Langmuir (1998) and pelagic clay composition of Taylor & McClennan (1985)] and altered oceanic crust ['super' composite of Staudigel *et al.* (1996)]. It should be noted that the high Nb/U ratios of 39–41°E MORB do not permit a significant contribution from either pelagic sediments or altered oceanic crust to their sources.

$^{206}Pb/^{204}Pb$ ratios and sufficiently high Δ7/4, Δ8/4 and $^{87}Sr/^{86}Sr$ values to explain the isotope composition of 39–41°E SWIR MORB via mixing with depleted MORB-source mantle (e.g. Menzies & Murthy, 1980; Cohen *et al.*, 1984; Rudnick *et al.*, 1986; Walker *et al.*, 1989; Huang *et al.*, 1995; Vervoort *et al.*, 2000). In contrast, mantle xenoliths from Proterozoic and younger continental terranes do not typically have sufficiently extreme Nd and Pb isotope compositions to constitute a credible mixing end-member for these lavas (e.g. McDonough & McCulloch, 1987; Lee *et al.*, 1996; Carlson *et al.*, 2004).

Distinguishing between ancient continental lithospheric mantle and lower continental crustal contamination of oceanic basalt sources has proven to be difficult and remains the subject of considerable controversy (e.g. Milner & le Roex, 1996; Douglass *et al.*, 1999; Hanan *et al.*, 2004), as these materials can have similar Sr, Nd and Pb isotope compositions (Cohen *et al.*, 1984; Rudnick *et al.*, 1986). Much of the isotopic variablility in kimberlite-borne cratonic peroditite xenoliths (constituting the vast majority of Archean peridotites analyzed), particularly in Pb isotope composition, may be due to infiltration of the xenolith by the host kimberlite (which compromises bulk analyses; Grégoire *et al.*, 2003) or precipitation of metasomatic clinopyroxene by kimberlitic magmas shortly before eruption (Simon *et al.*, 2003). These complications have made it very difficult to estimate the mean isotopic composition of cratonic Gondwanan lithospheric mantle.

Fortunately, recent trace element and isotopic studies have provided improved constraints on the incompatible element and isotopic composition of southern African cratonic lithospheric mantle and Precambrian lower crust. Grégoire *et al.* (2003) have presented an extensive set of *in situ* trace element data, obtained via laser ablation-ICPMS, of phases in a suite of representative peridotite xenoliths from the Archean Kaapvaal Craton of southern Africa. These data allow calculation of the bulk compositions of Archean southern African peridotites for a large suite of incompatible elements, free of contamination by the host kimberlite. The trace element patterns of these peridotites fall into two categories suggestive of different metasomatic agents or processes. Type 1 peridotites, as defined by Grégoire *et al.* (2003), display fairly smooth trace element patterns, similar to what might be expected for metasomatism by silicate melts derived by moderate degrees of melting of a depleted asthenospheric source. Type 2 peridotites have some characteristics in common with the 39–41°E SWIR lavas, including strong relative enrichments in Ba and the LREE, depletions in U, Th, Hf, Zr and Ti (Fig. 13) and relatively high $(Lu/Hf)_N/(Sm/Nd)_N$ ratios (mean = 1·4), all of which may be attributable to metasomatism by a volatile-rich melt or fluid (Grégoire *et al.*, 2003).

New high-precision whole-rock trace element concentration data have also been presented recently for a suite of southern African lower crustal granulite xenoliths (Schmitz *et al.*, 2004; M. D. Schmitz, unpublished data, 2004). These data indicate that each of three mineralogically defined granulite types (mafic, felsic and sedimentary) is also characterized by distinct incompatible element compositions (Fig. 13a). Felsic and sedimentary granulites have roughly similar incompatible element patterns, with strong enrichments in Ba, Th, U and Pb and sharp depletions in Nb. Mafic granulites show similarities to the 39–41°E MORB in that they have enrichments in Ba but depletions in Th and U, and are generally without Nb anomalies. Like the type 2 peridotities, the mafic granulites also have high $(Lu/Hf)_N/(Sm/Nd)_N$ ratios (mean = 1·6).

We have carried out mixing–melting models to determine how well mixtures of depleted MORB-source mantle with southern African lower crust or metasomatized cratonic peridotite can approximate the incompatible element compositions of SWIR MORB from 39 to 41°E. In these simple models, compositions were calculated for bulk mixtures of depleted mantle (Workman & Hart, 2005) with the mean compositions of each of the two types of metasomatized southern African peridotite (Grégoire *et al.*, 2003; Table 5) or each of the three types of southern African lower crustal granulite (Schmitz *et al.*, 2004; M. D. Schmitz, unpublished data, 2004; Table 5). Non-modal partial melt compositions of these mixed source compositions were then calculated and compared

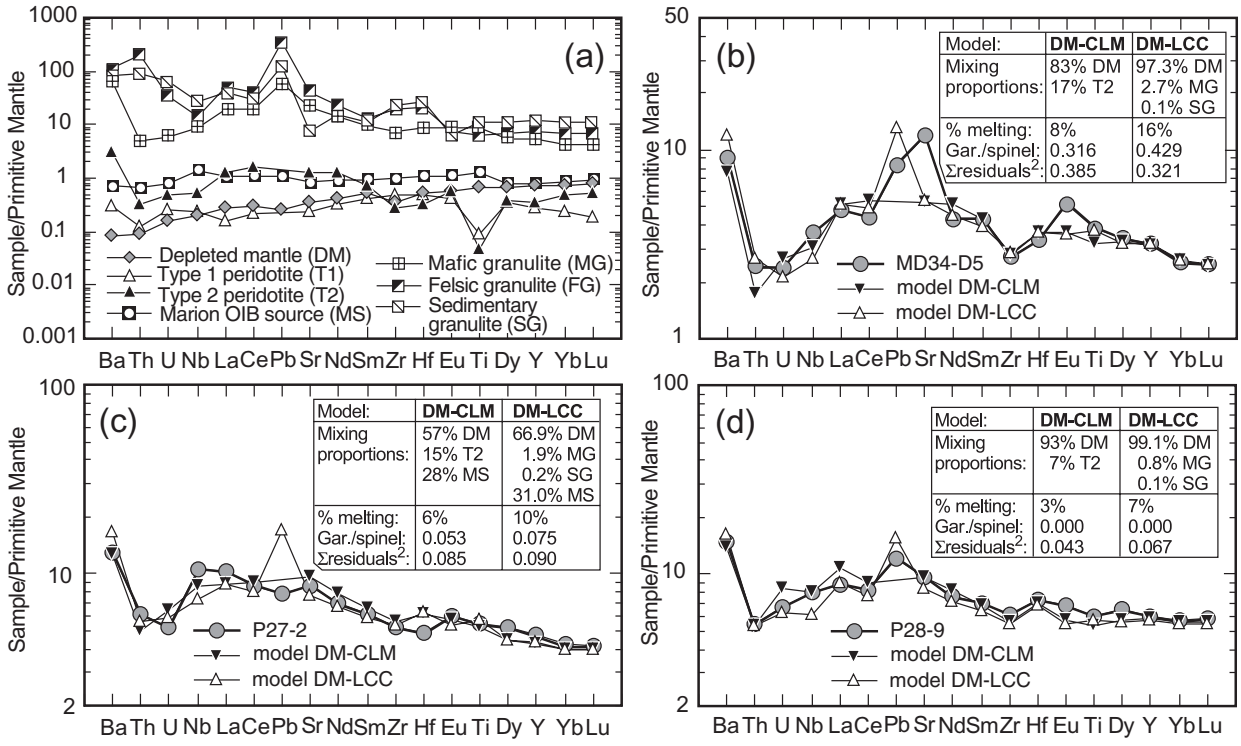

Fig. 13. Primitive mantle-normalized incompatible element diagrams showing (a) incompatible element patterns of potential mantle and crustal source materials of the 39–41°E SWIR MORB (see Table 5 for compositions and data sources), and incompatible element patterns of samples and mixing–melting forward model output for samples (b) MD34-D5, (c) P27-1 and (d) P28-9. Mixing–melting models attempt to simulate the incompatible element abundances of these samples by mixing depleted mantle with metasomatized cratonic peridotite or lower crustal granulite and subjecting the mixture to batch partial melting. The tables in (b)–(d) show the optimized free parameters: the types and proportions of mixing end-members used, the percentage of batch partial melting and the garnet/spinel ratio in the mixture undergoing melting. Partition coefficients, modes and melt contributions used for mantle phases are given in Table 6. The sum of residuals squared indicates the goodness of fit of the models, a perfect match having a value of zero. (See text for description of modeling procedure.)

with the incompatible element abundances of each of the three most primitive MORB samples from 39 to 41°E (i.e. MD34-D5, P27-2 and P28-9; Fig. 13b, c and d). The free parameters in these models are the mixing proportions of the various source materials, the degree of partial melting and the spinel/garnet ratio in the source. Fixed parameters are the modal and melt contribution proportions for olivine, orthopyroxene, clinopyroxene and spinel + garnet and the trace element partition coefficients (Table 6). For one sample that displays trace element evidence suggesting contamination by Marion plume material (sample P27-2, with a slight positive Nb anomaly), we also included a Marion plume source composition (see Table 5 legend for explanation) as a possible mixing component in the models. Residuals, representing the difference between the concentration generated by the model and that of the sample's measured concentration, were calculated for each element using the following equation:

$$R_i = C_{m,i}/C_{s,i} - 1 \quad (2)$$

where R_i is the residual for element i, $C_{m,i}$ is the concentration of element i calculated by the model and $C_{s,i}$ is the concentration of element i in the sample. Simulation of the incompatible element abundances of each of the three samples was performed for mixtures of depleted mantle with metasomatized peridotite and lower crustal granulite, respectively, by iteratively tuning the free parameters of the model to minimize the sum of the square of the residuals. Residuals for all elements were given a weighting value of one, except for Sr and Eu, which were given values of 0·5 because some samples appear to have experienced plagioclase accumulation or fractionation. Because Pb concentrations were not measured by Grégoire *et al.* (2003) in many peridotite phases, Pb is not included in the residual calculations for the depleted mantle-metasomatized peridotite models, nor (to keep the comparisons on an equal basis) for the depleted mantle–lower crustal models, although it is shown in Fig. 13 for illustrative purposes.

Our simple modeling shows that melts of mixtures of depleted mantle with between 7 and 18 wt %

Table 5: Elemental and isotopic compositions of model components used in this paper

	Depleted mantle end-member[a]	Type 1 peridotite[b]	Type 2 peridotite[b]	Mafic granulite[c]	Sedimentary granulite[c]	Felsic granulite[c]	Marion source[d]	Mean depleted mantle[e]	Mean global subducted sediment[f]	Fluid from subducted sediment[g]	Pelagic sediment $t = 1{\cdot}5$ Ga[h]	Pelagic sediment $t = 0$ Ga[i]
Ba (ppm)	0·563	2	21	444	574	797	5·2					
Th (ppm)	0·0079	0·005	0·027	0·42	7·9	17	0·058					
U (ppm)	0·0032	0·005	0·010	0·12	1·3	0·73	0·017					
Nb (ppm)	0·149	0·17	0·38	6·1	18·9	10·3	1·0					
La (ppm)	0·192	0·11	0·91	13·7	27·1	35·3	0·72					
Ce (ppm)	0·550	0·37	2·9	34·2	52·0	69·6	1·9					
Pb (ppm)	0·018			4·4	8·8	25·2	0·08					
Sr (ppm)	7·66	4·5	27	433	160	862	18	11·3	327	301		
Nd (ppm)	0·581	0·42	1·7	19·7	21·3	30·5	1·2	0·951	27	21·6		
Sm (ppm)	0·239	0·17	0·32	4·39	4·98	5·69	0·41	0·348	5·8	3·01		
Zr (ppm)	5·08	6·9	3·9	101	325	269	13·7					
Hf (ppm)	0·157	0·15	0·10	2·61	8·05	6·62	0·34	0·228	4·1	1·62		
Eu (ppm)	0·096	0·068	0·10	1·46	1·05	1·26	0·18					
Ti (wt %)	0·141	0·020	0·010	1·86	2·51	1·41	0·27					
Dy (ppm)	0·505	0·26	0·28	4·05	8·28	5·22	0·60					
Y (ppm)	3·33	1·2	1·6	24·3	53·6	33·8	3·5					
Yb (ppm)	0·365	0·10	0·25	2·18	5·61	3·32	0·40					
Lu (ppm)	0·058	0·013	0·038	0·32	0·82	0·49	0·069	0·064	0·41	0·33		
$^{87}Rb/^{86}Sr$				0·133				0·022	0·49	0·969		
$^{87}Sr/^{86}Sr$				0·70600				0·70245			0·7074	0·7118
$^{147}Sm/^{144}Nd$				0·142				0·221	0·13	0·085		
$^{143}Nd/^{144}Nd$				0·512022				0·51320			0·51040	0·51218
$^{176}Lu/^{177}Hf$				0·0387				0·038	0·014	0·028		
$^{176}Hf/^{177}Hf$				0·282959				0·28327			0·28163	0·28265

[a]Depleted mantle composition is from Workman & Hart (2005).
[b]Average Type 1 and Type 2 metasomatized peridotite compositions were calculated from the mineral composition and mineral mode data of Grégoire *et al*. (2003).
[c]Mean trace element compositions of southern African mafic, sedimentary and felsic granulite are calculated from the data of Schmitz *et al*. (2004) and M. D. Schmitz (unpublished data, 2004). Mean isotopic composition of mafic granulite is based on data from the previous two sources as well as Huang *et al*. (1995); all data are age-corrected to 150 Ma.
[d]Marion source was calculated from the mean composition of the three Marion and Prince Edward Island lavas presented in Table 2, assuming that this mean represents a 5% batch partial melt of a mantle source with the mineral modes and melting proportions given in Table 6, and a garnet/spinel ratio of one.
[e]Mean depleted mantle composition is based on that of Kempton *et al*. (2002), except that the $^{176}Hf/^{177}Hf$ ratio has been adjusted so that the composition lies on the Nd–Hf mantle array. The difference between the 'depleted mantle end-member' and 'mean depleted mantle' is that the former is an extreme compositional end-member and the latter is meant to be an approximate average composition of the Atlantic–Pacific N-MORB source.
[f]Global subducted sediment composition is from Plank & Langmuir (1998).
[g]Fluid from subducted sediment was calculated from the mobility factors for Rb, Sr, Nd, Sm and Yb measured by Aizawa *et al*. (1999) and assumed that the mobility of Hf (mobility factor not determined) was half of that of Yb.
[h]Pelagic sediment ($t = 1{\cdot}5$ Ga) is from Rehkämper & Hofmann (1997) and Kempton *et al*. (2002).
[i]Pelagic sediment ($t = 0$) composition represents the average composition of modern pelagic sediments reported by Ben Othman *et al*. (1989) and Vervoort *et al*. (1999). Pelagic sediment of all ages is assumed to have the same Rb, Sr, Nd, Sm, Lu and Hf abundances as global subducted sediments.

metasomatized cratonic peridotite (dominantly Type 2 peridotite), or between 1 and 2 wt % lower continental crust (dominantly mafic granulite) can both closely simulate the incompatible element patterns of 39–41°E SWIR MORB. In one case each, metasomatized cratonic peridotite and continental lower crust provide the best fit to a sample's incompatible element pattern (to samples MD34-D5 and P28-9, respectively), and in the third case,

Table 6: Partition coefficients and mineral proportions used in melting models

Element	Olivine	Orthopyroxene	Clinopyroxene	Spinel	Garnet
Ti	0·006[a]	0·024[a]	0·45[b]	0·048[a]	0·69[b]
Rb	0·00018[a]	0·0006[a]	0·011[a]	0·0001	0·0007[a]
Sr	0·00019[a]	0·007[a]	0·067[a]	0·0001	0·01[b]
Y	0·001[c]	0·06[d]	0·738[d]	0·001	2·33[d]
Zr	0·0033[c]	0·036[d]	0·204[d]	0·001	0·499[d]
Nb	0·01[a]	0·002[d]	0·031[d]	0·001	0·015[d]
Ba	0·0001[e]	0·001	0·0058[b]	0·001	0·0007[b]
La	0·0004[d]	0·009[d]	0·08[d]	0·01[a]	0·005[d]
Ce	0·0005[e]	0·005[d]	0·148[d]	0·01[a]	0·012[d]
Nd	0·001[e]	0·014[d]	0·258[d]	0·01[a]	0·091[d]
Sm	0·0014[e]	0·022[d]	0·494[d]	0·01[a]	0·337[d]
Eu	0·0016[e]	0·04[d]	0·60[d]	0·01[a]	0·60[d]
Dy	0·0017[e]	0·06[d]	0·69[d]	0·01[a]	2·0[d]
Yb	0·0015[e]	0·092[d]	0·713[d]	0·01[a]	6·07[d]
Lu	0·0015[e]	0·119[d]	0·718[d]	0·01[a]	7·68[d]
Hf	0·001[a]	0·036[d]	0·344[d]	0·01	0·596[d]
Pb	0·0001[a]	0·001[a]	0·072[f]	0·001	0·0005[a]
Th	0·0001[a]	0·0001[a]	0·006[d]	0·001	0·006[d]
U	0·0001[a]	0·0001[a]	0·007[d]	0·001	0·021[d]
Mineral mode	0·5	0·3	0·12	0·08	
Melt contribution	0·25	0·25	0·36	0·14	

These partition coefficients are used in the melting–mixing models shown in Figs 13 and 18. They are taken and/or interpolated from the following sources: [a]McKenzie & O'Nions (1991); [b]Hauri *et al.* (1994); [c]Salters *et al.* (2002); [d]Salters & Longhi (1999); [e]Beattie (1994); [f]Hart & Dunn (1993). Other partition coefficients were estimated. Mineral mode and melt contribution figures are shown for garnet + spinel, as the garnet/spinel ratio is a free parameter in some models.

both provide roughly equal fits (to sample P27-2). Although the new trace element data do not allow us to exclude either continental lithospheric mantle or lower crust as likely contributors to the source of 39–41°E MORB, our modeling does indicate that addition of either of these materials to the Indian Ocean upper mantle can account for the incompatible element characteristics of these unusual basalts. This strongly supports a role for continental material (crust and/or mantle) in the genesis of the 39–41°E MORB.

An important additional constraint on the possible role of lithospheric peridotite and continental lower crust in the genesis of the 39–41°E MORB is provided by new Nd–Hf isotope data obtained on Gondwanan cratonic peridotites and lower crustal granulite xenoliths. The Nd–Hf isotope compositions of clinopyroxene and garnet mineral separates of southern African cratonic peridotites (Simon *et al.*, 2002; Bedini *et al.*, 2004; Fig. 14) tend to fall well above the Nd–Hf mantle array with mostly positive and extremely variable ε_{Hf} (−5 to +470) and mostly negative ε_{Nd} values. These data indicate that mixtures of metasomatized Archean cratonic mantle with depleted MORB-source mantle could have the strong negative ε_{Nd} and moderate positive $\Delta\varepsilon_{Hf}$ values necessary to account for the 39–41°E MORB samples. However, such mixtures would need to contain a large proportion of the lithospheric mantle component, between roughly 10 and 25%, to explain the Nd isotopic compositions of the 39–41°E samples (assuming Nd concentrations and ε_{Nd} values of 0·9 and 4·0 ppm and +10 and −12 ε units, respectively, for depleted mantle and Archean lithospheric mantle; Bedini *et al.*, 2004).

Nd–Hf isotope data have also recently been reported for lower crustal granulite xenoliths from eastern Australia (Vervoort *et al.*, 2000) and southern Africa (Schmitz *et al.*, 2004). The Australian crustal xenolith data have Nd isotopic compositions ranging between $\varepsilon_{Nd} = +9{\cdot}5$ and −18 and, with the exception of one sample, plot within 8 ε_{Hf} units of the Nd–Hf isotopic mantle array line (mean $\Delta\varepsilon_{Hf} = +2$; Vervoort *et al.*, 2000). The southern African lower crustal xenolith data, which are more relevant to the SWIR given their proximity, are much more isotopically heterogeneous (Fig. 14). These granulite xenoliths span large ranges of present-day Nd and Hf isotopic compositions ($\varepsilon_{Nd} = -25$ to +134, $\varepsilon_{Hf} = -26$ to +38, mean $\Delta\varepsilon_{Hf} = -22$) falling between 45 ε_{Hf} units above and 218 ε_{Hf} units below the mantle array (Schmitz *et al.*, 2004; Fig. 14). Of the three granulite xenolith types defined by Schmitz *et al.* (2004), only the mafic granulites have isotopic compositions that typically plot above the mantle array ($\Delta\varepsilon_{Hf} = -3$ to +45) at unradiogenic Nd isotopic compositions ($\varepsilon_{Nd} = -7$ to −12; Fig. 14). Thus, mixtures of depleted mantle with 5–10% of continental lower crust can also explain the Nd and Hf isotopic composition of 39–41°E samples, but only if this material was dominantly composed of mafic granulite (Schmitz *et al.*, 2004).

One piece of evidence that appears to support the involvement of lithospheric mantle over lower continental crust in the genesis of the 39–41°E samples is their isotopic resemblance to the Ejeda–Bekily dikes from southern Madagascar (Mahoney *et al.*, 1991). These alkalic and basanitic dikes are relatively unfractionated and show little to no major or trace element evidence for crustal contamination (Dostal *et al.*, 1992). On the basis of their incompatible element and isotopic compositions (including their isotopic dissimilarity to Marion hotspot lavas), the Ejeda–Bekily dikes have been interpreted by Mahoney *et al.* (1991) and Storey *et al.* (1998) to represent melts of Archean or Early Proterozoic Madagascan lithospheric mantle. The dikes and the 39–41°E SWIR lavas have similar Hf isotopic compositions, both falling above the mantle array in Nd–Hf isotope space (Fig. 7), and the

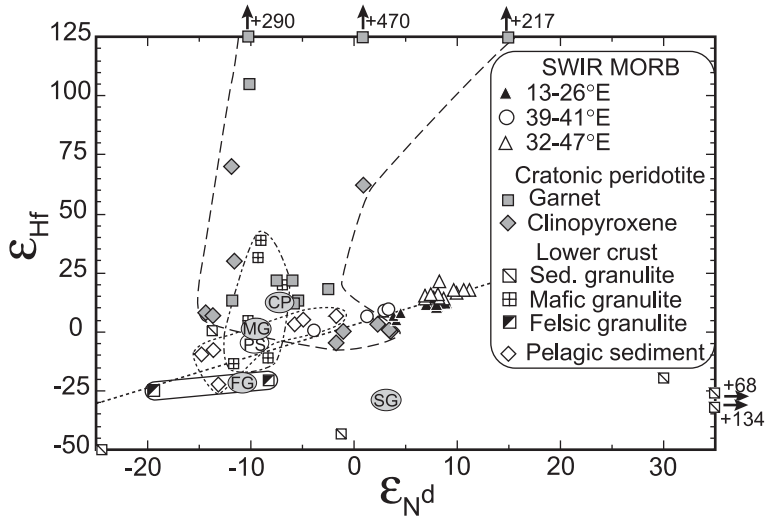

Fig. 14. Nd–Hf isotope diagram showing the compositions of clinopyroxene and garnet mineral separates from Archean southern African cratonic peridotites (Simon *et al.*, 2002; Bedini *et al.*, 2004), southern African lower crustal granulite xenoliths (Schmitz *et al.*, 2004), pelagic sediments (Ben Othman *et al.*, 1989; Vervoort *et al.*, 1999) and 13–47°E central SWIR MORB (including MD34-D4; Chauvel & Blichert-Toft, 2001). Ovals labeled CP, MG, FG, SG and PS indicate the mean ε_{Nd} and ε_{Hf} values of cratonic perioditite, mafic, felsic and sedimentary granulite and pelagic sediments, respectively, weighted by sample Nd and Hf contents.

dike samples plot closely to the 39–41°E MORB trends in most diagrams of $\Delta\varepsilon_{Hf}$ vs isotope and trace element ratios (Figs 9 and 10). The resemblance in isotope and trace element ratios between the Ejeda–Bekily dikes and 39–41°E SWIR MORB strongly suggests that both shared similar mantle sources. Because these silica-undersaturated dikes have major and trace element compositions consistent with being derived from an enriched continental lithospheric mantle source (Storey *et al.*, 1998) their strong isotopic resemblance to 39–41°E MORB would therefore seem to support a major role for continental lithospheric mantle in the sources of these MORB as well.

Escrig *et al.* (2004) came to a different conclusion and inferred that lower continental crust, rather than continental lithospheric mantle, was the most plausible contaminant responsible for the extreme isotope compositions of the 39–41°E MORB. This inference was based on measurement of a radiogenic $^{187}Os/^{188}Os$ ratio (~0·335) in sample MD34-D5, the most isotopically extreme of the 39–41°E MORB samples. Although such a radiogenic Os isotope composition would indeed argue for a source dominated by a crustal, rather than a mantle component, the amount of crust needed to reach this radiogenic an Os isotopic composition is extremely large (>50%), given possible Re and Os concentrations and Os isotopic composition estimates for lower crust and MORB-source peridotite. Assuming $^{187}Os/^{188}Os$ values of 0·80 and 0·129 and Os concentrations of 0·1 and 2 ppb for lower continental crust and MORB-source mantle, respectively (Meisel *et al.*, 1996; Saal *et al.*, 1998), it would require a mixture with nearly 90% lower crust to explain the Os isotope composition of sample MD34-D5. It seems unlikely that a source that contained such a large amount of crustal material could produce a basalt with the major and trace element composition of this sample. An alternative possibility is that this sample is contaminated by seawater Os, which is very radiogenic (Williams & Turekian, 2004), and, given the low Os concentration of this and most other MORB (6 ppt Os for MD34-D5; Escrig *et al.*, 2004), is a significant concern with Os isotope measurements in MORB.

A small but non-trivial portion of the continental rifting that dispersed central Gondwana occurred within Archean cratonic lithosphere (in East Antarctica, southern Africa, Madagascar and Southern India; e.g. Groenewald *et al.*, 1991; Tucker *et al.*, 1999; Fig. 15). If it can be assumed that the mantle portion of this lithosphere had chemical and isotopic traits similar to that of South African cratonic peroditite, then the separation and mixing of portions of this lithospheric mantle into the adjacent asthenosphere (probably via thermal erosion by the Marion mantle plume; Mahoney *et al.*, 1992; Storey *et al.*, 1998) appears to offer the simplest explanation for the geochemical signature of 39–41°E MORB and its location adjacent to the trace of the Marion hotspot.

Distribution of depleted components beneath the SWIR

Two main isotopic components dominate the Sr, Nd and Pb isotopic compositions of N-MORB from the

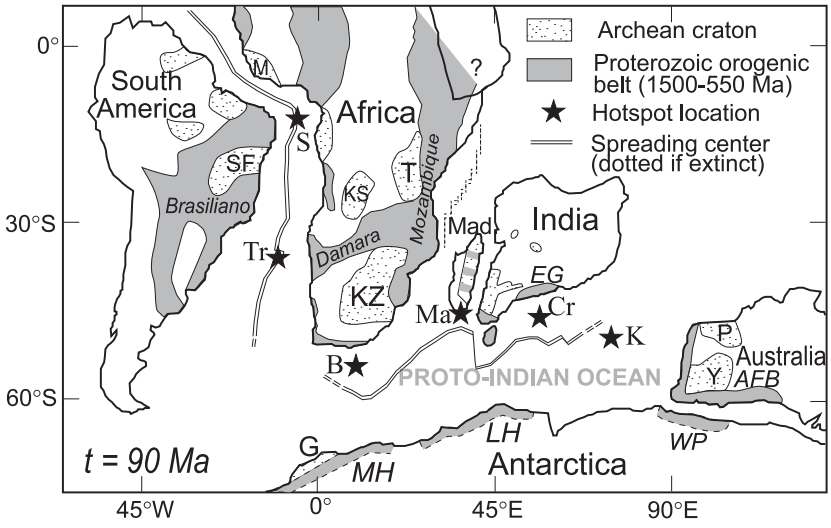

Fig. 15. Simplified tectonic map of the Gondwana continents at 90 Ma showing the distribution of Archean cratons, Meso- and Neoproterozic orogenic belts and hotspot locations. AFB, Albany–Fraser Belt; B, Bouvet hotspot; Cr, Crozet hotspot; EG, Eastern Ghats province; G, Grunehogna craton; K, Kerguelen hotspot; KS, Kasai craton; KZ, Kaapvaal–Zimbabwe craton; LH, Lützow–Holm Bay province; M, Man craton; Ma, Marion hotspot; Mad., Madagascar; MH, Maudheim province; P, Pilbara craton; S, Saint Helena hotspot; SF, São Francisco craton; T, Tanzanian craton; Tr, Tristan hotspot, WP, Wilkes province; Y, Yilgarn craton. Map was compiled using Scotese (2004) as a base map. Craton and orogenic belt boundaries are from Bernasconi (1983), Grunow *et al.* (1996), Haggerty (1999), Tucker *et al.* (1999), Meert (2003), and Hanson (2003). Hotspot locations are from Storey (1995) and Storey *et al.* (1998). The alternating gray and stippled pattern on Madagascar indicates that this area is underlain by Archean crust, but has been superimposed by Neoproterozoic arc magmatism (Handke *et al.*, 1999). It should be noted that Proterozoic orogenic belts nearly surround the proto-Indian Ocean basin.

central SWIR (Mahoney *et al.*, 1992). One, an Atlantic–Pacific-type N-MORB-source component, characterized by moderately radiogenic $^{206}Pb/^{204}Pb$, low Δ7/4 and Δ8/4 values and unradiogenic $^{87}Sr/^{86}Sr$, is dominant from 17 to 26°E along the western SWIR (Mahoney *et al.*, 1992). It also appears to be present, although variably overprinted by contamination from the Bouvet plume, westward to the Bouvet triple junction (le Roex *et al.*, 1983, 1992). The other component, an Indian Ocean-type N-MORB source, is characterized by relatively unradiogenic $^{206}Pb/^{204}Pb$ and high Δ7/4 and Δ8/4 values and by moderately elevated $^{87}Sr/^{86}Sr$ relative to most Atlantic and Pacific MORB. This latter component is present east of 32°E, but its most extreme expression is in the 42–47°E region, from the Discovery II to the Indomed fracture zone (Figs 1 and 4).

The data presented here clearly show that the Indian Ocean and Atlantic–Pacific N-MORB signatures in SWIR MORB are also distinct in terms of their Hf isotope compositions (Fig. 4), with samples dominated by the Indian Ocean MORB source tending to lie above the Nd–Hf mantle array at a wide range of ε_{Nd} values (+7 to +11), and those dominated by the Atlantic–Pacific N-MORB source tending to lie below it at a narrower range of ε_{Nd} values (+7 to +9). The distinct Hf–Nd isotopic compositions of these two MORB sources provide important clues to their origins.

The Atlantic–Pacific mantle signature

From about 43°E to 10°E on the SWIR (excluding the 39–41°E segment) there is a gradual decrease in ε_{Nd} and ε_{Hf} and a gradual increase in $^{206}Pb/^{204}Pb$ ratios ranging from values typical of Indian Ocean-type N-MORB to those similar to Bouvet OIB (Fig. 4). Sr isotopes reveal that this gradual isotopic transition is not simply the result of binary mixing between an Indian Ocean-type N-MORB source and material from the Bouvet plume, but rather is the result of both of these components mixing with an Atlantic–Pacific-type N-MORB source component with unradiogenic Sr, but intermediate Nd, Hf and Pb isotope ratios (Mahoney *et al.*, 1992). The Hf isotope ratios of SWIR lavas dominated by the Atlantic–Pacific signature are lower than those of most MORB from the northern MAR or EPR (Salters, 1996; Nowell *et al.*, 1998; Chauvel & Blichert-Toft, 2001). However, Andres *et al.* (2002) found that there is a general southward decrease in $\Delta\varepsilon_{Hf}$ from 40° to 55°S along the southern MAR. Further, MORB from the few portions of the MAR south of 49°S uncontaminated by the 'LOMU' and Shona geochemical anomalies (Douglass *et al.*, 1999; Le Roux *et al.*, 2002*a*) have moderate ε_{Nd} and negative $\Delta\varepsilon_{Hf}$ values that are nearly identical to those of Atlantic–Pacific-type MORB from 17° to 26°E on the SWIR (Andres *et al.*, 2002; Fig. 7). This Nd–Hf isotopic similarity strongly suggests that the western SWIR N-MORB are derived from MORB-source mantle similar to that

beneath the southernmost MAR and this, along with the gradual eastward increase in $\Delta\varepsilon_{Hf}$ values from the western to the eastern SWIR, confirms the finding of Mahoney *et al.* (1992) that the western boundary of the Indian Ocean mantle domain is largely gradational in nature and is located east of 26°E on the SWIR. On the basis of ε_{Hf}–ε_{Nd} and ε_{Hf}–$^{87}Sr/^{86}Sr$ isotopic and Lu/Hf ratio variations, we propose that the boundary is more precisely located between 26°E and 32°E.

The Indian Ocean mantle signature

In most respects, MORB from the 42–47°E section of the SWIR lie at the opposite end of the isotopic spectrum from the Atlantic–Pacific-type MORB source expressed at 17–26°E (Fig. 4). But normal and transitional MORB from this region, which includes the Discovery II and Indomed fracture zones and the spreading segments between them, are unusually heterogeneous, particularly in Sr and Nd isotope ratios (e.g. $^{87}Sr/^{86}Sr = 0{\cdot}7023$–$0{\cdot}7033$, $\varepsilon_{Nd} = +7$ to $+11{\cdot}2$; Mahoney *et al.*, 1992; Figs 5 and 6). Samples from this region encompass the most radiogenic Nd and Hf isotope compositions reported thus far for the Indian Ocean outside the AAD (Mahoney *et al.*, 1992; Chauvel & Blichert-Toft, 2001), as well as among the lowest $^{206}Pb/^{204}Pb$ values reported for the SWIR outside the 39–41°E segment (Price *et al.*, 1986; Mahoney *et al.*, 1992). However, Nd–Hf–Sr isotope systematics reveal that there are at least two depleted end-members sampled by MORB at 42–47°E, indicated by the isotopic differences between the samples with the most radiogenic Nd and Hf isotope ratios (e.g. P29-34 with $\varepsilon_{Nd} = +11{\cdot}2$, $\varepsilon_{Hf} = +17$, $^{87}Sr/^{86}Sr = 0{\cdot}7026$ vs MD34-D4 with $\varepsilon_{Nd} = +8{\cdot}4$, $\varepsilon_{Hf} = +21$ and $^{87}Sr/^{86}Sr = 0{\cdot}7030$; Mahoney *et al.*, 1992; Chauvel & Blichert-Toft, 2001; Fig. 7).

The range of isotopic compositions present in MORB from the 42–47°E area provides important clues to mixing processes occurring beneath the east–central SWIR and has implications for the way in which the Indian Ocean mantle signature is produced. The seven samples from six dredge hauls with reported Sr, Nd, Pb and Hf isotope data from this region fall into three distinct isotopic categories. Samples P29-34 and P30-75 have isotope compositions that fall within the fields for Atlantic and Pacific MORB in Sr–Nd–Hf–Pb and Pb–Pb isotope space, although near the low $^{206}Pb/^{204}Pb$–ε_{Nd} and high $^{208}Pb/^{204}Pb$ edges of these fields (Table 3, Figs 5 and 6). These samples also have $\Delta\varepsilon_{Hf}$ values between $+0{\cdot}5$ and -1. All of these traits suggest an isotopic affinity with depleted Atlantic–Pacific-type MORB sources. Samples P37-1 and P37-2 display anomalous isotope compositions indicative of long-term large ion lithophile and LREE enrichment and intermediate U/Pb ratios (e.g. $^{87}Sr/^{86}Sr = 0{\cdot}7033$–$0{\cdot}7038$, $\varepsilon_{Nd} = +2{\cdot}9$ to $+6{\cdot}8$, $^{206}Pb/^{204}Pb = 18{\cdot}04$–$18{\cdot}35$; Mahoney *et al.*, 1992). These samples fall above the Nd–Hf mantle array line, but only slightly ($\Delta\varepsilon_{Hf} \leq +1{\cdot}7$). Finally, samples P41-49, P42-11 and MD34-D4 have Sr, Nd and (except for MD34-D4) $^{206}Pb/^{204}Pb$ isotope ratios intermediate between the depleted and enriched groups ($^{87}Sr/^{86}Sr = 0{\cdot}7029$–$0{\cdot}7032$, $\varepsilon_{Nd} = +7{\cdot}0$ to $+8{\cdot}4$, $^{206}Pb/^{204}Pb = 17{\cdot}8$–$18{\cdot}2$; Hamelin & Allègre, 1985), but have $\Delta\varepsilon_{Hf}$ values higher than either group ($+2{\cdot}3$ to $+6{\cdot}7$). These latter samples also have $\Delta7/4$ and $\Delta8/4$ values (of $5{\cdot}1$–$5{\cdot}4$ and 37–65, respectively) significantly higher than those of the depleted P29-34 and P30-75 samples. It is this last group, characterized by Nd and Sr isotope ratios intermediate between Atlantic–Pacific MORB and OIB, low to moderate $^{206}Pb/^{204}Pb$ with elevated $\Delta7/4$ and $\Delta8/4$ and moderate to high positive $\Delta\varepsilon_{Hf}$ values, that is most characteristic of Indian Ocean MORB as a whole (e.g. Michard *et al.*, 1986; Mahoney *et al.*, 1989; Salters, 1996; Chauvel & Blichert-Toft, 2001; Hanan *et al.*, 2004).

The fact that depleted MORB similar to that from the Atlantic and Pacific Oceans exists in a region of the SWIR otherwise characterized by Indian Ocean-type isotope compositions (Figs 4–8) strongly supports the idea that the Indian Ocean MORB source is the product of an 'Indian Ocean component' (or a range of components) that has variably contaminated an upper mantle originally having an isotopic character similar to that beneath Atlantic and Pacific ridges (Storey *et al.*, 1989; Mahoney *et al.*, 1989, 1992). The preservation of relatively uncontaminated Atlantic–Pacific-type MORB source mantle in this region may be attributable to inefficient mixing beneath the east–central SWIR as a result of the cold upper mantle temperatures inferred for this region from seismic tomography (Debayle & Leveque, 1997). The good correlations between $\Delta\varepsilon_{Hf}$ and $^{87}Sr/^{86}Sr$, $\Delta7/4$, $\Delta8/4$, Ba/Nb and Ba/Th displayed by SWIR MORB from east of 32°E (excluding 39–41°E), as well as most other Indian Ocean MORB (Figs 9 and 10), are clear indications that high $\Delta\varepsilon_{Hf}$ values are as intrinsic to this component as elevated $^{87}Sr/^{86}Sr$, high $\Delta7/4$ and $\Delta8/4$ and enrichment in large ion lithophile elements. The lack of good correlations between $\Delta\varepsilon_{Hf}$ and $^{206}Pb/^{204}Pb$ (Fig. 9b) and between Nd and Hf isotope ratios (Fig. 7) in Indian Ocean MORB suggests either that the Indian Ocean component spans a wide range of Nd and Pb isotope compositions or, perhaps more likely, that the Atlantic–Pacific-type MORB source was already heterogeneous in these isotope ratios before being contaminated.

Hf isotope constraints on the origin of the Indian Ocean MORB isotopic signature

Several possible scenarios have been proposed for the origin of a component responsible for the isotopic

differences between Indian Ocean and Atlantic–Pacific MORB. These include: (1) contamination of the Indian Ocean upper mantle by plume material derived either from the Kerguelen plume alone (Storey *et al.*, 1989; Weis & Frey, 1996), or from a combination of central Indian Ocean plumes (e.g. Marion, Crozet and Kerguelen) mixed with delaminated continental lithospheric mantle (Mahoney *et al.*, 1992); (2) focused recycling of pelagic sediments and subducted oceanic crust into the Indian Ocean upper mantle (Dupré & Allègre, 1983; Rehkämper & Hofmann, 1997); (3) foundering and mixing of continental lower crust into the Indian Ocean upper mantle during or after the opening of the Indian Ocean (e.g. Escrig *et al.*, 2004; Hanan *et al.*, 2004); (4) mobilization or delamination of subduction-modified mantle wedge material formed during Paleozoic subduction beneath eastern Gondwana (Kempton *et al.*, 2002).

As pointed out by other workers (Mahoney *et al.*, 1992; Hanan *et al.*, 2004), Kerguelen and all other known Indian Ocean plumes have $^{206}Pb/^{204}Pb$ values that are too radiogenic (~18 to ~19; Salters & White, 1998; Yang *et al.*, 1998) to explain the bulk of the Indian Ocean MORB data by mixing with an Atlantic–Pacific-type MORB source. A mixture of plume material with continental lithospheric mantle, on the other hand, might be able to produce an Indian Ocean component with an appropriate isotopic composition to account for Indian Ocean MORB (Mahoney *et al.*, 1992). However, this seems unlikely for two reasons. First, mixing relations require that for an Indian Ocean component to have a plausible $^{206}Pb/^{204}Pb$ value of about 17·25 or less, either unrealistically large proportions of lithospheric mantle would be required (>50%) or this lithospheric mantle material must have had an extremely low mean $^{206}Pb/^{204}Pb$ value of 16·5 or less [assuming Pb abundances of 0·08 and 0·16 ppm for plume material (from Table 5) and lithospheric mantle (McDonough, 1990), respectively, and a $^{206}Pb/^{204}Pb$ ratio of 18·5 for the plume material]. Such unradiogenic Pb isotope compositions have been reported for Archean cratonic peridotites (e.g. Cohen *et al.*, 1984) but not for peridotites of Proterozoic age (see Lee *et al.*, 1996; Carlson *et al.*, 2004). However, the great majority of the continental rifting that resulted in the breakup of central and eastern Gondwana to form the Indian Ocean involved Proterozoic lithosphere rather than Archean cratons (Meert, 2003; Fig. 15). Thus, unless there was major delamination of the Archean keels beneath Gondwanan cratons in response to Mesozoic plume-head impact, which is not supported by seismic and heat flow studies (e.g. Gupta, 1991; James *et al.*, 2001), there was little opportunity for widespread mixing of plume material and/or Indian Ocean asthenosphere with low-$^{206}Pb/^{204}Pb$ Archean mantle.

Second, the arrays defined by the 39–41°E MORB samples on plots of $\Delta\varepsilon_{Hf}$ versus other isotope ratios,

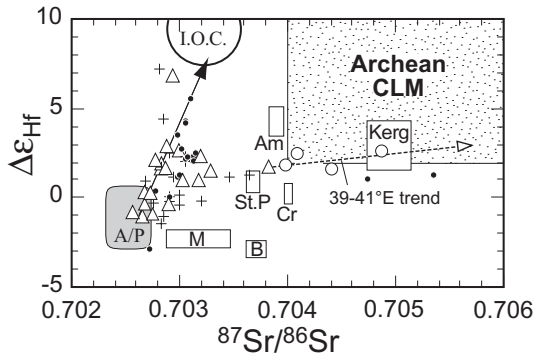

Fig. 16. $^{87}Sr/^{86}Sr$ vs $\Delta\varepsilon_{Hf}$, showing 32–68°E SWIR MORB, other Indian Ocean MORB and fields for oceanic islands in the central and western Indian Ocean. Data sources as in Figs 6 and 7. Mixing between Atlantic–Pacific (A/P)-type MORB, such as that present beneath the western SWIR, with high-$\Delta\varepsilon_{Hf}$ plume sources or Archean continental lithospheric mantle (CLM) component (with which the 39–41°E SWIR MORB appears to be mixing) will yield mixtures with higher $^{87}Sr/^{86}Sr$ and/or lower $\Delta\varepsilon_{Hf}$ than that inferred for the Indian Ocean mantle component (I.O.C.).

which we attribute mainly to mixing between Indian Ocean asthenosphere and cratonic lithospheric mantle, have slopes that are highly oblique to the trends defined by the Indian Ocean-type SWIR MORB outside 39–41°E and other Indian Ocean MORB (Fig. 16). The 39–41°E samples appear to be pointing toward a component with markedly lower $^{206}Pb/^{204}Pb$ and higher $^{87}Sr/^{86}Sr$, $\Delta 7/4$ and $\Delta 8/4$ for a given $\Delta\varepsilon_{Hf}$ value than the main trend of Indian Ocean MORB data. The extreme Hf isotope heterogeneity of mineral separates from Archean cratonic peridotite (Fig. 14) certainly permits this material to have a wide range of $\Delta\varepsilon_{Hf}$ values. However, the isotopic similarity between the Ejeda–Bekily dikes from southern Madagascar and 39–41°E MORB appears to support our contention that the high $^{87}Sr/^{86}Sr$, low $^{206}Pb/^{204}Pb$ component tapped by these MORB represents Gondwanan Archean lithospheric mantle probably disrupted by the Marion plume in the late Cretaceous. If this inference is correct, it suggests that no mixture of this ancient, low $^{206}Pb/^{204}Pb$ lithospheric mantle with the Kerguelen, Marion or other Indian Ocean plumes would have sufficiently high $\Delta\varepsilon_{Hf}$ values to explain the highest-$\Delta\varepsilon_{Hf}$ SWIR MORB, such as MD34-D4 (Fig. 16). Moreover, because of the relatively high $^{87}Sr/^{86}Sr$ ratios of Gondwanan Archean lithospheric mantle (e.g. Menzies & Murthy, 1980; Walker *et al.*, 1989) and those Indian Ocean plumes with positive $\Delta\varepsilon_{Hf}$ values (e.g. Yang *et al.*, 1998; Doucet *et al.*, 2004), it seems unlikely that a mixture of these materials would have the mildly radiogenic $^{87}Sr/^{86}Sr$ (<~0·7036) required for the Indian Ocean component by the $^{87}Sr/^{86}Sr$–$\Delta\varepsilon_{Hf}$ array (Fig. 16), even if the $\Delta\varepsilon_{Hf}$ value of the cratonic lithosphere involved was significantly higher

than indicated by the 39–41°E MORB and Ejeda–Bekily dikes.

Addition of ancient pelagic sediments to the Indian Ocean upper mantle seems to offer a more plausible explanation for the differences between Atlantic–Pacific and Indian Ocean MORB than plume contamination, at least from a geochemical perspective. Although we cannot address why pelagic sediments should be preferentially recycled into the upper mantle beneath the Indian, rather than the Atlantic or Pacific Oceans, the estimated Sr, Nd and Pb isotope ratios of ancient (1–3 Ga) subducted pelagic sediments agree well with those required for the Indian Ocean mantle component, particularly if the sediments are mixed with variable quantities of subducted oceanic crust (Rehkämper & Hofmann, 1997). The moderately decoupled Nd and Hf isotopic ratios in pelagic sediments (Fig. 14), and their Nd/Hf ratios, which are up to 10 times higher than mantle values (e.g. Ben Othman *et al.*, 1989; Vervoort *et al.*, 1999), also seem to offer an explanation for the high $\Delta\varepsilon_{Hf}$ values observed in Indian Ocean MORB.

However, as pointed out by Kempton *et al.* (2002), the Nd and Hf isotope compositions of pelagic sediments are too unradiogenic, and the decoupling between Hf and Nd isotope ratios and concentrations is too limited, to explain the Nd–Hf isotopic compositions of at least one-third of analyzed Indian Ocean MORB samples, those having both $\varepsilon_{Nd} > +7$ and $\Delta\varepsilon_{Hf} > +2$ (Fig. 7). Even for the optimal case in which pelagic sediment is added without any accompanying recycled oceanic crust, mixtures of pelagic sediments and Atlantic–Pacific-type MORB-source mantle will lie two or more ε_{Hf} units above the Nd–Hf array only at ε_{Nd} values less than about +5. Thus, the Indian Ocean mantle component must consist of a material with an even greater decoupling of its Nd and Hf concentrations and isotope ratios and/or a more radiogenic Hf isotope composition.

Hanan *et al.* (2004) have proposed that just such a material formed in the lower continental crust adjacent to continental rift zones. Recent analysis of lavas from zone B4 of the AAD (125–126°E) showed that these Indian Ocean-type MORB (according to their low $^{206}Pb/^{204}Pb$ and high $^{208}Pb/^{204}Pb$ ratios) have extremely radiogenic Nd and Hf isotopic compositions ($\varepsilon_{Nd} = +9{\cdot}8$ to $+12{\cdot}9$, $\varepsilon_{Hf} = +22{\cdot}2$ to $+28{\cdot}8$; Hanan *et al.*, 2004), giving them the most radiogenic Hf isotope ratios yet published for any MORB, as well as the highest $\Delta\varepsilon_{Hf}$ values in the Indian Ocean (up to $+8{\cdot}5$). To explain the long-term high Lu/Hf ratios required by these radiogenic Hf isotopic compositions, Hanan *et al.* (2004) proposed that their source is the product of mixing Pacific-type upper mantle with a restite of garnet-bearing granulitic lower continental crust that underwent extensive melting during continental rifting. This melting would have had the effect of increasing Sm/Nd and dramatically raising Lu/Hf, as a result of the compatibility of Lu in garnet. Extremely high $(Lu/Hf)_N$ ratios, up to 38, have been measured in lower crustal granulite xenoliths from other continental rift environments (Scherer *et al.*, 1997). Over the ~80 Myr since the separation of Australia from Antarctica (Storey, 1995), this lower crustal restite could develop high ε_{Nd} and extremely high ε_{Hf} and $\Delta\varepsilon_{Hf}$ values suitable as a mixing end-member for zone B4 AAD MORB and high $\Delta\varepsilon_{Hf}$ Indian Ocean MORB elsewhere, whereas less melt-depleted lower crustal granulite could constitute a low ε_{Nd}–ε_{Hf} end-member to explain more enriched Indian Ocean MORB (Hanan *et al.*, 2004). The low U/Pb ratios of lower continental crust would also fit with the unradiogenic $^{206}Pb/^{204}Pb$ ratios measured in Indian Ocean MORB (Rudnick & Fountain, 1995; Hanan *et al.*, 2004).

Although the lower crustal contamination model of Hanan *et al.* (2004) offers a potential explanation for the Nd, Hf and Pb isotope differences between Indian Ocean-type and Atlantic–Pacific-type MORB, this hypothesis has one major problem. The $^{87}Sr/^{86}Sr$ values of Gondwanan lower crustal granulites tend to be rather high, even when corrected for radiogenic growth since the time of continental rifting (e.g. mean $^{87}Sr/^{86}Sr_{80\,Ma} = 0{\cdot}7072$ for Australian granulite xenoliths, mean $^{87}Sr/^{86}Sr_{150\,Ma} = 0{\cdot}7068$ for all southern African granulite xenoliths and 0·7060 for southern African mafic granulite xenoliths only; Rudnick *et al.* 1986; Rudnick, 1990; Huang *et al.*, 1995; M. D. Schmitz, unpublished data, 2004). Because melt depletion cannot lower Sr isotope ratios, the low $^{87}Sr/^{86}Sr$ ratio of the Indian Ocean component inferred from the main $^{87}Sr/^{86}Sr$–$\Delta\varepsilon_{Hf}$ correlation (Fig. 16) seriously limits the degree to which lower crustal granulite could be incorporated into sources of Indian Ocean MORB. Figure 17 shows that for mixtures of depleted mantle with mean Australian granulite or mean southern African mafic granulite, addition of <1% of the granulite end-member is required to explain the vast majority of Indian Ocean MORB with $^{87}Sr/^{86}Sr$ ratios of <0·7035. Such small proportions of lower crustal granulite are not nearly sufficient to explain the Nd and Hf isotopic ranges of Indian Ocean MORB (Fig. 17a), regardless of whether one uses a mean Australian or southern African granulite composition or the hypothetical high-ε_{Hf} and -ε_{Nd} 'lower crustal granulite' (LCG) end-member of Hanan *et al.* (2004). It is true that $^{87}Sr/^{86}Sr$ ratios in lower crustal granulite can extend to values as low as 0·7024 in Australian and 0·7020 in southern African granulites (Rudnick *et al.*, 1986; M. D. Schmitz, unpublished data, 2004); however, these values are extremely unrepresentative. Such low $^{87}Sr/^{86}Sr$ ratios could potentially explain the unradiogenic Sr isotope compositions in a localized area, such as zone B4 of the AAD, but it is highly implausible that low $^{87}Sr/^{86}Sr$ ratios would be a general characteristic of

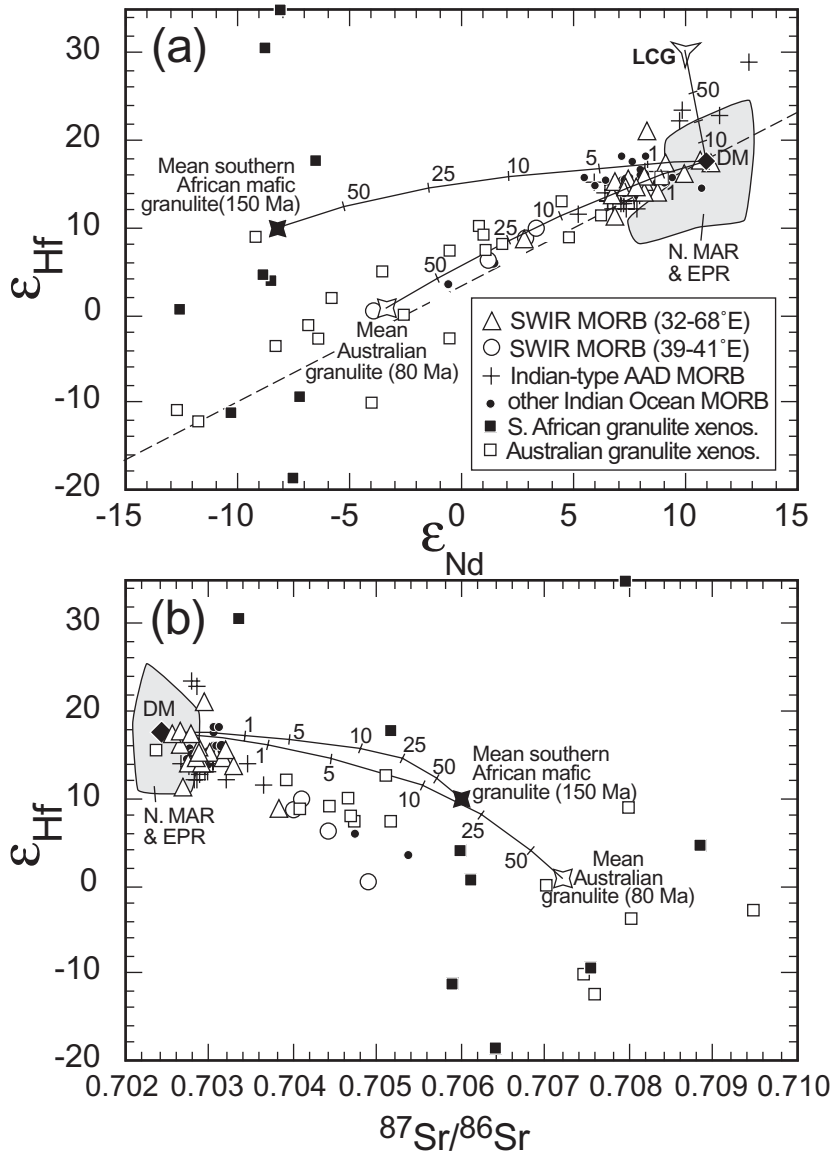

Fig. 17. Plots of (a) ε_{Nd}, and (b) $^{87}Sr/^{86}Sr$ both vs ε_{Hf} showing data for Australian and southern African granulite xenoliths age-corrected to the time of local Indian Ocean opening (80 and 150 Ma, respectively). Approximately one-third of the southern African and one-fifth of the Australian lower crustal granulite data fall outside the ranges of these plots, particularly toward higher $^{87}Sr/^{86}Sr$ and lower ε_{Hf} values. Also shown are 32–68°E SWIR and other Indian Ocean MORB, as well as mixing curves between an Atlantic–Pacific-type depleted mantle (DM) composition and mean Australian lower crustal granulite (Rudnick *et al.*, 1986; Rudnick, 1990; Vervoort *et al.*, 2000; with Hf, Sr and Nd contents of 2·6, 335 and 16 ppm) and mean southern African mafic granulite (Schmitz *et al.*, 2004; M. D. Schmitz, unpublished data, 2004; see Table 5 for trace element and isotopic composition). The end-member marked LCG is the hypothetical high ε_{Nd}–ε_{Hf} lower crustal granulite restite component of Hanan *et al.* (2004). It should be noted that the relatively large proportions of lower crust required to explain the Nd–Hf isotope compositions of most Indian MORB are inconsistent with the relatively unradiogenic Sr isotope compositions of these samples.

a lower crustal granulite contaminant present throughout the Indian Ocean mantle domain.

Another environment where extreme decoupling of Lu/Hf and Sm/Nd ratios is expected to occur is in the mantle wedge of a subduction zone. During subduction, the mantle wedge is subjected to pervasive infiltration by hydrous, slab-derived fluids, and possibly sediment melts, and experiences partial melting due to the solidus-lowering effect of these fluids. Experimental evidence suggests that aqueous fluids driven off a subducting slab will have elevated Nd/Hf ratios as a result of the relative immobility of Hf (e.g. Ayers *et al.*, 1997). Recent Hf isotope data from 'fluid-dominated' volcanic arcs do suggest that slab-derived fluids can transport significant

quantities of Hf into the sub-arc mantle (Woodhead *et al.*, 2001), but data for the Mariana arc system, which has been most studied for Hf isotope systematics (Pearce *et al.*, 1999; Woodhead *et al.*, 2001), suggest that the Nd/Hf ratio of the fluid component added to the sub-arc mantle may be up to three times higher than that of the local subducting sediments. Thus, because of the high Nd/Hf ratios and relatively low ε_{Nd} and ε_{Hf} values of fluids derived from subducting sediments and oceanic crust, the likely net effect of fluid addition with respect to the Nd and Hf isotopes systems is a significant decrease in $^{143}Nd/^{144}Nd$ and Sm/Nd ratio, a mild decrease in $^{176}Hf/^{177}Hf$ and a significant increase in Lu/Hf ratio, relative to mantle melting residues that had not experienced fluid addition. Fluid-mobile elements such as Sr and especially Pb and Rb would also be added, resulting in decreased U/Pb and increased Rb/Sr ratios in the mantle wedge (e.g. Aizawa *et al.*, 1999; Green & Adam, 2003).

Over hundreds of millions of years, the elemental and isotopic fractionations produced in the mantle wedge would result in it having radiogenic $^{176}Hf/^{177}Hf$ and $^{87}Sr/^{86}Sr$ and relatively unradiogenic $^{143}Nd/^{144}Nd$ and $^{206}Pb/^{204}Pb$ ratios, qualitatively similar to the contaminant inferred to be responsible for the Indian Ocean MORB source (Kempton & Pearce, 2003; Zhang *et al.*, 2005). Indeed, positive $\Delta\varepsilon_{Hf}$ values are characteristic of suprasubduction zone magmas, particularly from long-lived, fluid-dominated arc systems (e.g. the Mariana and Tonga–Kermadec arcs; Pearce *et al.*, 1999; Kempton *et al.*, 2000). Kempton *et al.* (2002) advocated addition of such fluid-modified, melt-depleted mantle wedge material to the Indian Ocean upper mantle to explain the Nd–Hf isotopic differences between Indian Ocean- and Atlantic–Pacific-type MORB, both for the AAD (their study area) and for the greater Indian Ocean mantle domain. Their hypothesis is consistent with recent evidence (Gurnis *et al.*, 1998) that the AAD overlies a stranded, westward-dipping slab from a subduction zone that was active on the Pacific margin of Gondwana from the Late Paleozoic to the Early Cretaceous.

Although there is no evidence for ancient subduction zones beneath spreading centers elsewhere in the Indian Ocean, it is important to note that the continental rifting that separated Africa, Antarctica, Indo-Madagascar and Australia to form the Indian Ocean occurred mostly within Meso- and Neoproterozoic (550–1500 Ma) orogenic belts (e.g. Groenewald *et al.*, 1991; Meert, 2003; Fig. 15). These belts consist of high-grade metamorphic and igneous terranes amalgamated during the assembly of Gondwana and its precursor, Rodinia (e.g. Jacobs *et al.*, 1998; Dalziel *et al.*, 2000). Many of these terranes contain igneous and meta-igneous rocks with clear suprasubduction zone geochemical signatures (e.g. Cornell *et al.*, 1996; Kröner *et al.*, 1997, 2001; Paulsson & Austrheim, 2003), which appear to have formed in intra-oceanic arc and Andean-type continental margin environments (e.g. Stern, 1994; Handke *et al.*, 1999). It is likely that slab-derived fluids and/or sediment melts were introduced to significant portions of the Proterozoic lithospheric mantle beneath these orogenic belts during the periods of subduction with which these magmatic rocks are associated.

Continental rifting during the Early Cretaceous may have resulted in the destabilization and delamination of some of this subduction-modified Meso- and Neoproterozoic lithospheric mantle, which could have foundered in and mixed with the upper mantle beneath the nascent Indian Ocean. If the subduction modification took place a sufficiently long time ago, addition of such mantle wedge material could explain the high ε_{Hf} values and strong Nd–Hf isotopic decoupling of samples such as MD34-D4 from the 42–47°E section of the SWIR (Chauvel & Blichert-Toft, 2001), and the MORB from zone B4 of the AAD (Hanan *et al.*, 2004) and could also explain the mildly elevated $^{87}Sr/^{86}Sr$ ratios of these samples.

We present a set of models (Fig. 18) for the development of a range of subduction-modified mantle (SMM) compositions, formed at times from 250 to 1500 Ma, in Nd–Hf and Sr–Hf isotope space. In these models, various amounts of a subduction component (either mean global subducting sediments or a slab-derived fluid) are added to an age-corrected Atlantic–Pacific-type depleted mantle composition (Table 5). The resulting mixture is then immediately subjected to partial melt extraction and the present-day isotope composition of the melt residue is calculated. The assumptions of these models are that: (1) the REE and Hf contents of the fluid are entirely derived from subducting sediments (Table 5; these elements appear to be essentially immobile in igneous oceanic crust during dehydration; Green & Adam, 2003); (2) the mobility of Hf from subducting sediments into a fluid phase is 50% lower than that of Lu, similar to the mobilities of Ti and Nb determined in sediment dehydration experiments (Aizawa *et al.*, 1999); (3) the Sr isotopic composition of the fluid can be estimated by assuming that 30% of the Sr in the fluid is derived from igneous oceanic crust (with a depleted mantle isotopic composition) and 70% is derived from mean pelagic sediments (this is an approximation based on the lower $^{87}Sr/^{86}Sr$ ratios in lavas from 'fluid-dominated' relative to 'sediment-dominated' arcs; e.g. Davidson, 1986; Lin *et al.*, 1990); (4) following sediment or fluid addition, the resulting mixture is subjected to removal of a 6% nonmodal batch partial melt (in the spinel stability field) to simulate extraction of arc magmas (see Table 6 for partition coefficients and melting assemblage). This degree of melting is at the lower end of the range estimated for most arc magmas (e.g. Baker *et al.*, 1994), but

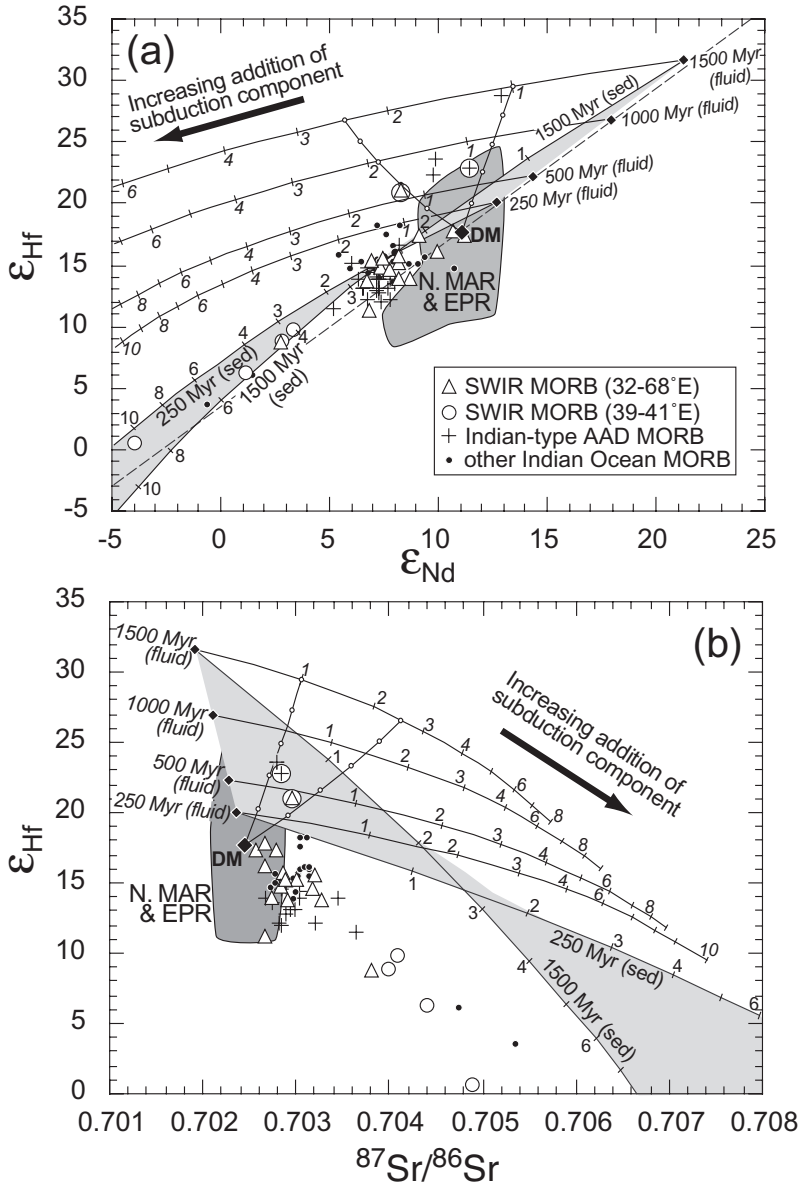

Fig. 18. Plots of ε_{Hf} vs (a) ε_{Nd}, and (b) $^{87}Sr/^{86}Sr$ showing the compositions of subduction-modified mantle (SMM) formed at 250, 500, 1000 and 1500 Ma, along with MORB from the SWIR and other Indian Ocean spreading centers. Labels on the curves indicate the age of the subduction modification and the relative percentage of subduction component added, either as bulk sediment (sed) or fluid. For clarity, the range of 1500 to 250 Ma SMM (sed) compositions is shown with a light gray field and only the 250 and 1500 Ma sediment addition trajectories are shown in detail. Circled samples MD34-D4 (△, Hamelin & Allègre, 1985; Chauvel & Blichert-Toft, 2001) and MW8801 23-1 (+, Pyle *et al.*, 1992; Hanan *et al.*, 2004) are modeled by mixing curves (small circles mark 20% increments) between Atlantic–Pacific-type depleted mantle (DM) and SMM compositions. Calculation of model SMM compositions was based on the values in Table 5 for the Sr, Nd and Hf isotopic and trace element composition of mean pelagic sediments (interpolated from the 1·5 Ga and modern values) and mean depleted mantle. Melt residue compositions were calculated using the mineral modes, melting proportions and partition coefficients listed in Table 6, but with no involvement of garnet. Because the mass balance parameters for slab fluid generation and reaction with mantle wedge peridotite are poorly known, the percentage figures for fluid component addition are quantitative only in a relative sense.

was chosen to approximate the mean degree of melting experienced by the entire mantle wedge. Increasing the degree of melting by as much as a factor of two will not significantly affect the model results. The details of the model calculations are presented in the caption to Fig. 18 and in Table 6.

The subduction-modified mantle (SMM) compositions produced by addition of bulk subducting sediments yield

ε_{Nd} and ε_{Hf} values that lie relatively close to the mantle array ($\Delta\varepsilon_{Hf}$ less than +3 between $\varepsilon_{Nd} = +5$ and $\varepsilon_{Nd} = +15$). This is because the effects of sediment addition and partial melting on SMM act in opposite directions and maintain good coupling between Sm/Nd and Lu/Hf ratios. The combination of slab fluid addition and partial melting, on the other hand, sharply lowers Sm/Nd relative to Lu/Hf. This results in the fluid-modified SMM trajectories lying above the Nd–Hf mantle array and having much shallower slopes. About 25% of the Indian Ocean MORB samples in Fig. 18a have $\Delta\varepsilon_{Hf}$ values that are too high to be explained by involvement of sediment-dominated SMM. In contrast, all high-$\Delta\varepsilon_{Hf}$ Indian Ocean MORB can be explained by mixing between Atlantic–Pacific-type MORB source mantle and fluid-modified SMM, although the samples with the highest $\Delta\varepsilon_{Hf}$ values require mixing with SMM components that formed at least 1000–1500 Myr ago.

The SMM trajectories in Sr–Hf isotope space do not provide equally strong constraints on the age or nature of a possible SMM component involved in the genesis of Indian Ocean MORB. Both sediment- and fluid-modified SMM compositions can explain the mildly elevated $^{87}Sr/^{86}Sr$ and radiogenic ε_{Hf} values of the highest $\Delta\varepsilon_{Hf}$ Indian MORB. However, the fluid-modified SMM compositions in both Nd–Hf and Sr–Hf isotope space give more consistent results when attempting to reproduce the compositions of particular samples by mixing SMM with depleted mantle (Fig. 18). For example, in both Nd–Hf and Sr–Hf isotope ratio space, the high-$\Delta\varepsilon_{Hf}$ SWIR MORB sample MD34-D4 can be approximated by mixing depleted mantle with ~30% of a 1500 Ma fluid-modified SMM component and, similarly, AAD zone B4 MORB sample MW8801 23-1 (one of only two with Sr isotope data; Pyle *et al.*, 1992) can also be reproduced by mixing depleted mantle with ~40% of a 1500 Ma SMM component, but one having experienced somewhat less fluid addition.

Mixing between an Atlantic–Pacific-type MORB source and ancient SMM variably modified by slab-derived fluids can simply explain why Indian Ocean MORB is characterized by high $\Delta\varepsilon_{Hf}$ values and a diverse range of Nd isotope compositions. That this hypothesis also explains why Indian MORB tend to have mildly, but not highly, elevated Sr isotopic compositions is also a point in its favor. Determining whether SMM is the most appropriate material to explain the Pb isotope compositions of Indian Ocean MORB will require better constraints on the mean relative contributions of U, Th and Pb from oceanic crust and sediments to slab-derived fluids, as well as more precisely determined partition coefficients for these elements during melting of hydrous peridotite, than are currently available in the published literature.

The fact that MORB from 43°E on the SWIR (sample MD34-D4; Chauvel & Blichert-Toft, 2001) and from zone B4 of the AAD (Hanan *et al.*, 2004) lie on or above the curve of 500 Ma fluid-modified SMM compositions indicates that the Nd–Hf isotopic characteristics of all high-$\Delta\varepsilon_{Hf}$ Indian Ocean MORB cannot be explained by westward advection of mantle wedge material from the Pacific margin of Gondwana (see Kempton *et al.*, 2002). Subduction at this margin appears to have begun only in the Early Paleozoic (~500 Ma; Grunow *et al.*, 1996), which would not allow sufficient time to develop the necessary decoupling of Nd and Hf isotopic compositions. It seems likely that, at least in some locations, this isotopic signature was acquired via destabilization and foundering of lithospheric mantle beneath the Proterozoic orogenic belts that border the Indian Ocean. We cannot, however, rule out a role for advected Paleozoic-age SMM in the genesis of Indian Ocean lavas with only mildly positive $\Delta\varepsilon_{Hf}$ values.

If the hypothesis is correct that the distinct isotope characteristics of Indian Ocean MORB are derived from contamination of the Indian Ocean upper mantle by delaminated or detached mantle lithosphere underlying Proterozoic orogenic belts, an important question remains: why does MORB from the Atlantic Ocean bear a closer isotopic resemblance to MORB of the Pacific rather than that of the Indian Ocean? Like the Indian Ocean, the Atlantic also formed as the result of Mesozoic continental breakup. A potential clue comes from the fact that geochemical signatures of contamination by continental and/or subduction components do exist in portions of the Mid-Atlantic Ridge, but these tend to be fairly localized (i.e. less than 500 km in extent along ridge; Shirey *et al.*, 1987; Douglass *et al.*, 1999; Kamenetsky *et al.*, 2001; Le Roux *et al.*, 2002*a*). Similar geochemical anomalies are absent along the East Pacific Rise (e.g. White *et al.*, 1987; Mahoney *et al.*, 1994). We speculate that the isotopic differences between MORB from the Indian and Atlantic Oceans is due two main factors. First, continental breakup leading to the formation of the Indian Ocean was much more complex, and involved a larger number of continents (and microcontinents) than that leading to the formation of the Atlantic Ocean (Fig. 15). Hence, there was a much longer zone of contact between rifted continental lithosphere and asthenosphere where delamination of continental mantle lithosphere could occur. Second, the Indian Ocean is bordered mainly by Proterozoic orogenic belts, whereas the central and South Atlantic is bordered by a much higher proportion of Archean cratons (e.g. Bernasconi, 1983; Black & Liegeois, 1993; Hanson, 2003; Fig. 15), which are probably less dense and more rigid than orogenic belts (e.g. Lenardic *et al.*, 2003), and thus may be less susceptible to delamination.

ACKNOWLEDGEMENTS

We are grateful to Andreas Späth for technical assistance with the ICPMS system at UCT and for his hospitality to the first author on two trips to Cape Town to do the trace element work. Mary Horan and Tim Mock generously provided critical laboratory and mass spectrometry assistance at DTM. Mark Schmitz generously provided unpublished trace element and isotope data for his lower crustal xenolith suite. Robert L. Fisher shared his knowledge of the geology of the western Indian Ocean and provided the Marion Island and Prince Edward Island samples. John Mahoney is thanked for supplying several key samples from the SWIR and Madagascar, and for useful comments on an early draft of this paper. We also express sincere thanks to Warren Smith and the Scripps Institution of Oceanography Geological Collections for assistance in obtaining several MORB samples used in this study. This paper benefited from the detailed and insightful reviews of Catherine Chauvel, Dominique Weis and Tiffany Barry, as well as the Editor. This work was supported by US NSF grants OCE 9907173 to P.E.J. and R.W.C., OCE 0221368 to P.E.J. and by funding from the South African National Research Foundation, to A.L.R.

SUPPLEMENTARY DATA

Supplementary data for this paper are available at *Journal of Petrology* online.

REFERENCES

Aizawa, Y., Tatsumi, Y. & Yamada, H. (1999). Element transport by dehydration of subducted sediment: implications for arc and ocean island magmatism. *The Island Arc* **8**, 39–46.

Andres, M., Blichert-Toft, J. & Schilling, J.-G. (2002). Hafnium isotopes in basalts from the southern Mid-Atlantic Ridge from 40°S to 55°S: Discovery and Shona plume–ridge interactions and the role of recycled sediments. *Geochemistry, Geophysics, Geosystems* **3**, doi: 10.1029/2002GC000324.

Asimow, P. D., Hirschmann, M. M. & Stolper, E. M. (1997). An analysis of variations in isentropic melt productivity. *Philosophical Transactions of the Royal Society, Series A* **355**, 255–281.

Ayers, J. C., Dittmer, S. K. & Layne, G. D. (1997). Partitioning of elements between peridotite and H_2O at 2·0–3·0 GPa and 900–1100°C, and application to models of subduction zone processes. *Earth and Planetary Science Letters* **150**, 381–398.

Baker, M. B., Grove, T. L. & Price, R. (1994). Primitive basalts and andesites from the Mt. Shasta region, N. California: products of varying melt fraction and water content. *Contributions to Mineralogy and Petrology* **118**, 111–129.

Beattie, P. (1994). Systematics and energetics of trace element partitioning between olivine and silicate melts: implications for the nature of mineral–melt partitioning. *Chemical Geology* **117**, 57–71.

Bedini, R. M., Blichert-Toft, J., Boyet, M. & Albarède, F. (2004). Isotopic constraints on the cooling of the continental lithosphere. *Earth and Planetary Science Letters* **223**, 99–111.

Ben Othman, D., White, W. M. & Patchett, J. P. (1989). The geochemistry of marine sediments, island arc magma genesis and crust–mantle recycling. *Earth and Planetary Science Letters* **94**, 1–21.

Bernasconi, A. (1983). The Archean terranes of central eastern Brazil—a review. *Precambrian Research* **23**, 107–131.

Black, R. & Liegeois, J.-P. (1993). Cratons, mobile belts, alkaline rocks and continental lithospheric mantle: the Pan-Africa testimony. *Journal of the Geological Society, London* **150**, 89–98.

Blichert-Toft, J. & Albarède, F. (1997). The Lu–Hf isotope geochemistry of chondrites and the evolution of the mantle–crust system. *Earth and Planetary Science Letters* **148**, 243–258.

Blichert-Toft, J., Chauvel, C. & Albarède, F. (1997). Separation of Hf and Lu for high-precision isotope analysis of rock samples by magnetic sector-multiple collector ICP-MS. *Contributions to Mineralogy and Petrology* **127**, 248–260.

Blichert-Toft, J., Frey, F. A. & Albarède, F. (1999). Hf isotope evidence for pelagic sediments in the source of Hawaiian basalts. *Science* **285**, 879–882.

Blundy, J. D., Robinson, J. A. C. & Wood, B. J. (1998). Heavy REE are compatible on the spinel lherzolite solidus. *Earth and Planetary Science Letters* **160**, 493–504.

Bodinier, J. L., Guiraud, M., Fabries, J., Dostal, J. & Dupuy, C. (1987). Petrogenesis of layered pyroxenites from the Lherz, Freychinede and Prades ultramafic bodies (Ariege, French Pyrenees). *Geochimica et Cosmochimica Acta* **51**, 279–290.

Bourdon, B., Zindler, A., Elliott, T. & Langmuir, C. H. (1996). Constraints on mantle melting at mid-ocean ridges from global ^{238}U–^{230}Th disequilibrium data. *Nature* **384**, 231–235.

Bown, J. W. & White, R. S. (1994). Variation with spreading rate of oceanic crustal thickness and geochemistry. *Earth and Planetary Science Letters* **121**, 435–449.

Cannat, M., Rommevaux-Jestin, C., Sauter, D., Deplus, C. & Mendel, V. (1999). Formation of the axial relief at the very slow spreading Southwest Indian Ridge (49–69°E). *Journal of Geophysical Research* **104**, 22825–22843.

Carlson, R. W., Irving, A. J., Schulze, D. J. & Hearn, B. C. (2004). Timing of Precambrian melt depletion and Phanerozoic refertilization events in the lithospheric mantle of the Wyoming Craton and adjacent Central Plains Orogen. *Lithos* **77**, 453–472.

Chauvel, C. & Blichert-Toft, J. (2001). A hafnium isotope and trace element perspective on melting of the depleted mantle. *Earth and Planetary Science Letters* **190**, 137–151.

Cohen, R. S. & O'Nions, R. K. (1982). Identification of recycled continental material in the mantle from Sr, Nd and Pb isotope investigations. *Earth and Planetary Science Letters* **61**, 73–84.

Cohen, R. S., O'Nions, R. K. & Dawson, J. B. (1984). Isotope geochemistry of xenoliths from East Africa: implications for development of mantle reservoirs and their interaction. *Earth and Planetary Science Letters* **68**, 209–220.

Cornell, D. H., Thomas, R. J., Bowring, S. A., Armstrong, R. A. & Grantham, G. H. (1996). Protolith interpretation in metamorphic terranes: a back-arc environment with Besshi-type base metal potential for the Quha Formation, Natal Province, South Africa. *Precambrian Research* **77**, 243–271.

Dalziel, I. W. D., Mosher, S. & Gahagan, L. M. (2000). Laurentia–Kalahari collision and the assembly of Rodinia. *Journal of Geology* **108**, 499–513.

Davidson, J. P. (1986). Isotopic and trace element constraints on the petrogenesis of subduction-related lavas from Martinique, Lesser Antilles. *Journal of Geophysical Research* **91**, 5343–5962.

Debayle, E. & Leveque, J. J. (1997). Upper mantle heterogeneities in the Indian Ocean from waveform inversion. *Geophysical Research Letters* **24**, 245–248.

Dick, H. J. B., Lin, J. & Schouten, H. (2003). An ultraslow-spreading class of ocean ridge. *Nature* **426**, 405–412.

Dosso, L., Bougault, H., Beuzart, P., Calvez, J.-Y. & Joron, J.-L. (1988). The geochemical structure of the South-East Indian Ridge. *Earth and Planetary Science Letters* **88**, 47–59.

Dostal, J., Dupuy, C., Nicollet, C. & Cantagrel, J. M. (1992). Geochemistry and petrogenesis of Upper Cretaceous basaltic rocks from southern Malagasy. *Chemical Geology* **97**, 199–218.

Doucet, S., Weis, D., Scoates, J., Debaille, V. & Giret, A. (2004). Geochemical and Hf–Pb–Sr–Nd isotopic constraints on the origin of the Amsterdam–St. Paul (Indian Ocean) hotspot basalts. *Earth and Planetary Science Letters* **218**, 179–195.

Douglass, J., Schilling, J. G. & Fontignie, D. (1999). Plume–ridge interactions of the Discovery and Shona mantle plumes with the southern Mid-Atlantic Ridge (40–55°S). *Journal of Geophysical Research* **104**, 2941–2962.

Dupré, B. & Allègre, C. J. (1983). Pb–Sr isotope variations in Indian Ocean basalts and mixing phenomena. *Nature* **303**, 142–146.

Eggins, S. M., Woodhead, J. D., Kinsley, L. P. J., Mortimer, G. E., Sylvester, P. J., McCulloch, M. T., Hergt, J. M. & Handler, M. R. (1997). A simple method for the precise determination of forty trace elements in geological samples by ICPMS using enriched isotope internal standardisation. *Chemical Geology* **134**, 311–326.

Elthon, D., Ross, D. K. & Meen, J. K. (1995). Compositional variations of basaltic glasses from the Mid-Cayman Rise spreading center. *Journal of Geophysical Research* **100**, 12497–12512.

Escrig, S., Capmas, F., Dupré, B. & Allègre, C. J. (2004). Osmium isotopic constraints on the nature of the DUPAL anomaly from Indian mid-ocean-ridge basalts. *Nature* **431**, 59–63.

Evensen, N. M., Hamilton, P. J. & O'Nions, R. K. (1978). Rare-earth abundances in chondritic meteorites. *Geochimica et Cosmochimica Acta* **42**, 1199–1212.

Fisher, R. L. & Goodwillie, A. M. (1997). The physiography of the Southwest Indian Ridge. *Marine Geophysical Researches* **19**, 451–455.

Fisher, R. L., Natland, J. H., Dick, H. J. B. & Meyer, P. S. (1985). *Shipboard Description and Inventory of Rocks Dredged on PROTEA Expedition, Leg 5, in the Southwest Indian Ocean. Scripps Institution of Oceanography Reference Series*, reference number 85-15, 223 pp.

Green, T. H. & Adam, J. (2003). Experimentally-determined trace element characteristics of aqueous fluid from partially dehydrated mafic oceanic crust at 3·0 GPa, 650–700°C. *European Journal of Mineralogy* **15**, 815–830.

Grégoire, M., Bell, D. R. & le Roex, A. P. (2003). Garnet lherzolites from the Kaapvaal craton (South Africa): trace element evidence for a metasomatic history. *Journal of Petrology* **44**, 629–657.

Groenewald, P. B., Grantham, G. H. & Watkeys, M. K. (1991). Geological evidence for a Proterozoic to Mesozoic link between southeastern Africa and Dronning Maud Land, Antarctica. *Journal of the Geological Society, London* **148**, 1115–1123.

Grunow, A., Hanson, R. & Wilson, T. (1996). Were aspects of Pan-African deformation linked to Iapetus opening? *Geology* **24**, 1063–1066.

Gupta, M. L. (1991). Heat-flow and heat generation in the Archean Dharwar cratons and implications for the southern Indian shield geotherm and lithospheric thickness. *Tectonophysics* **194**, 107–122.

Gurnis, M., Müller, R. D. & Moresi, L. (1998). Cretaceous vertical motion of Australia and the Australian–Antarctic Discordance. *Science* **279**, 1499–1504.

Haggerty, S. E. (1999). Earth and planetary sciences—a diamond trilogy: superplumes, supercontinents, and supernovae. *Science* **285**, 851–860.

Hamelin, B. & Allègre, C. J. (1985). Large-scale regional units in the depleted upper mantle revealed by an isotope study of the South-West Indian Ridge. *Nature* **315**, 196–199.

Hanan, B. B., Blichert-Toft, J., Pyle, D. G. & Christie, D. M. (2004). Contrasting origins of the upper mantle revealed by hafnium and lead isotopes from the Southeast Indian Ridge. *Nature* **432**, 91–94.

Handke, M. J., Tucker, R. D. & Ashwal, L. D. (1999). Neoproterozoic continental arc magmatism in west–central Madagascar. *Geology* **27**, 351–354.

Hanson, R. E. (2003). Proterozoic geochronology and tectonic evolution of southern Africa. In: Yoshida, M., Windley, B. F. & Dasgupta, S. (eds) *Proterozoic East Gondwana: Supercontinent Assembly and Breakup. Geological Society, London, Special Publications* **206**, 427–463.

Hart, S. R. (1984). A large-scale anomaly in the Southern Hemisphere mantle. *Nature* **309**, 753–757.

Hart, S. R. & Dunn, T. (1993). Experimental cpx/melt partitioning of 24 trace elements. *Contributions to Mineralogy and Petrology* **113**, 1–8.

Hart, S. R., Gerlach, D. C. & White, D. M. (1986). A possible new Sr–Nd–Pb mantle array and consequences for mixing. *Geochimica et Cosmochimica Acta* **50**, 1551–1557.

Hartnady, C. J. H. & le Roex, A. P. (1985). Southern Ocean hotspot tracks and the Cenozoic absolute motion of the African, Antarctic, and South American plates. *Earth and Planetary Science Letters* **75**, 245–257.

Hauri, E. H., Wagner, T. P. & Grove, T. L. (1994). Experimental and natural partitioning of Th, U, Pb and other trace elements between garnet, clinopyroxene and basaltic melts. *Chemical Geology* **117**, 149–166.

Hirschmann, M. M. & Stolper, E. M. (1996). A possible role for garnet pyroxenite in the origin of the 'garnet signature' in MORB. *Contributions to Mineralogy and Petrology* **124**, 185–208.

Hofmann, A. W. (1988). Chemical differentiation of the Earth: the relationship between mantle, continental crust and oceanic crust. *Earth and Planetary Science Letters* **90**, 297–314.

Huang, Y.-M., Van Calsteren, P. & Hawkesworth, C. J. (1995). The evolution of the lithosphere in southern Africa: a perspective on the basic granulite xenoliths from kimberlites in South Africa. *Geochimica et Cosmochimica Acta* **59**, 4905–4920.

Irving, A. J. & Frey, F. A. (1978). Distribution of trace elements between garnet megacrysts and host volcanic liquids of kimberlitic to rhyolitic composition. *Geochimica et Cosmochimica Acta* **42**, 771–787.

Jacobs, J., Fanning, C. M., Henjes-Kunst, F., Olesch, M. & Paech, H.-J. (1998). Continuation of the Mozambique Belt into East Antarctica: Grenville-age metamorphism and polyphase Pan-African high-grade events in central Dronning Maud Land. *Journal of Geology* **106**, 385–406.

Jacobsen, S. B. (1999). The Geochemical Earth Reference Model: composition and evolution of the depleted mantle. *EOS Transactions, American Geophysical Union* **80**, F1173.

James, D. E., Fouch, M. J., VanDecar, J. C. & van der Lee, S. (2001). Tectospheric structure beneath southern Africa. *Geophysical Research Letters* **28**, 2485–2488.

Johnson, C. M. & Beard, B. L. (1993). Evidence from hafnium isotopes for ancient sub-oceanic mantle beneath the Rio-Grande Rift. *Nature* **362**, 441–444.

Kamenetsky, V. S., Maas, R., Sushchevskaya, N. M., Norman, M. D., Cartwright, I. & Peyve, A. A. (2001). Remnants of Gondwanan continental lithosphere in oceanic upper mantle: evidence from the South Atlantic Ridge. *Geology* **29**, 243–246.

Kempton, P. D. & Pearce, J. A. (2003). Indian MORB-source mantle: not just a case of plume contamination or sediment recycling. *Geophysical Research Abstracts* **5**, abstract 04017 (CD-ROM).

Kempton, P. D., Pearce, J. A. & Tappin, D. (2000). Hf isotope evidence for mantle domain boundaries in the western Pacific. *Journal of Conference Abstracts* **5**, 576.

Kempton, P. D., Pearce, J. A., Barry, T. L., Fitton, J. G., Langmuir, C. & Christie, D. M. (2002). Sr–Nd–Pb–Hf isotope results from ODP Leg 187: evidence for mantle dynamics of the Australian–Antarctic Discordance and origin of the Indian MORB source. *Geochemistry, Geophysics, Geosystems* **3**, doi: 10.1029/2002GC000320.

Klein, E. M. & Langmuir, C. H. (1987). Global correlations of ocean ridge basalt chemistry with axial depth and crustal thickness. *Journal of Geophysical Research* **92**, 8089–8115.

Kröner, A., Sacchi, R., Jaeckel, P. & Costa, M. (1997). Kibaran magmatism and Pan-African granulite metamorphism in northern Mozambique: single zircon ages and regional implications. *Journal of African Earth Sciences* **25**, 467–484.

Kröner, A., Willner, A. P., Hegner, E., Jaeckel, P. & Nemchin, A. (2001). Single zircon ages, *PT* evolution and Nd isotopic systematics of high-grade gneisses in southern Malawi and their bearing on the evolution of the Mozambique belt in southeastern Africa. *Precambrian Research* **109**, 257–291.

Lassiter, J. C., Hauri, E. H., Reiners, P. W. & Garcia, M. O. (2000). Generation of Hawaiian post-erosional lavas by melting of a mixed lherzolite/pyroxenite source. *Earth and Planetary Science Letters* **178**, 269–284.

Lee, D.-C., Halliday, A. N., Davies, G. R., Essene, E. J., Fitton, J. G. & Temdjim, R. (1996). Melt enrichment of shallow depleted mantle: a detailed petrological trace element and isotopic study of mantle-derived xenoliths and megacrysts from the Cameroon line. *Journal of Petrology* **37**, 415–441.

Lenardic, A., Moresi, L. & Muhlhaus, H. (2003). Longevity and stability of cratonic lithosphere: insights from numerical simulations of coupled mantle convection and continental tectonics. *Journal of Geophysical Research* **108**, article number 2303.

le Roex, A. P. (1985). Geochemistry, mineralogy and magmatic evolution of the basaltic and trachytic lavas from Gough Island, South Atlantic. *Journal of Petrology* **26**, 149–186.

le Roex, A. P. & Erlank, A. J. (1982). Quantitative evaluation of fractional crystallization in Bouvet Island lavas. *Journal of Volcanology and Geothermal Research* **13**, 309–338.

le Roex, A. P., Dick, H. J. B., Erlank, A. J., Reid, A. M., Frey, F. A. & Hart, S. R. (1983). Geochemistry, mineralogy and petrogenesis of lavas erupted along the Southwest Indian Ridge between the Bouvet triple junction and 11 degrees east. *Journal of Petrology* **24**, 267–318.

le Roex, A. P., Dick, H. J. B., Reid, A. M., Frey, F. A., Erlank, A. J. & Hart, S. R. (1985). Petrology and geochemistry of basalts from the American–Antarctic Ridge, Southern Ocean: implications for the westward influence of the Bouvet mantle plume. *Contributions to Mineralogy and Petrology* **90**, 367–380.

le Roex, A. P., Dick, H. J. B. & Fisher, R. L. (1989). Petrology and geochemistry of MORB from 25°E to 46°E along the Southwest Indian Ridge: evidence for contrasting styles of mantle enrichment. *Journal of Petrology* **30**, 947–986.

le Roex, A. P., Dick, H. J. B. & Watkins, R. T. (1992). Petrogenesis of anomalous K-enriched MORB from the Southwest Indian Ridge: 11°53′E to 14°38′E. *Contributions to Mineralogy and Petrology* **110**, 253–268.

Le Roux, P. J., le Roex, A. P., Schilling, J. G., Shimizu, N., Perkins, W. W. & Pearce, N. J. G. (2002*a*). Mantle heterogeneity beneath the southern Mid-Atlantic Ridge: trace element evidence for contamination of ambient asthenospheric mantle. *Earth and Planetary Science Letters* **203**, 479–498.

Le Roux, P. J., le Roex, A. P. & Schilling, J.-G. (2002*b*). MORB melting processes beneath the southern Mid-Atlantic Ridge (40–55°S): a role for mantle plume-derived pyroxenite. *Contributions to Mineralogy and Petrology* **144**, 206–229.

Lin, P. N., Stern, R. J., Morris, J. & Bloomer, S. H. (1990). Nd and Sr-isotopic compositions of lavas from the northern Mariana and southern Volcano arcs: implications for the origin of island arc melts. *Contributions to Mineralogy and Petrology* **105**, 381–392.

Mahoney, J. J., Natland, J. H., White, W. M., Poreda, R., Bloomer, S. M., Fisher, R. L. & Baxter, A. N. (1989). Isotopic and geochemical provinces of the western Indian Ocean spreading centers. *Journal of Geophysical Research* **94**, 283–296.

Mahoney, J. J., Nicollet, C. & Dupuy, C. (1991). Madagascar basalts: tracking oceanic and continental sources. *Earth and Planetary Science Letters* **104**, 350–363.

Mahoney, J. J., le Roex, A. P., Peng, Z., Fisher, R. L. & Natland, J. H. (1992). Southwestern limits of Indian Ocean Ridge mantle and the origin of low $^{206}Pb/^{204}Pb$ mid-ocean ridge basalts: isotope systematics of the Southwest Indian Ridge (17°–50°E). *Journal of Geophysical Research* **97**, 19771–19790.

Mahoney, J. J., Sinton, J. M., Kurz, M. D., Macdougall, J. D., Spencer, K. J. & Lugmair, G. W. (1994). Isotope and trace element characteristics of a super-fast spreading ridge: East Pacific Rise, 13–23°S. *Earth and Planetary Science Letters* **121**, 173–193.

Mahoney, J. J., Graham, D. W., Christie, D. M., Johnson, K. T. M., Hall, L. S. & Vonderhaar, D. L. (2002). Between a hotspot and a cold spot: isotopic variation in the Southeast Indian Ridge asthenosphere, 86°E–118°E. *Journal of Petrology* **43**, 1155–1176.

Mattielli, N., Weis, D., Blichert-Toft, J. & Albarède, F. (2002). Hf isotope evidence for a Miocene change in the Kerguelen mantle plume composition. *Journal of Petrology* **43**, 1327–1339.

McDonough, W. F. (1990). Constraints on the composition of the continental lithospheric mantle. *Earth and Planetary Science Letters* **101**, 1–18.

McDonough, W. F. & McCulloch, M. T. (1987). The southeast Australian lithospheric mantle: isotopic and geochemical constraints on its growth and evolution. *Earth and Planetary Science Letters* **86**, 327–340.

McKenzie, D. & O'Nions, R. K. (1991). Partial melt distributions from inversion of rare-earth element concentrations. *Journal of Petrology* **32**, 1021–1091.

Meert, J. G. (2003). A synopsis of events related to the assembly of East Gondwana. *Tectonophysics* **362**, 1–40.

Meisel, T., Walker, R. J. & Morgan, J. W. (1996). The osmium isotopic composition of the Earth's primitive upper mantle. *Nature* **383**, 517–520.

Menzies, M. A. & Murthy, V. R. (1980). Enriched mantle: Nd and Sr isotopes in diopsides from kimberlite nodules. *Nature* **283**, 634–636.

Michard, A., Montigny, R. & Schlich, R. (1986). Geochemistry of the mantle beneath the Rodriguez triple junction and the South-East Indian Ridge. *Earth and Planetary Science Letters* **78**, 104–114.

Milner, S. C. & le Roex, A. P. (1996). Isotope characteristics of the Okenyenya igneous complex, northwestern Namibia: constraints on the composition of the early Tristan plume and the origin of the EM 1 mantle component. *Earth and Planetary Science Letters* **141**, 277–291.

Mühe, R., Devey, C. W. & Bohrmann, H. (1993). Isotope and trace element geochemistry of MORB from the Nansen–Gakkel Ridge at 86°N. *Earth and Planetary Science Letters* **120**, 103–109.

Mühe, R., Bohrmann, H., Garbe-Schönberg, D. & Kassens, H. (1997). E-MORB glasses from the Gakkel Ridge (Arctic Ocean) at 87°N: evidence for the Earth's most northerly volcanic activity. *Earth and Planetary Science Letters* **152**, 1–9.

Müller, M. R., Robinson, C. J., Minshull, T. A., White, R. S. & Bickle, M. J. (1997). Thin crust beneath Ocean Drilling Program

borehole 735B at the Southwest Indian Ridge? *Earth and Planetary Science Letters* **148**, 93–107.

Nelson, D. R., Chivas, A. R., Chappell, B. W. & McCulloch, M. T. (1988). Geochemical and isotopic systematics in carbonatites and implications for the evolution of ocean island sources. *Geochimica et Cosmochimica Acta* **52**, 1–17.

Niu, Y. & Batiza, R. (1991). An empirical method for calculating melt compositions produced beneath mid-ocean ridges: applications for axis and off-axis (seamounts) melting. *Journal of Geophysical Research* **96**, 21753–21777.

Nowell, G. M., Kempton, P. D., Noble, S. R., Fitton, J. G., Saunders, A. D., Mahoney, J. J. & Taylor, R. N. (1998). High precision Hf isotope measurements of MORB and OIB by thermal ionisation mass spectrometry: insights into the depleted mantle. *Chemical Geology* **149**, 211–233.

O'Neill, H. S. C. (1981). The transition between spinel lherzolite and garnet lherzolite, and its use as a geobarometer. *Contributions to Mineralogy and Petrology* **77**, 185–194.

Patchett, P. J. & Tatsumoto, M. (1980*a*). Hafnium isotope variations in oceanic basalts. *Geophysical Research Letters* **7**, 1077–1080.

Patchett, P. J. & Tatsumoto, M. (1980*b*). A routine high-precision method for Lu–Hf isotope geochemistry and chronology. *Contributions to Mineralogy and Petrology* **75**, 263–267.

Patchett, P. J., White, W. M., Feldmann, H., Kielinczuk, S. & Hofmann, A. W. (1984). Hafnium/rare earth element fractionation in the sedimentary system and crustal recycling into the Earth's mantle. *Earth and Planetary Science Letters* **69**, 365–378.

Paulsson, O. & Austrheim, H. (2003). A geochronological and geochemical study of rocks from Gjelsvikfjella, Dronning Maud Land, Antarctica—implications for Mesoproterozoic correlations and assembly of Gondwana. *Precambrian Research* **125**, 113–138.

Pearce, J. A., Baker, P. E., Harvey, P. K. & Luff, I. W. (1995). Geochemical evidence for subduction fluxes, mantle melting and fractional crystallization beneath the South Sandwich Island Arc. *Journal of Petrology* **36**, 1073–1109.

Pearce, J. A., Kempton, P. D., Nowell, G. M. & Noble, S. R. (1999). Hf–Nd element and isotope perspective on the nature and provenance of mantle and subduction components in western Pacific arc–basin systems. *Journal of Petrology* **40**, 1579–1611.

Pertermann, M. & Hirschmann, M. M. (2003). Partial melting experiments on a MORB-like pyroxenite between 2 and 3 GPa: constraints on the presence of pyroxenite in basalt source regions from solidus location and melting rate. *Journal of Geophysical Research* **108**, paper number 2000JB000118.

Plank, T. & Langmuir, C. H. (1998). The chemical composition of subducting sediment and its consequences for the crust and mantle. *Chemical Geology* **145**, 325–394.

Price, R. C., Kennedy, A. K., Riggs-Sneeringer, M. & Frey, F. A. (1986). Geochemistry of basalts from the Indian Ocean triple junction: implications for the generation and development of Indian Ocean ridge basalts. *Earth and Planetary Science Letters* **78**, 379–396.

Pyle, D. G., Christie, D. M. & Mahoney, J. J. (1992). Resolving an isotopic boundary within the Australian–Antarctic discordance. *Earth and Planetary Science Letters* **112**, 161–178.

Pyle, D. G., Christie, D. M., Mahoney, J. J. & Duncan, R. A. (1995). Geochemistry and geochronology of ancient southeast Indian and southwest Pacific seafloor. *Journal of Geophysical Research* **100**, 22261–22282.

Rehkämper, M. & Hofmann, A. W. (1997). Recycled ocean crust and sediment in Indian Ocean MORB. *Earth and Planetary Science Letters* **147**, 93–106.

Rehkämper, M. & Halliday, A. N. (1998). Accuracy and long-term reproducibility of lead isotopic measurements by MC-ICP-MS using an external method for correction of mass discrimination. *International Journal of Mass Spectrometry and Ion Processes* **58**, 123–133.

Robinson, C. J., White, R. S., Bickle, M. J. & Minshull, T. A. (1996). Restricted melting under the very slow-spreading Southwest Indian Ridge. In: MacLeod, C. J., Tyler, P. A. & Walker, C. L. (eds) *Tectonic, Magmatic, Hydrothermal and Biological Segmentation of Mid-Ocean Ridges. Geological Society, London, Special Publications* **118**, 131–141.

Rudnick, R. L. (1990). Nd and Sr isotopic compositions of lower crustal xenoliths from North Queensland, Australia: implications for Nd model ages and crustal growth processes. *Chemical Geology* **83**, 195–208.

Rudnick, R. L. & Fountain, D. M. (1995). Nature and composition of the continental crust: a lower crustal perspective. *Reviews of Geophysics* **33**, 267–309.

Rudnick, R. L., McDonough, W. F., McCulloch, M. T. & Taylor, S. R. (1986). Lower crustal xenoliths from Queensland, Australia: evidence for deep crustal assimilation and fractionation of continental basalts. *Geochimica et Cosmochimica Acta* **50**, 1099–1115.

Saal, A. E., Rudnick, R. L., Ravizza, G. E. & Hart, S. R. (1998). Re–Os isotope evidence for the composition, formation and age of the lower crust. *Nature* **393**, 58–61.

Salters, V. J. M. (1996). The generation of mid-ocean ridge basalts from the Hf and Nd isotope perspective. *Earth and Planetary Science Letters* **141**, 109–123.

Salters, V. J. M. & Dick, H. J. B. (2002). Mineralogy of the mid-ocean-ridge basalt source from neodymium isotopic composition of abyssal peridotites. *Nature* **418**, 68–72.

Salters, V. J. M. & Hart, S. R. (1989). The hafnium paradox and the role of garnet in the source of mid-ocean-ridge basalts. *Nature* **342**, 420–422.

Salters, V. J. M. & Hart, S. R. (1991). The mantle sources of ocean ridges, islands and arcs: the Hf-isotope connection. *Earth and Planetary Science Letters* **104**, 364–380.

Salters, V. J. M. & Longhi, J. (1999). Trace element partitioning during the initial stages of melting beneath mid-ocean ridges. *Earth and Planetary Science Letters* **166**, 15–30.

Salters, V. J. M. & Stracke, A. (2004). Composition of the depleted mantle. *Geochemistry, Geophysics, Geosystems* **5**, doi: 10.1029/2003GC000597.

Salters, V. J. M. & White, W. M. (1998). Hf isotopic constraints on mantle evolution. *Chemical Geology* **145**, 447–460.

Salters, V. J. M., Longhi, J. E. & Bizimis, M. (2002). Near mantle solidus trace element partitioning at pressures up to 3·4 GPa. *Geochemistry, Geophysics, Geosystems* **3**, doi: 10.1029/2001GC000148.

Scherer, E. E., Cameron, K. L., Johnson, C. M., Beard, B. L., Barovich, K. M. & Collerson, K. D. (1997). Lu–Hf geochronology applied to dating Cenozoic events affecting lower crustal xenoliths from Kilbourne Hole, New Mexico. *Chemical Geology* **142**, 63–78.

Schmitz, M. D., Vervoort, J. D., Bowring, S. A. & Patchett, J. P. (2004). Decoupling of the Lu–Hf and Sm–Nd systems during the evolution of granulitic lower crust beneath southern Africa. *Geology* **32**, 405–408.

Scotese, C. R. (2004). A continental drift flipbook. *Journal of Geology* **112**, 729–741.

Shirey, S. B., Bender, J. F. & Langmuir, C. H. (1987). Three-component isotopic heterogeneity near the Oceanographer Transform, Mid-Atlantic Ridge. *Nature* **325**, 217–223.

Simon, N. S. C., Carlson, R. W., Pearson, D. G. & Davies, G. R. (2002). The Lu–Hf isotope composition of cratonic lithosphere: disequilibrium between garnet and clinopyroxene in kimberlite xenoliths. *Geochimica et Cosmochimica Acta* **66**(Supplement), A717.

Simon, N. S. C., Carlson, R. W., Davies, G. R., Nowell, G. M. & Pearson, D. G. (2003). Os–Sr–Nd–Hf isotope evidence for the ancient depletion and subsequent multi-stage enrichment history of the Kaapvaal cratonic lithosphere. In: *Extended Abstracts of the Eighth International Kimberlite Conference*, abstract number 117 (CD-ROM).

Staudigel, H., Plank, T., White, W. M. & Schminke, H. U. (1996). Geochemical fluxes during seafloor alteration of the basaltic upper crust: DSDP Sites 417 and 418 (Overview). In: Bebout, G. E., Scholl, D. W., Kirby, S. H. & Platt, J. P. (eds) *Subduction: Top to Bottom. Geophysical Monograph, American Geophysical Union* **96**, 19–38.

Stern, R. J. (1994). Arc-assembly and continental collision in the Neoproterozoic East African orogen: implications for the consolidation of Gondwanaland. *Annual Review of Earth and Planetary Sciences* **22**, 319–352.

Storey, B. C. (1995). The role of mantle plumes in continental breakup: case histories from Gondwanaland. *Nature* **377**, 301–308.

Storey, M., Saunders, A. D., Tarney, J., Gibson, I. L., Norry, M. J., Thirlwall, M. F., Leat, P., Thompson, R. N. & Menzies, M. A. (1989). Contamination of Indian Ocean asthenosphere by the Kerguelen–Heard mantle plume. *Nature* **338**, 574–576.

Storey, M., Mahoney, J. J. & Saunders, A. D. (1998). Cretaceous basalts in Madagascar and the transition between plume and continental lithosphere mantle sources. In: Mahoney, J. J. & Coffin, M. F. (eds) *Large Igneous Provinces. Geophysical Monograph, Washington American Geophysical Union* **100**, 95–122.

Subbarao, K. V. & Hedge, C. E. (1973). K, Rb, Sr and $^{87}Sr/^{86}Sr$ in rocks from the Mid-Indian Ocean Ridge. *Earth and Planetary Science Letters* **18**, 223–228.

Sun, S.-S. (1980). Lead isotopic study of young volcanic rocks from mid-ocean ridges, ocean islands and island arcs. *Philosophical Transactions of the Royal Society of London, Series A* **297**, 409–445.

Sun, S.-S. & McDonough, W. F. (1989). Chemical and isotopic systematics of oceanic basalts: implications for mantle composition and processes. In: Saunders, A. D. & Norry, M. J. (eds) *Magmatism in the Ocean Basins. Geological Society, London, Special Publications* **42**, 313–345.

Taylor, S. R. & McClennan, S. M. (1985). *The Continental Crust: its Composition and Evolution*. Oxford: Blackwell Scientific.

Todt, W., Cliff, R. A., Hanser, A. & Hofmann, A. W. (1996). Evaluation of a ^{202}Pb–^{205}Pb double spike for high-precision lead isotope analysis. In: Basu, A. & Hart, S. R. (eds) *Earth Processes: Reading the Isotopic Code. Geophysical Monograph, American Geophysical Union* **95**, 429–437.

Tucker, R. D., Ashwal, L. D., Handke, M. J., Hamilton, M. A., Le Grange, M. & Rambeloson, R. A. (1999). U–Pb geochronology of the Archean and Proterozoic rocks of north–central Madagascar. *Journal of Geology* **107**, 135–153.

Vervoort, J. D., Patchett, P. J., Blichert-Toft, J. & Albarède, F. (1999). Relationships between Lu–Hf and Sm–Nd isotopic systems in the global sedimentary system. *Earth and Planetary Science Letters* **168**, 79–99.

Vervoort, J. D., Patchett, J. P., Albarède, F., Blichert-Toft, J., Rudnick, R. & Downes, H. (2000). Hf–Nd isotopic evolution of the lower crust. *Earth and Planetary Science Letters* **181**, 115–129.

Walker, R. J., Carlson, R. W., Shirey, S. B. & Boyd, F. R. (1989). Os, Sr, Nd and Pb isotope systematics of southern African peridotite xenoliths: implications for the chemical evolution of subcontinental mantle. *Geochimica et Cosmochimica Acta* **53**, 1583–1595.

Weaver, B. L., Wood, D. A., Tarney, J. & Joron, J. L. (1986). Role of subducted sediment in the genesis of ocean island basalts: geochemical evidence from South Atlantic Ocean islands. *Geology* **14**, 275–278.

Weis, D. & Frey, F. A. (1996). Role of the Kerguelen Plume in generating the eastern Indian Ocean seafloor. *Journal of Geophysical Research* **101**, 13831–13849.

White, W. M., Hofmann, A. W. & Puchelt, H. (1987). Isotope geochemistry of Pacific mid-ocean ridge basalt. *Journal of Geophysical Research* **92**, 4881–4893.

Williams, G. A. & Turekian, K. K. (2004). The glacial–interglacial variation of seawater osmium isotopes as recorded in Santa Barbara Basin. *Earth and Planetary Science Letters* **228**, 379–389.

Woodhead, J. D., Hergt, J. M., Davidson, J. P. & Eggins, S. M. (2001). Hafnium isotope evidence for 'conservative' element mobility during subduction zone processes. *Earth and Planetary Science Letters* **192**, 331–346.

Workman, R. K. & Hart, S. R. (2005). Major and trace element composition of the depleted MORB mantle (DMM). *Earth and Planetary Science Letters* **231**, 53–72.

Yang, H.-J., Frey, F. A., Weis, D., Giret, A., Pyle, D. G. & Michon, G. (1998). Petrogenesis of the flood basalts forming the northern Kerguelen Archipelago: implications for the Kerguelen Plume. *Journal of Petrology* **39**, 711–748.

Zhang, S.-Q., Mahoney, J. J., Mo, X.-X., Ghazi, A. M., Milani, L., Crawford, A. J., Guo, T.-Y. & Zhao, Z.-D. (2005). Evidence for a widespread Tethyan upper mantle with Indian Ocean-type isotopic characteristics. *Journal of Petrology* **46**, 829–858.